Cell Culture Impedance Sensing with Thin Film ITO Electrodes

Katja Sofie Støren Sverdlilje

Master thesis in the Materials, Energy, and Nanotechnology (MENA) Programme

60 ECTS credits

Department of Physics & Department of Chemistry

UNIVERSITY OF OSLO

August 2016

© Katja Sofie Støren Sverdlilje – Department of Physics and Department of Chemistry, University of Oslo.

2016

Cell Culture Impedance Sensing with Thin Film ITO Electrodes

Katja Sofie Støren Sverdlilje

http://duo.uio.no/

Printed by: University Print Centre, University of Oslo

Acknowledgements and Dedication

This thesis was written as part of the master degree programme Materials, Energy and Nanotechnology (MENA) at the departments of Physics and Chemistry at the University of Oslo (UiO), in the Nanotechnology and Functional Materials (NAFUMA) group.

Big thanks go to my supervisors: Prof. Ola Nilsen (main supervisor), Chemistry Department, UiO; Prof. Ørjan Martinsen, Physics Department, UiO; and Jon Roger Eidet, MD, PhD, Department of Ophthalmology, Oslo University Hospital, all of whom have made the work on this thesis interesting and engaging, and whose support and input has been invaluable.

Thanks to the people and institutions whose equipment I have used and whose help, instruction and advice were all instrumental in making the experimental part of this thesis possible: Leva Momtazi and Jon Bratvold in the NAFUMA group; Rune Bjørnestøl at the UiO Chemistry Department Instrument Workshop; Tom Thorsen and Behzad Foroughinejad at the UiO Chemistry Department Electronics Workshop; Elijah Jeremiah Aller at the UiO Chemistry Department Glassblowing Workshop; Klaus Magnus Håland Johansen, Per Lindberg, and Stig Bengt Mikael Sjödin at the NorFab MiNa lab in Oslo; Catherine Jackson and Sjur Reppe at the cell culture lab at Oslo University Hospital; and Krister Borge, Adrian Helle, and Soheil Dabestani at Sonen lab at the Institute for Informatics, UiO.

Julie Nitsche Kvalvik, thanks for your support, input and help. It would have been a lot more difficult without you.

Special thanks go to my co-students and office buddies Hanna Elina Melteig and Ina Aune Grosås for all the co-procrastinative, informative and interesting discussions on biochemistry, "ordinary" chemistry, biophysics, politics, epidemics, evolutionary psychology, environment, and a host of other interesting subjects of variable relevance. It would have been a lot less enjoyable without you. Thanks for your support and encouragement.

And thanks to Per Anders Hansen and all of you at the NAFUMA soup lunches for all the diverse culinary experiences and conversations. It would have been a lot less tasty without you.

* * *

This thesis is dedicated to my fantastic wife Vanja, who puts up with my weirdness and work hours in the most loving and supportive way possible, as well as brightening each and every day; and Benedicte and Sol-Maria, who are, with absolute certainty, the best kids in the world.

Katja Sofie Støren Sverdlilje

Abstract

The intent of the thesis has been to investigate the suitability of micrometer-scaled interdigitated indium tin oxide (ITO) electrodes for impedance sensing of a monolayer human retinal pigment epithelium (RPE) culture, and to assess atomic layer deposition (ALD) coating as a tool to functionalise the electrode and substrate surfaces. Building a impedance sensing device for cell cultures was part of the work.

A cell culture impedance sensing device utilising micrometer-scaled interdigitated ITO electrodes has been designed, prototyped and produced to measure electric properties of a monolayer human RPE cell culture of the ARPE-19 cell line. Design was performed in a CAD tool, plastic parts were printed with a 3D printer; the electrodes were created using laser ablation of a glass plate coated with a 350 nm ITO film; the cell well was cut from a SiO_2 glass tube. Equivalent circuit analysis and finite element method (FEM) simulation were performed based on existing research documentation. Toxicity tests for adhesives for the well attachment were performed, resulting in the use of aquarium silicone as adhesive.

Interdigitated electrodes with 24 µm and 192 µm digits were used to measure the impedance of an ARPE-19 cell culture. Separate experiments with substrates coated by atomic layer deposition (ALD) technique with titanium tetraisopropoxide (TTIP) and glycine, and with $CaCO_3$ were performed.

Impedance measurements indicating cell attachment and proliferation on the different types of substrates and for different electrode dimensions were performed with an impedance analyser; phase contrast optical microscope observations of the cells were performed in parallel. Measurements indicated that the ITO electrodes allowed ARPE-19 cell attachment and proliferation, and were sensitive to the resulting impedance changes. The TiO_2/glycine-coated electrodes allowed cell attachment and proliferation but were both unsuccessful in regards to measurement purposes.

Abbreviations and Conventions

AC	Alternating current
ALD	Atomic layer deposition
CAD	Computer assisted design
CPE	Constant phase element
CVD	Chemical vapour deposition
DC	Direct current
DMEM	Dulbecco's modified Eagle's medium
DPBS	Dulbecco's phosphate-buffered saline
ECG	Electrocardiograph
ECM	Exctracellular matrix
EDR	Electrodermal response
FDA	Food and Drug Administration
FEM	Finite element method
ITO	Indium tin oxide
QCM	Quartz crystal microbalance
RPE	Retinal pigment epithelium
TTIP	Titanium tetraisopropoxide

Complex variables are written in bold, e.g. **Z**. Scalar variables are written in italic, e.g. *R*.

Where spelling differs between British and American convention, i.e. "utilise" vs. "utilize", the former, British convention is utilised. Latin expressions are written in italic, e.g. *in vitro.*

Specific equipment used in work in this thesis is presented within its corresponding method section. For reference, a list of them is given in Appendix D.

Unless otherwise indicated, vector graphics drawings were made in Inkscape, renders and technical drawing of cell culture sensing device were generated in Solidworks, Maple plots were generated in Maple, and measurement plots were generated in Origin.

Contents

1 Introduction

This chapter describes the goal for this thesis and the background of the project, followed by a presentation of and historical overview of bioimpedance and cell culture.

The goal of this thesis has been to investigate the suitability of micrometer-scaled interdigitated indium tin oxide (ITO) electrodes for impedance measurements of retinal pigment epithelium (RPE) cells of the ARPE-19 cell line, and to look into the benefits of coating the electrodes with a $CaCO_3$ or titanium tetraisopropoxide (TTIP)/glycine nanofilm deposited by atomic layer deposition (ALD) as an attachment-promoting layer. As part of the thesis, a cell culture impedance sensing device is designed, prototyped and produced.

The thesis is part of a project at Oslo University Hospital, which investigates growing and storing of layers of the human retina, in order to enable tissue engineering techniques for repair or replacement of a retina which has been damaged or become detached.

Cell culture is an important tool in medical and biological research and production, including vaccine production and toxicology, and also the rapidly growing field of tissue engineering, i.e. the technique of creating living tissue by growing or arranging cells in laboratory conditions, typically with the intent replacing or repairing damaged or sick tissue as a therapy.

One of the challenges of cell culture is monitoring the growth, state and attributes of the cells being cultured. The sizes of most mammalian cells lie in the range of 10 μm to 100 μm, meaning that microscopy is required for optical observation and measurements; this can be time consuming. Often, the main desired statistic is proliferation, which for detached cells can be measured by a cell counter; for attached cells, however, a method which enables monitoring of cell attachment and proliferation without detaching the cells from the substrate is desirable, since detachment may harm the cells.

Impedance sensing for cell culture has been developed to provide a method for recording proliferation and other characteristics of the cells and their processes. Electrodes, either in the form of probes in a cell suspension, or integrated in the substrate of the cell culture vessel, record impedance data for the cell culture, and can thus measure cell proliferation and viability, along with the potential to measure cell health. In the case of the substrate-integrated electrodes, the intrusiveness of the measurement can be minimal, depending on the electrode properties. Currents should be held at an acceptable level and frequency in order to sustain the integrity of the cells and the cell culture.

Current technology in cell culture substrate impedance sensing equipment use electrodes with dimensions down to approximately 2 μm, although larger dimensions are more common. Substrates are often covered with an attachment-promoting layer, e.g. collagen or lysine.

The work is interdisciplinary, drawing on:

- Biophysics, by the techniques and theory for measuring bioimpedance and analysing the results as dielectric spectroscopy.
- Cell biology, by the workings of a cell culture lab and the techniques and theory of cell culture.
- Nanotechnology and materials science, by the choice of materials and manufacture of electrode equipment.

There is also a prominent engineering element present, in the design, prototyping and construction of the sensing device.

An introduction to electrics and dielectrics can also be found in Appendix B.

Calculations in this thesis are not always presented with all steps included; complete calculations can be found in Appendix G.

1.1 History of Bioimpedance and Bioelectricity

Bioelectricity was observed early in human history in the form of numbing effects from animals capable of delivering an electric discharge. Among those is the torpedo ray (Figure 1 and Figure 2), which was mentioned in Hippocrates' texts[1]. Electric discharges from animals may deliver currents up to 5 A, and, in the case of the electric eel (*Electrophorus electricus* – actually a knifefish, not an eel) may reach voltages over 500 V [1].

Figure 1 - Lesser electric ray, *Narcine bancroftii*.From [2].

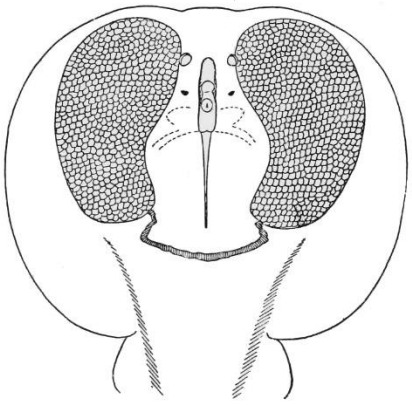

Figure 2 - Electric organs of the torpedo ray. From [3].

Georg Wilhelm Richmann was a Russian physicist of German descent, who in 1763 arguably had the doubtful honour of being the first person on record to die in an electrical experiment, during a thunderstorm (Figure 3). Incidentally, this may also be the first recorded experiment where bioimpedance was directly involved, albeit unintended. The event was published worldwide, and highlighted the need for caution when dealing with strong currents [4].

[1] Michael Faraday would study the electrical discharge from torpedo rays centuries later, in 1813.

Figure 3 - G. W. Richmann is killed by lightning during an electricity experiment in 1763. From [5].

The first recorded experiment with bioelectricity also marks the start of experiments with flowing currents, while the previous experiments had been concerned with static electricity.

In 1780, Luigi Galvani discovered that frogs' muscles moved when their spinal cords were stimulated [4]. The outdated term *galvanic current* stems from Galvani's experiments and legacy. Modern terminology for galvanic current is direct current (DC).

Conduction parameters for tissue were described in the mid- to late 19th century, when the conduction velocity of a nerve cell axon was measured around 1850 by Hermann von Helmholtz, and the capacitive and anisotropic properties of tissue, based on alternating current (AC) measurements, were described by Hermann Müller in the 1870s. An early form of the electroencephalogram (EEG) was recorded in 1875 by Richard Caton [4], followed by the electrocardiogram (ECG) in 1887 by August Waller.

James Clark Maxwell, whose set of partial differential equations, published in 1873, form the basis of classical electrodynamics, would build on Faraday's works on bioelectricity. He calculated the resistance of spheres in suspension as a function of their concentration. This is still used as the basic mathematical model for cell suspensions [4].

In 1910, Rudolf Höber demonstrated the existence of cell membranes by comparing electric properties at high and low frequency currents.

Hugo Fricke introduced a descriptive model in 1932 where he highlighted and described how the electrode polarisation capacitance varies with the frequency of the current, formulated in Fricke's Law [6].

The brothers Kenneth S. and Robert H. Cole published several seminal papers on tissue impedance, conductance and permittivity in 1928 and later in 1932 and 1940. The Cole-Cole equation, Cole-Cole plot and constant phase element (CPE) were introduced by them. They forged the basis of mathematical treatment of immitivity and permittivity for living tissues, as well as a mathematical expression for impedance dispersion corresponding to the circular arc in the Cole-Cole plot. They also proposed electrical circuit equivalents for the Cole-Cole equation [7-10].

Herman Paul Schwan worked on electric properties of blood, cell counting, tissue relaxation and electrode polarization, and in 1950 he described the frequency dependency of capacitance of muscle tissue. The important concept of dispersion was introduced by Schwan [11].

Giaever and Keese proposed a system in 1984 for monitoring cells in tissue culture by impedance measurements. They monitored complex impedance over time during cell seeding in the cell culture vessel, attachment, proliferation and death, registering that the impedance of the system increased as the cells attached. They also noticed that there were small fluctuations of impedance in the system, which they attributed to either movement in the cells or chemical changes [12]. They later confirmed that the fluctuations occurred due to cell micromotion (Figure 4) [13]. During the 1990s, they continued to develop measurement techniques and derived data, and in the 2000s, the Electric Cell-Substrate Impedance Sensing (ECIS) system was released to the market, which has been followed by several manufacturers since, producing cell impedance measurement equipment in various forms and configurations.

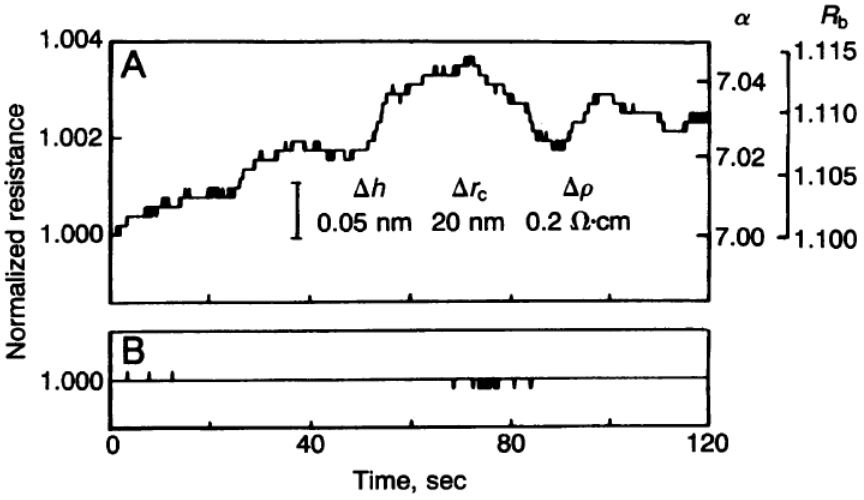

Figure 4 - Microfluctuations in live cells (top), compared to dead cells (bottom). From [13].

Equipment for various uses of bioimpedance and bioelectricity techniques has been developed throughout the previous century and into the current one. Some of them are described in sections 1.1.1 and 0. Of special interest to this thesis is the development of techniques for impedance measurements of cell cultures.

1.1.1 Uses of Bioimpedance and Bioelectricity Techniques

Bioimpedance and/or bioelectricity techniques are used in various monitoring and therapeutical equipment, e.g.:

- Impedance sensing of cell culture, where the impedance of a material is measured and analysed, and the focus of this thesis.
- Impedance plethysmography, where volume changes and blood pressure in living tissue can be derived from impedance measurement.
- Electrodermal response (EDR) measurement, which mainly measures sweat activity in the skin, and is utilised in screening for neurological diseases and psycho-physiological measurements, e.g. emotional response to activity or stimulus. The 'lie detector' is an EDR instrument, which evaluates stress response to the subject's own statements by measuring sweat activity in the skin.
- Coulter counter, a cell counter where cells in suspension are passed through a microchannel, and the impedance between the two sides of this microchannel is measured. An increase in impedance signifies a cell passing through the microchannel. The microchannel's width is typically 50 or 100 μm, to accommodate cells of different sizes.
- Impedance cardiogram (ICG), where a low current is applied to the heart region and the total impedance is measured to discern cardiodynamic parameters such as stroke volume and cardiac output. ICG measures mechanical changes and activity in the chest region. ICG electrodes simultaneously measure the electrocardiography (ECG) signal.
- Electrical impedance tomography (EIT), where impedance measurements are made to create images of body tissue, exploiting the fact that blood and muscle tissue have higher conductivity than fat, bone and lung tissue.
- Biopotential measurements, including electroencephalography (EEG), which measures biopotentials in the brain; ECG, which measures biopotentials in the heart; electrooculography (EOG) and electroretinography (ERG), which both measure biopotentials in the eye; and electromyography (EMG), which measures the biopotentials in muscle fibres. Here, bioelectricity is measured, but often the current source and the electrodes are separated by tissue, which necessarily imposes bioimpedance considerations.

Other uses include heart defibrillators, electrosurgery, pacemakers, electrotherapy, body composition analysis, cell sorting by electrorotation and dielectrophoresis, fingerprint

detection and recognition, muscle exercise by electrostimulation and electroconvulsive therapy, as well as the fatal and counter-therapeutic execution method of electrocution.

Among the latest developed bioimpedance techniques is a device which makes electrical impedance spectroscopy measurements of the skin to detect malignant melanomas (skin cancer) [14]. Currently in development is a sweat measurement device which can warn of hypoglycemia (low blood sugar), aimed at diabetics [15]. For examples of impedance sensing in cell culture, see section 1.1.1.

1.1.2 Measurement Capabilities of Cell Culture Impedance Sensing

Following are some examples that may shed light on what information about cells and cell cultures can currently be derived from impedance measurements, with substrate electrodes and attached cells as the main focus.

Proliferation is a measure of how much the cells multiply and spread, and can be measured by e.g. multiple, small substrate electrodes [16]. When cells spread over a surface, the system impedance is expected to increase, and one or more *dispersion* is expected in impedance profile (see section 2.1.2 for an introduction to dispersions). This thesis is an attempt to measure proliferation with ITO electrodes with or without ALD coating.

When cells rupture, their electrical properties change significantly, with a drop in impedance and phase angle [17] [18].

Micromotions are small fluctuations in the cells' shape and position, detectable over a course of minutes, and indicative of viable cells, contrary to dead ones, which don't move and fluctuate on the substrate [13].

Apoptosis and necrosis are two different processes of cell death. Apoptosis is self-induced, programmed cell death in multicellular organisms, where the individual cell's death is an intended part of the organism's functioning, and as such is usually beneficial to the organism as a whole. Necrosis is unintended cell death caused by external factors like infection, trauma, or toxins, and is usually detrimental to the organism, potentially fatal.

During apoptosis, cells shrink while the cell's interior deteriorates, before the cell membrane integrity is lost and the cell contents are absorbed by the organism. In bioimpedance measurements, this translates to a steady decline in capacitance as apoptosis progresses. Necrotic cells swell until their plasma membrane ruptures and the cell contents are released to the surroundings. This translates to sudden dips in the capacitance for the cells [19].

Differentiation is the process a cell undergoes when it changes from one cell type to another, generally from a more general type to a more specialised one, e.g. from a stem cell to a specialised cell. Induced stem cells, i.e. stem cells produced by modifying or reprogramming differentiated cells [20], is one of the resources necessary for the development of regenerative

medicine. Hildebrandt *et al*. measured differentiation of human mesenchymal stem cells into osteogenic cells[2]. In one study, impedance more than doubled after differentiation [21].

Capacitance correlates with the glutamine consumption rate of the cell, which again correlates to cell activity [22].

Cytotoxicity means poisonous to cells, from *cyto*-, Latinized form of Greek *Kutos* for cell/receptacle, and *toxicum,* Latin for poisonous. Cytotoxicity can be monitored by measuring viability and/or attachment of cells in response to introduction of toxins, compared to a toxin-free culture [23].

Similar measurements have been performed to detect viral infection in fish cells, with cell death and resulting drop in capacitance as the indicator or viral infection [24].

Virus detection is possible, as was demonstrated by Wang *et al*, who used 15 µm wide interdigitated gold electrodes covered with protein A of *Staphylococcus aureus* bacteria, which again had antibodies attached. Viruses were captured by the antibodies, with a resulting change in impedance, after which red blood cells were captured by the viruses for amplification of the measurements [25].

1.2 History of Cell Culture

The discipline of cell culture started in 1907, when cells, in this case explant frog cells, were first shown to grow and proliferate *in vitro* by Ross Harrison [26]. Over the next hundred years, tissue culture would develop as a research and production tool, in some cases reducing or eliminating the need for experiments on live animals.

During the 1900s, tissue culture techniques were developed and refined. Mammalian cells were successfully cultivated, and in 1952 cervical cancer cells from a human were used to establish the first cell line, HeLa, which derived its name from the woman the biopsy was performed on, Henrietta Lacks, who died later the same year from the tumour.

Development of co-culture techniques can allow study of interactions between cells [26] and prolong their proliferation period, which increases the possible expansion of the cell culture.

The 1980s saw a rapid increase in the research activity around artificially grown implants, and in 1997, the first manufactured living human organ that was recommended to the US Food and Drug Administration (FDA) by an advisory board, Apligraf (Graftskin) Human Skin Equivalent, was approved as a therapy for venous leg ulcers.

[2] Mesenchymal cells may differentiate into fibroblasts (muscle cells), chondrocytes (cartilage cells), adipocytes (fat cells), or osteoblasts (bone cells). The differentiation into osteoblasts progresses via the osteogenic cell, which in turn differentiates into the osteoblast.

1.2.1 Tissue Engineering

Spearheading the present forefront of cell culture technique is tissue engineering, the branch of medicine in which biological tissue is grown or coaxed into growing. Regenerative medicine utilises tissue engineering techniques and uses the resulting tissue to repair or substitute damaged or sick tissue in a patient.

Cells are harvested, ideally from the patient, cultured, structured into tissue, and introduced into the patient. Tissue can be grown *ex vivo* and then implanted or grown directly *in vivo.*

Transplants are accompanied by the serious risks of infection and rejection, and indeed, infection will probably always be a risk when a patient is surgically treated, although the risk is reduced by antibiotics. Rejection will always be an issue when the transplanted tissue consists of cells from another person (an allogenic transplant). In this case the recipient must take immunosuppressive drugs to avoid rejection.

The problem of rejection can be circumvented if the transplanted tissue is engineered from the patient's own cells (an autologous transplant). This is one of the advantages of tissue engineering. The discipline is currently pushing towards growing 3-dimensional, structured tissue. Until recently, only 2-dimensional tissue types like skin, bladder walls and membranes have been successfully grown. 2D structures are, as the name implies, uniform sheets of tissue. In 3D structures, different types of cells have to be positioned in the right places with the right immediate environment; particularly blood vessels and nerves, which most tissues need, but also the ECM, the collection of molecules situated between the cells, where they constitute a supporting scaffold holding the cells together, and comprise an essential part of the biochemical environment of the cell. These requirements complicate regenerative medicine therapies.

The first successfully grown 3-dimensional tissue was reported in 2005, when a functioning heart valve was produced [27]. This was the first proof of concept for growing 3D tissue, and implied that various 3D tissue structures could be manufactured. In 2013, transplantation of nerve cells led to re-establishment of sensory and, in one case, motor function in 3 patients treated for complete spinal injury (total loss of motor and sensory function) [28].

Central to the discipline of tissue engineering is the access to stem cells. In adults, stem cells are relatively rare, and diminish with age. When pluripotent stem cells were induced from differentiated cells in 2007 [29], this lead to the researchers receiving the Nobel prize in Physiology or Medicine in 2012 [30]. This type of cells was recently utilised to develop healthy RPE that was transplanted to the retina of a patient with a disorder called age-related macular degeneration [31]. This disorder is associated with a degenerated RPE and is one of the most common causes of blindness in the western world.

2 Methods and Theory

This chapter gives a brief introduction to the history and theory of bioimpedance, impedance sensing, and cell culture, as well as a summary of material properties of ITO, the process of ALD, and the characterisation technique of spectroscopic ellipsometry.

2.1 Bioimpedance

Bioimpedance is the field of science that describes the effects living tissue and electric currents have on each other and can more specifically be described as the study of passive electrical properties of biological tissue. Related to the field of bioimpedance is bioelectricity, which describes electric potentials and currents generated by living tissue, and how tissue can be controlled by electric fields. The two subjects are often intertwined, for example in the workings of ECG, where the polarisation of the cells in the heart, triggered by the body itself, is measured through electrodes typically attached to the arms and a leg. The signal being measured – the polarisation of the heart cells – is a bioelectricity phenomenon, while the measurement and interpretation of the signal, which travels through the chest cavity and part of the arms, involve bioimpedance phenomena.

Techniques of bioimpedance measurements exploit the different impedance responses of different materials and tissue types, and/or the interaction of those materials, when subjected to an external voltage source[3]. Measurements can be performed using a variety of electrode configurations, where the simplest one involves two electrodes carrying some form of electric current and registering measurements, as in the experiments performed in this thesis. More complex configurations with separate sets of current-carrying (CC) electrodes and pick-up (PU) electrodes can offer higher sensitivity and more detailed data, but are more complicated to assemble, run and interpret.

One of the main problems with bioimpedance measurements is prediction. The measured systems are, by definition, comprised of some biological matter, and are therefore complex and varied by any standards of physics, in which simplification is often the key to understanding and prediction. In biological systems, simplification is certainly possible, but reproducing accurately the conditions of one measurement is often difficult. In measurements of a tissue, a researcher will encounter cell membranes, cell interiors with a plethora of organelles with different electrical properties, cell growth medium, and extracellular matrix (ECM). These different elements are complex in themselves: the cell membrane has ion channels that increase conductivity and may open or close; the cell's adherence to the substrate is dependent on focal adhesions; cell growth medium containing animal serum will never be completely reproducible.

[3] The voltage source may be imbedded in, and may be seen as internal to the *organism*, as with an implanted pacemaker, but the voltage is not generated by the tissue itself. In cases where tissue itself generates current or voltage, the term bioelectricity is used.

To describe the frequency-dependent electrical properties of a material, it is useful to use the complex values *impedance* and *admittance*, collectively known as *immittance*.

Impedance **Z** is defined as

$$\mathbf{Z} = R + jX \quad [\Omega] \tag{1}$$

where R and X are resistance reactance, both measured in ohm (Ω). $j = \sqrt{-1}$, the imaginary unit, is in bioimpedance theory often denoted j instead of the more usual i to avoid confusion with the symbol for current, usually denoted i or I. Reactance X for a sinusoidal signal in a uniform dielectric with no edge effects and no induction is $X = -\frac{1}{\omega C}$, where ω is angular frequency of the signal and C is the capacitance of the dielectric.

Admittance **Y** is defined as

$$\mathbf{Y} = G + jB \quad [\Omega] \tag{2}$$

where G and B are conductance and susceptance, both measured in ohm. Susceptance (not to be confused with susceptibility) for a sinusoidal signal in a uniform dielectric with no edge effects and no induction is $B = \omega C$.

See Appendix B for an overview of relevant basic electrics and dielectrics.

2.1.1 Tissue Conductance

Impedance measurements of biological tissue usually involve weak AC. The conductance of body fluids and their cell culture counterpart, cell growth medium, is electrolytic, i.e. the charges in motion are comprised of ions in the medium. Since the charge carriers in the measuring equipment, wires and electrodes are electrons, the electrode-tissue interface presents a barrier to the charge carriers, where they either have to stop or change. If the voltage is one-directional and strong enough, the ions will undergo red-ox reactions at the electrodes, releasing gases [4] which are usually harmful to the tissue or cell culture. For *in vivo* applications, the consequences of gas release into the bloodstream can be serious, as they can become potentially fatal embolisms.

Central to the measurement and understanding of bioimpedance measurements is the concept of *dispersion* (Figure 5). Dispersion in this context means dispersions in the real part of the system's relative permittivity with respect to frequency. The dispersion phenomenon is caused by the relaxation mechanisms and relaxation times for different types of charge carriers. A relaxation mechanism can be thought of as the way a charge carrier falls back to equilibrium after an electric field is turned off. The relaxation time is defined as 63 % of the time it takes for the charge carrier to relax back to a state undisturbed by the electric field [4]. An example is a molecular dipole like H_2O which is rotated by an electric field to align with it, but when the electric field disappears, the dipole, affected by other forces, settles back to a position similar to its original state, before the electric field disturbed it. Figure 5 shows a rough overview of different relaxation mechanisms and their associated dispersion frequency bands.

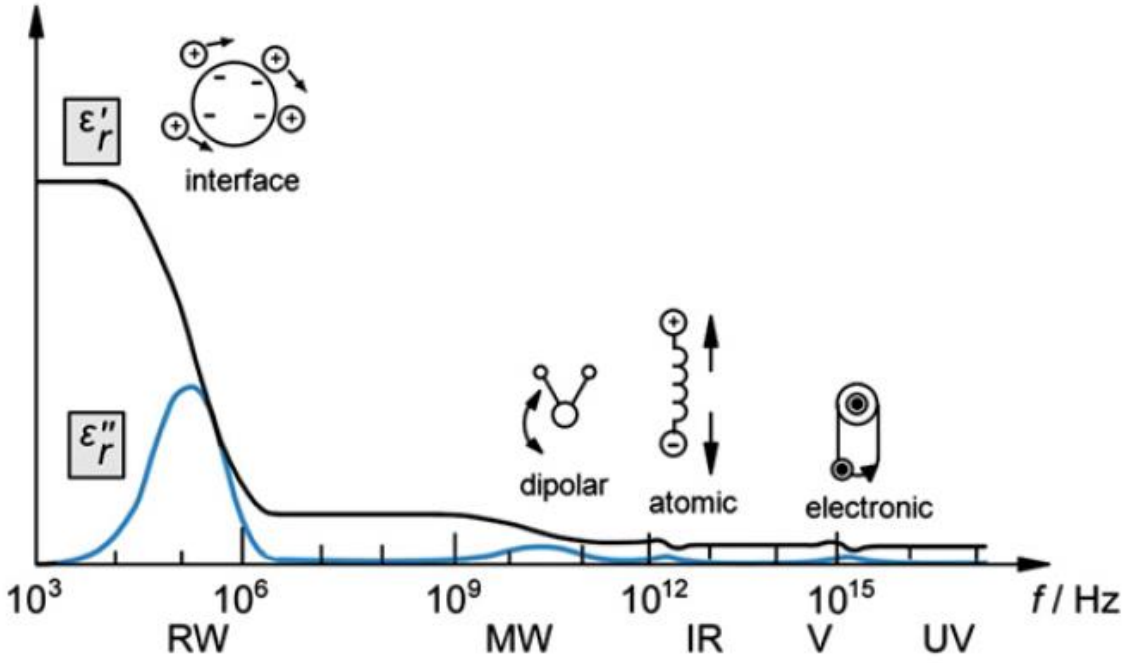

Figure 5 - Dispersions shown with entities responding to different frequencies. From low to high frequencies: A whole, living cell; a dipolar atom; atomic level vibration, and electronic response. From [32].

Different types of charges and dipoles have different relaxation times, and the dispersion signature of a material can tell us something about its composition. In general, bigger dipoles/charge carriers have longer relaxation times than smaller ones. E.g. a large bipolar molecule takes longer to re-set to a rest position than an atom.

In muscle tissue, permittivity decreases in dispersions as shown in Figure 6. The different dispersion correspond to different relaxation mechanisms [4]:

- α-dispersion, in the mHz to kHz range, stems from ionic diffusion, intracellular structures, and counterion effects at the membrane surfaces.
- β-dispersion, in the kHz to 100 MHz range, stems from membrane capacitance, protein molecules, Maxwell-Wagner effects (processes at interfaces between dielectrics).
- γ-dispersion, in the GHz range, stems from dipolar molecular or ionic mechanisms, e.g. water molecules, salts, and proteins. This is the only dispersion present in saline.

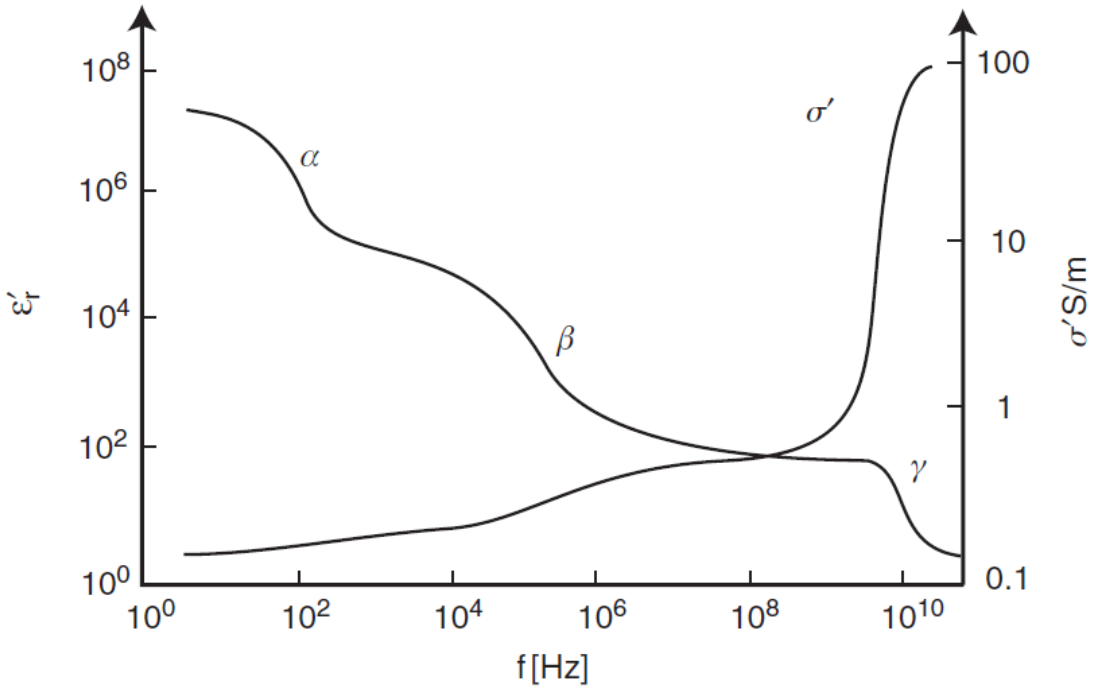

Figure 6 – α-, β-, and γ-dispersions manifest as relative permittivity decreases and conductivity increases as a function of frequency. From [4].

Dispersions are dependent on material, and other possible dispersions may be due to e.g. atomic relaxation, which happen at frequencies in the infra-red spectrum, i.e. the higher GHz frequencies, or electronic relaxation, which take place in the frequency range of visible light, i.e. the higher THz range [33]. Clearly separated dispersions are not the norm for tissue, but may be found in cell suspensions [4].

The dispersion of a dielectric system manifest in a complex plane plot (also called a Wessel[4] diagram) as a semi-circle, as seen in the plot for water in Figure 7. However, biological systems are rarely purely dielectric or purely conductive, and a plot of tissue may show broad dispersions which may overlap [4]; some of them may be difficult to discern. The plots then become more difficult to interpret. As in many other situations, simplifying a model of a bioimpedance system too much will make the model too inaccurate or inadequate.

The semi-circular plot of complex permittivity in the complex plane indicates a significant change in both the real and imaginary parts of a system's permittivity over a dispersion. Usually, dispersions denote a decrease in permittivity as frequency increases (see Figure 5), and this change in the real part of the permittivity is in this case accompanied by a temporary

[4] Caspar Wessel, a Norwegian-Danish cartographer and mathematician, described complex numbers as points in a plane in his work "On the Analytical Representation of Direction" from 1797, which also introduced an early version of the vector concept. He was the younger brother of the well-known poet Johan Herman Wessel.

change in the imaginary part of the permittivity, which is the part that is frequency dependent.

The characteristic frequency f_c is the frequency corresponding to the apex of the complex plane impedance plot.

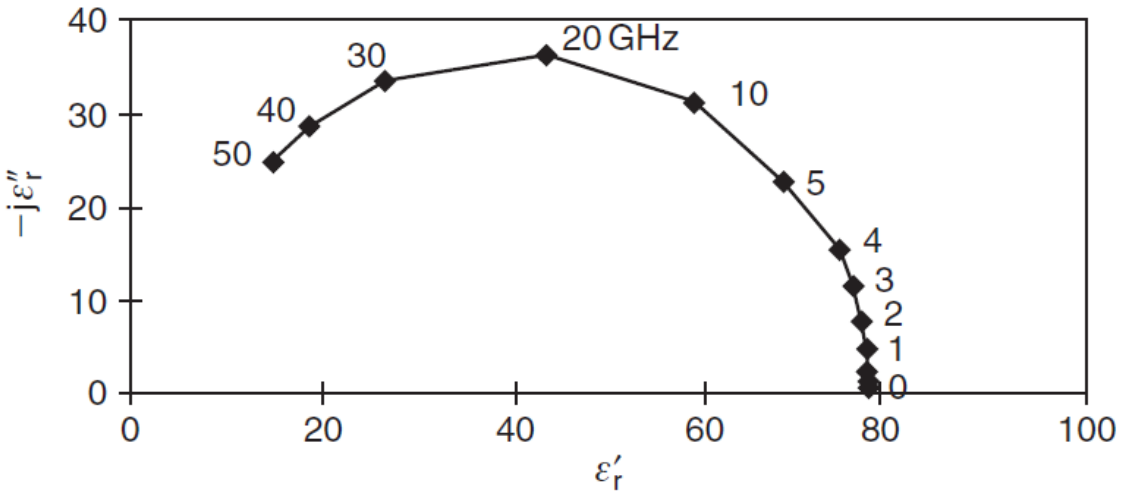

Figure 7 - Cole-Cole plot for water. The characteristic frequency f_c is close to 20 GHz. From [4].

The different parts of a cell culture are dominated by different electrical properties. Cell membranes act like capacitors [33]; as long as the cell remains intact and alive, the entire cell may be treated as a capacitor as well, since the cell membrane isolates the cell interior from the surroundings[22]. The assumption of persistence of the whole cell capacitance has to be treated with some caution, though, as ion channels in the membrane may open and change the capacitance, e.g. if they are subjected to a high enough electric potential [4]. Cell growth medium acts like a conductive electrolyte due to the electrolyte constituents.

To complicate matters, cells that attach to each other reduce the overall capacitance, and some cells that adhere to each other open gap junctions between them – nanometre-size channels in the membranes that connect the electrolytic interiors of the cells to each other and thereby increase conductivity but reduce capacitance [34]; cells that adhere to the substrate create focal contacts as described in section 2.3.3 [35], resulting in a contact impedance with the electrodes which vary over the contact area of the cell, with higher conductance at the focal contacts than where the attachment layer is thicker.

2.1.2 Medium Conductivity

The cell growth medium is a water-based solution of with various different ions, nutrients, hydrocarbons, growth factors, and whatever else the specific cell culture needs. Electrically, the medium behaves like an electrolytic conductor with conductivity and permittivity

comparable to that of saline, i.e. $\sigma \approx 1$ S/m and $\varepsilon_r \approx 80$. Both conductivity and permittivity are independent of frequency at frequencies below 10 MHz [4].

At interfaces between media, particularly when a solid and a liquid is involved, a double layer will usually form. Surface charges in the solid attract ions in the liquid, and a liquid layer of ions build at the surface of the solid. The two layers of charges, one in the solid and one in the liquid, are called the double layer. This double layer also forms on cell membranes and contributes to the system capacitance and one of the dispersions of living tissue (see section on "Dispersions").

2.1.3 Extracellular Matrix conductivity

For a cell-substrate distance of 75 ± 7 nm, in a bath with a resistivity of 66 Ω cm, a resistance of 7.7 MΩ was measured for the sheet of extracellular attachment proteins. When the resistivity of the bath was increased, the resistance of the sheet increased proportionally, indicating a close relationship between the resistivities of the sheet and the bulk electrolyte. The resistivity of the ECM was reported as being controlled by and indistinguishable from that of the bulk electrolyte [36].

2.1.4 Electric Properties of the Cell

The cell is a complex structure which includes a cell membrane enclosing a nucleus, golgi apparatus, endoplasmic reticulum, mitochondria with their own membranes, as well as other organelles [37]. All of those elements in the cell have different electric properties, several of which are unknown.

The membrane is a bilipid layer that insulates the interior of the cell chemically and electrically, something which makes a simplifying approximation possible. The cell can be viewed as an electrolytic interior with an insulating and capacitive membrane. As long as the interior structures and organelles of the cell are not in contact with the exterior, they only contribute to the capacitance of the cell. If the membrane is compromised and the contents come into contact with the exterior, the capacitance of the system will drop and the conductance increase.

The cell membrane has a capacitance of approximately 1 μF/cm^2 [4].

There are a number of channels in the membrane that facilitate ion exchange between the interior and exterior of the cell. When these are opened, it may change the impedance and admittance of the system. In addition, a strong current can lead to *electroporation* of cells, i.e. forced opening of ion channels in the cell membrane [4]. This changes the conductivity of the cells and is usually harmful to them. Therefore, currents used to measure cells must be weak to insure the integrity of the cells and the consistency of measurements. Typically, currents in the nA to low mA range are used, with voltages in the mV range and frequencies in the Hz to MHz range.

2.1.5 Double Layer Effects

When a voltage is applied by electrodes over an electrolyte, ions in the electrolyte will concentrate at the electrode surfaces. This allows charge to build up in the surface layers of the electrode. These two layers of charge are called the double layer, and can add a significant capacitance to the system [4].

2.2 Impedance Sensing

Impedance sensing involves characterisation of a material by measuring its electric properties, specifically impedance or admittance. Dielectric spectroscopy (DS) involves measuring impedance and/or admittance over a range of current frequencies. DS allows continuous, quick, harmless in-line measurements of the cell culture impedance at different frequencies. In the terminology of DS, the sample is the dielectric. The DS measurement can be performed by an electrode probe in a suspension or by electrodes on the cell culture substrate, in which case the cells attach directly onto the electrodes.

2.2.1 Impedance Measurements

Impedance measurements are made with a configuration of equipment including electrodes of some sort, connected to an analyser. In suspension, the electrodes usually take the form of a probe with electrodes, while in attached cultures the electrodes are usually part of the cell attachment substrate.

Tissue and cell culture suspensions are *volume conductors,* i.e. the current travels through the bulk of the material, with different current densities at different points in the material, depending on the conductivity of the material and the nature and source of current. Conductivity is often not uniform in biological tissue; high conductivity results in higher current density, as does proximity to electrodes.

2.2.1.1 Electrode Properties

The properties of the electrodes influence how and what is measured, and the desired data derived from the impedance measurement heavily influences electrode design:

Smaller electrodes may monitor cell proliferation and / or attachment very accurately, particularly if they are placed in a 2-dimensional array on the substrate. As cells proliferate and gradually cover the electrodes, the time difference in the onset of impedance changes for the electrodes allows the proliferation speed to be calculated [16]. The measured impedance is dependent on how large a portion of the electrode is covered by cell(s), so a single cell will have a greater relative effect on a smaller electrode than on a bigger one.

Electrodes with larger surface area will pick up more cells than smaller ones, allowing for measurement of total and average properties for a larger number of cells.

For single cell measurements, the electrode should necessarily be small, comparable in size to the cell. To ensure single cells are measured, a channel or trap to capture the cells may be needed; the trap should be wide enough for the cells to enter, but small enough that only a very few cells do [19].

Interdigitated electrodes (Figure 8) may be suitable for several types of measurements, as they have a relatively high surface area, and pick up a large number of cells, while having a relatively high resolution due to the narrow fingers, or digits, of the electrodes. The measurement sensitivity and depth is dependent on interdigit distance [4], with shorter range and higher sensitivity for smaller interdigit distances. Capacitance of the electrodes may become a problem if the digits are close together, and should be considered when calculating values for the system.

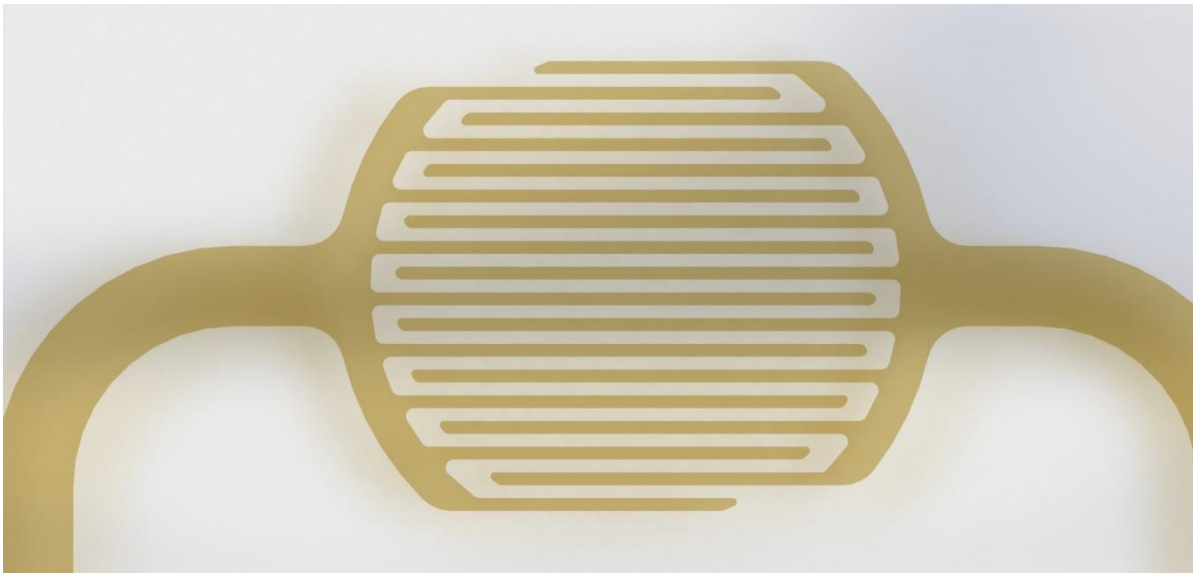

Figure 8 - Interdigitated electrodes.

For a suspension probe, the distance between the electrodes governs the sensitivity and the number of cells measured simultaneously. A small aperture with electrodes on each side may measure single cells, as in a coulter counter. However, if large numbers of cells need to be measured, larger electrodes with greater distance between may be needed.

2.2.1.2 Electrode Material

When choosing electrode material for a cell culture, it is important to consider the cytotoxicity of the electrode in a solution, together with the projected timespan of the measurement. If the cells are to be measured over any considerable time and/or it is desirable that the cells stay viable, healthy, and unaffected by the measurement process, electrodes should interfere minimally with the cells. For an attached cell culture with substrate electrodes, electrodes used must be biocompatible, as the cells necessarily will share the cell growth medium with the electrodes over some time. Gold is a common choice, as it fulfils both biocompatibility and attachment criteria. ITO has shown very promising in this regard,

with very good attachment values [38], and was chosen for this thesis for its combination of conductivity and transparency. Platinum has also been used [39].

The electrode material can significantly affect the voltage profile of the system. At the electrode/electrolyte interface, metal ions may be released from the electrodes, building a charge difference between the electrode and the electrolyte. How many ions are released depends on the metal; e.g. noble metals release ions at a slow rate, as one might expect. If the electrodes are made from different materials, the build-up of charge creates an electric field and an electric potential difference between the electrodes, resulting in current. This voltage may exceed 1 V, depending on the electrode materials. The e*quilibrium potential* (EP) is the voltage needed in the external circuit to ensure zero current. The EP of an ITO electrode in a 1 M NaOH electrolyte has been reported to be + 0.15 V to + 0.20 V versus a Ag/AgCl reference electrode [40]. An AgCl electrode has an EP of + 0.22 V [4], indicating that the EP of ITO is + 0.37 V to 0.42 V.

If the electrodes are of the same material, the voltage will negate each other and the EP is 0. In cell culture measurements, electrodes are usually chosen from the same material and the EP is not a problem. The bio-inertness and slow ion release of noble metals make them doubly suitable for electrodes in cell culture [4].

2.2.1.3 Electrode Shape and Distance

The shape of and distance between the electrodes also matter to the measurements. The sensitivity of the electrodes is dependent on the current density in the material it measures (Figure 9). If the electrodes are close together, the current density will be higher immediately between them than otherwise. Proximity of the electrodes also means that their sensitivity will be focused closer to the electrodes, since the sensitivity is dependent on the current density. If measuring depth is important, the distance between the electrodes will need to be considered.

If the electrode has a sharp edge or point, this may also cause high current densities, depending on the direction of the current and the conductivity of the tissue (Figure 10) [4]. High current density may harm tissue.

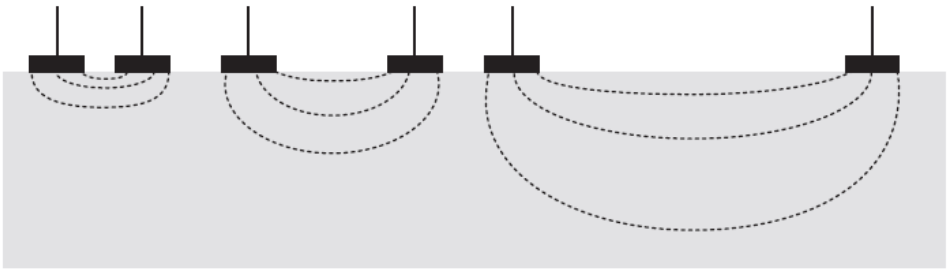

Figure 9 - Current density and sensitivity depends on proximity of electrodes. From [4].

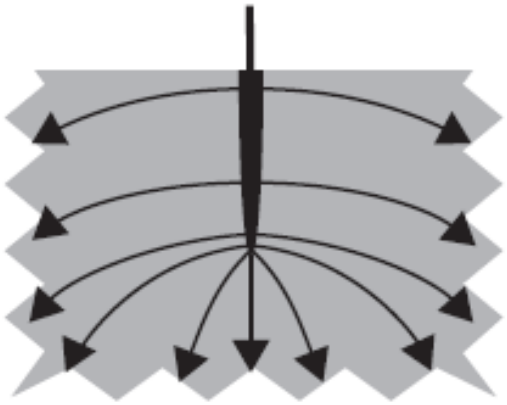

Figure 10 - Conduction profile of a needle electrode. From [4].

2.2.1.4 Capacitance of Interdigitated Electrodes

The capacitance of interdigitated electrodes is potentially an issue. As the electrodes consist of several parallel digits with an electrolyte in between, the capacitance of the electrode might "drown out" measurements of the cells. To alleviate this, one can view trends in the measurements instead of absolute values. A measurement of the cell growth medium without cells will give an idea of the system's resistive and capacitive values without the cells.

The capacitance C of interdigitated electrodes with digit length p, width w, interdigit spacing s, and overall electrode width q was shown by den Otter to be approximately

$$C = pq\frac{4}{\pi a}\varepsilon\sum_{n=1}^{\infty}\frac{1}{2n-1}J_0^2\left(\frac{(2n-1)\pi s}{2a}\right) \tag{3}$$

where a is the periodicity of the electrode digits so that $2a = 2(w + s)$, and J_0 is the zeroth Bessel function of the first kind [41]. See Appendix C for a brief description of Bessel functions.

The assumptions made to enable use of this approximation is that the width and spacing of the digits are small compared to the overall dimensions of the system, and that "the number of parallel strips is large" [41]. The specific requirements for "large" in this context are not investigated in den Otter's article.

2.2.1.5 Electrode Polarisation

Electrode polarisation may affect the measurements significantly. It is, in effect, an impedance generated by the electrode/electrolyte interface. Depending on electrode material and electrolyte content, electrode polarisation may be dependent on frequency and electrolyte concentration, and it is inversely proportional with the surface area of the electrode [42].

2.2.1.6 Signal Processing

The measurement of tissue and cell culture is usually made with sine wave AC with voltage in the mV range or lower, and frequencies in the higher kHz range or higher. This is to ensure that tissue and cells do not undergo electroporation, which affects the measurement and may be harmful to the cells, or lysing, by which is meant that the cell membrane integrity is lost completely, the cell dies and its contents are released to the surroundings.

If the system is subjected to an AC with constant amplitude *V*, the current magnitude *I* and phase ϕ is measured and compared to those of the voltage. The phase angle is a measure of the time difference between the peaks of the two sine waves, compared to the period of the sine wave, and from the phase angle and conductance, the capacitance of the system can be calculated (Figure 11).

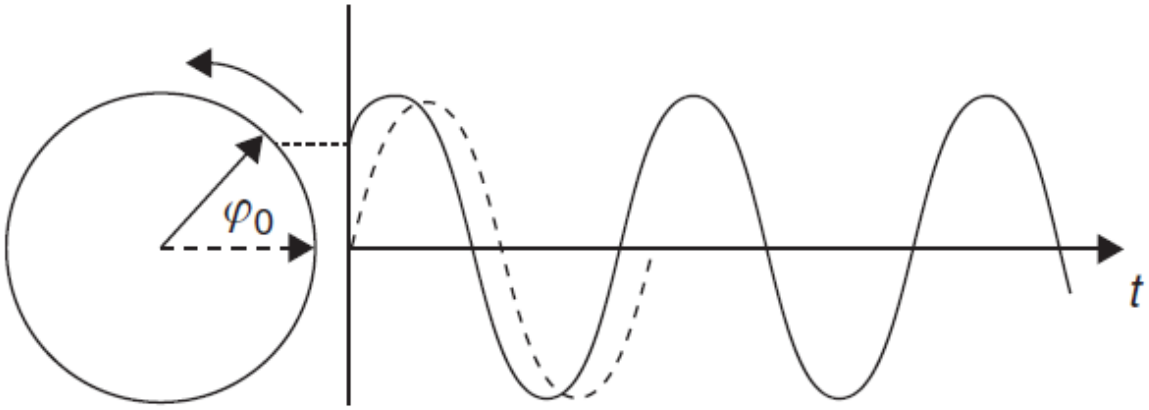

Figure 11 - Sine wave (solid) with reference wave (stippled) and phase angle ϕ_0. From [4].

2.2.1.7 Equivalent Circuits

When making impedance measurements, the calculations of values and interpretation of derived values depend on the model chosen to represent the system in question. The representation is often an electrical circuit equivalent of the system, with resistors and capacitors in series or parallel. These circuits need to take into account that tissue electrical properties are frequency dependent, in general with increasing admittance as frequency rises. One of the central models for this purpose is the Cole system (Figure 12). It utilises a *constant phase element* (CPE), where the components are frequency dependent, but where the immittance phase is frequency independent. The CPE of the Cole system is Fricke compatible, that is, the phase angle ϕ and the frequency exponent α (see equations 4 and 5 below) are dependent on each other but frequency independent [4].

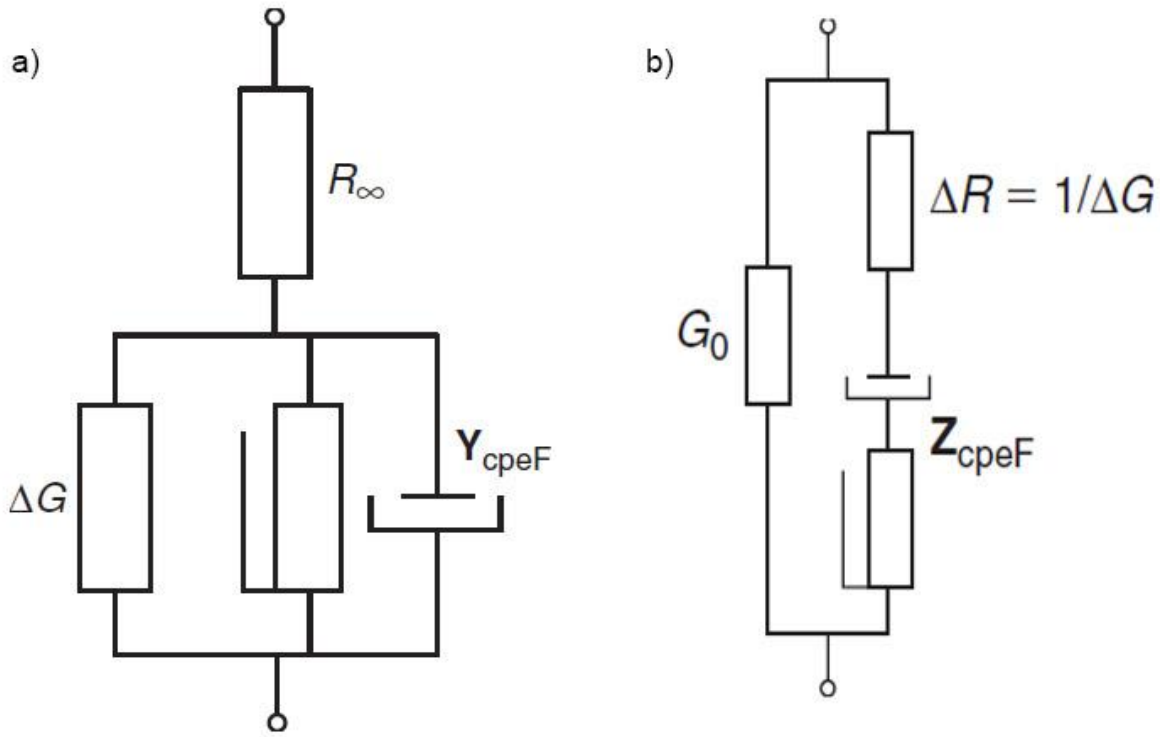

Figure 12 - Cole systems: a)Impedance version and b) admittance version. Subscripts indicate frequency. $\Delta G = G_\infty - G_0$,$\Delta R = R_0 - R_\infty$. cpeF indicates a Fricke-compatible CPE. Based on [4].

For a single dispersion, the impedance **Z** of the Cole impedance system (Figure 12 a, in series) is described by the equation:

$$\mathbf{Z} = R_\infty + \frac{\Delta R}{1 + (j\omega\tau_Z)^\alpha} \quad [\Omega] \tag{4}$$

where R_∞ is the resistance at infinite frequency, $\Delta R = R_0 - R_\infty$, R_0 is resistance at zero frequency (=DC), j is the imaginary unit, ω is the angular frequency of the current, τ_Z is the time constant, and α is dependent on the material modelled. The time constant τ_Z is defined by $\tau_Z\omega_c = 1$, where ω_c is the characteristic angle frequency of the system, where $\omega_c = 2\pi \cdot f_c$, where f_c is the characteristic frequency. The characteristic frequency f_c is the frequency corresponding to the apex of the complex plane plot of the impedance, i.e. the extreme value of its imaginary part in the dispersion frequency range.

Conversely, for a single dispersion, the admittance **Y** of a Cole admittance system (Figure 12 b, in parallel) is described by the equation:

$$\mathbf{Y} = G_0 + \frac{\Delta G}{1 + (j\omega\tau_Y)^{-\alpha}} \quad [S] \tag{5}$$

where G_0 is the conductance at zero frequency (=DC), $\Delta G = G_\infty - G_0$, G_∞ is conductance at infinite frequency, j is the imaginary unit, ω is the angular frequency of the current, τ_Y is the time constant, and α is dependent on the material modelled. The time constant τ_Y is, similarly to τ_Z, defined by $\tau_Y \cdot \omega_c = 1$.

Several Cole elements may be combined to model complex systems (Figure 13).

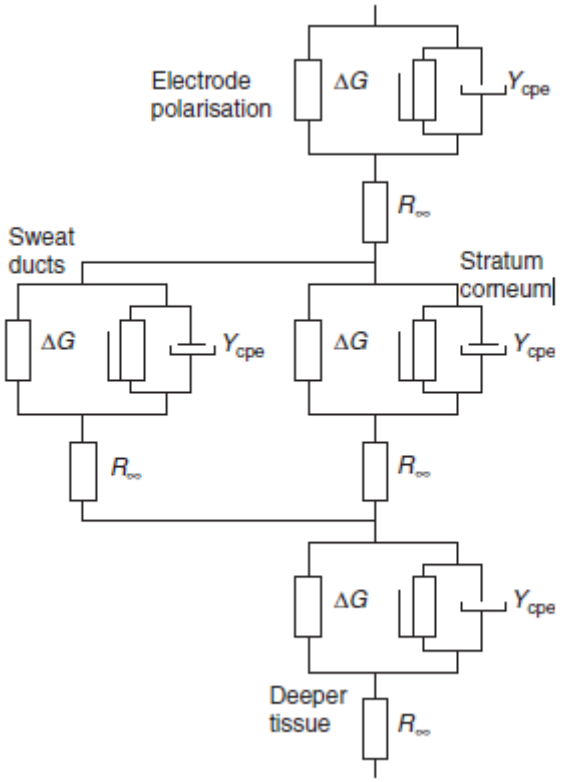

Figure 13 - Combination of Cole elements to model skin impedance measurement. From [4].

When measuring the system, the electrodes may contribute to the capacitance and resistance, and may require to be represented by their own Cole system in order to model the system accurately. As measurements are made, an initial measurement of the electrodes, and of the electrodes with growth medium will give some insight into how they affect the system, and allow the compensate for those effects, to allow more accurate calculation of the desired values, which are usually capacitance and resistance.

The cell membrane is capacitive, while the culture medium and ECM are electrolytically conductive. The system may be represented by a parallel cole element, where the capacitor represents the cell membrane(s), in series with the ECM, represented by a resistor. In parallel with these, the cell medium is represented by a resisitor.

2.2.1.8 Finite Element Method

It may be desirable to run a simulation of the system, to give an indication of what values might be expected and how the system is going to behave. As simulation of complex or fine-

detailed systems place strong demands on computing power, simplification may be important to enable the hardware to calculate values in reasonable time.

In the finite element method (FEM), the volume of the system is divided into 3-dimensional elements, with each element having its own parameters, and with values being calculated separately. The smaller the elements, the more accurate the simulation, and the more time-consuming it is. Each element is called a voxel (from ***vo***lume pi***xel***). The simulation may suffer from not being able to model smooth curves very well, if voxels are shaped as cubes. Simulation software like COMSOL divides the volume into non-cubic volume elements whose faces coincide with or approximate interfaces and borders between the different elements of the volume (Figure 14).

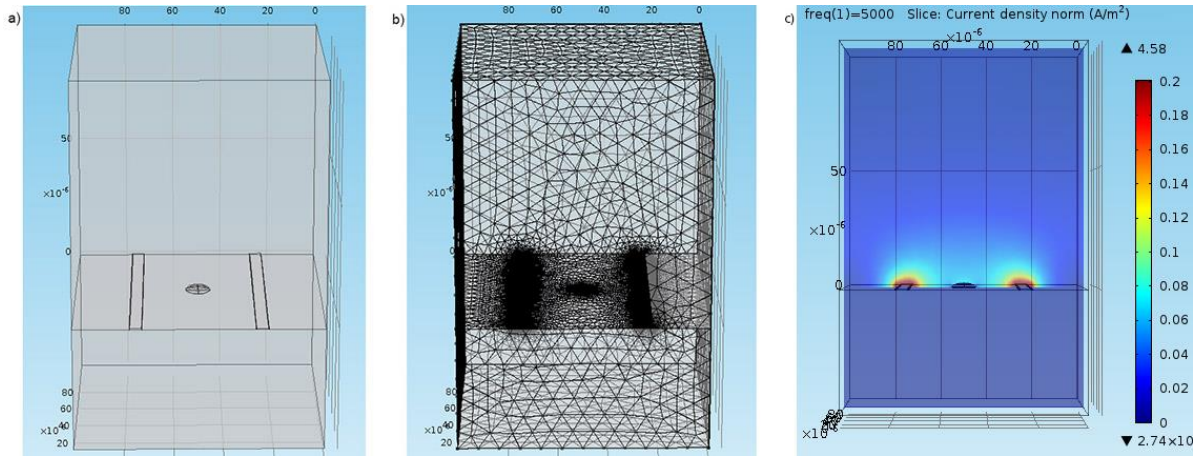

Figure 14 - Simple model of a cell (small disk in the middle) on a substrate, flanked by electrodes. a) Wireframe. b) Mesh for FEM simulation; finer geometry requires smaller elements to simulate system accurately. c) Current density plot.

The simulation in Figure 14 is a 3-dimensional simulation. If the geometry of the system is invariant in one of the directions, the simulation can be simplified to a 2-dimensional one reduces the required computing power.

2.3 Cell Culture

Cell culture is, in essence, the discipline of growing living cells in controlled conditions. It is an important and essential tool in biological and medical research and development [26], e.g. development and production of vaccines [43], toxicology [44] and the emerging techniques of tissue engineering [45].

2.3.1 *In Vitro - In Vivo - Ex Vivo*

The latin term *'in vitro',* which translates to 'in glass', signifies that the cells are taken out of their normal environment – an animal body, usually – and placed in artificial laboratory growth conditions; the converse term for growth or procedures performed inside a living

organism is '*in vivo'*, which translates to 'in the living'. '*Ex vivo*' means "out of the living," i.e. outside the given organism.

In vitro methods vary within certain parameters, but common to all cell cultures is the need for a growth medium with required nutrients, oxygen, and a physiological pH and temperature. Originally most experiments were performed in glass vessels - hence the name – and glass as a growth substrate is still used, but plastics have replaced much of their usage, often in the forms of plastic petri dishes and multi-well cell culture plates. 3-dimensional setups may sometimes be used, in the forms of e.g. collagen sponges or gels, depending on production needs and the type of cells [46].

2.3.2 The Cell Culture Laboratory

The cell culture laboratory contains equipment constructed to keep cell cultures alive, to observe the cells, to inhibit infection of the cell cultures from the outside world, and to inhibit infection of the outside world by the cell cultures.

2.3.2.1 Sterilisation

In any cell culture laboratory, sterilization is crucial. The definition of sterilization is "a process which removes all living things" [47].

The cells must not be exposed to unwanted substances or pathogens, and the laboratory personnel must be protected from any potentially harmful agents. Virus and bacteria thrive in cell cultures, which provide an ideal environment for them to proliferate in; the cell culture seeks to mimic the conditions inside a living organism, which is the very environment virus and bacteria have evolved to exploit. This requires any cell culture vessel to have the ability to withstand appropriate sterilization. Methods include dry heating, e.g. an oven; wet heating, e.g. an autoclave; irradiation, i.e. ultraviolet (UV) light or gamma rays; and chemical sterilization, e.g. ethanol [47].

The work area must be sterilised before and after use; this is usually accomplished by wiping it with ethanol. The operator should wear latex gloves or equivalent, and disinfect their gloves with ethanol or other suitable disinfectants before introducing them in the flow hood.

In any laboratory environment, achieving complete sterilisation is very hard. But achieving sufficient sterilisation is achieved by using proper sterilisation technique.

2.3.2.2 Vertical Laminar Flow Hood

The main workstation in the cell culture lab is the vertical laminar flow hood. For work with human cells, which carries a higher risk of operator infection with compatible pathogens, a class II microbiological safety cabinet should be used. The class II cabinet is essentially a box with an opening for the operator's hands and arms, and which injects a flow of filtered air from its ceiling. The air flow is sucked into ventilation grilles in the workbench surface, fed through a filter and partly circulated back into the hood, partly ejected as exhaust. Since part

of the air flow is ejected from the circulation, there is necessarily an air intake, which is the opening in the front window. Since this hole functions as an air intake, potentially harmful specimens are hindered from leaving the flow hood (Figure 15) [26].

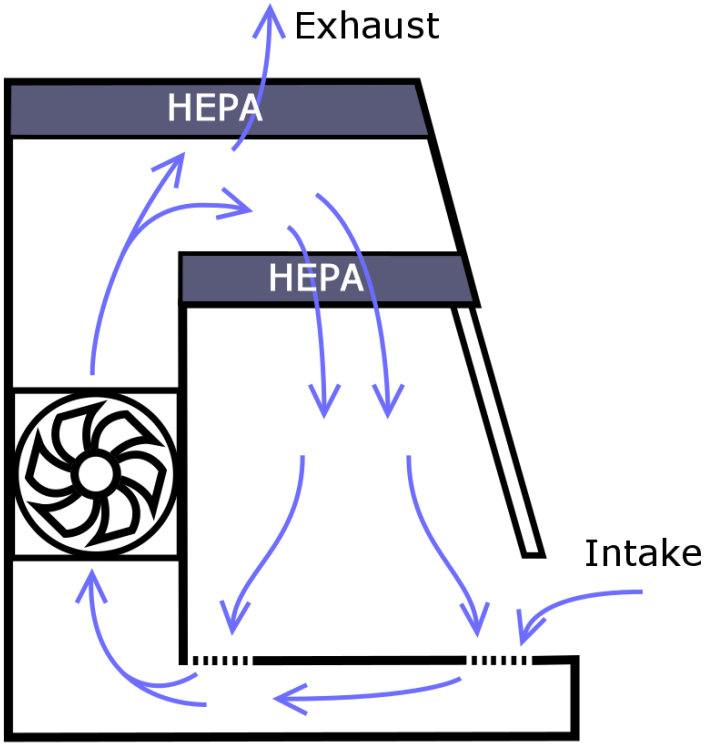

Figure 15 – Side view of a class II microbiological safety cabinet, a high safety version of the vertical laminar flow hood. Air is sucked in through the opening in/under the frontal glass window and through air vents in front of and behind the work surface, then pushed through a HEPA filter before either being expelled as exhaust or reinserted into the flow hood through its ceiling.

2.3.2.3 Incubator

The environment needed for cell culture is maintained by an incubator: essentially an insulated box with air filter, regulated heating, CO_2 supply, and humidity control. Standard CO_2 levels are 5 % and 10 %, and culture media are produced with either of these in mind. The standard temperature for a mammalian cell culture is 37 °C. The humidity is maintained e.g. by a wide water pan inside the incubator.

2.3.2.4 Phase Contrast Microscope

To observe the cells visually, an optical microscope is usually used. Cells can be almost completely transparent, and a technique is needed to enhance observation. Staining the cells with dye make them easier to observe visually; a less invasive method is the use of a phase contrast microscope, which makes staining unnecessary. The technique is based on diffraction of visible light when passing through cells. The light is first shaped into a hollow cone by an annular aperture and condenser. When collected again after passing through the specimen, an opaque ring matching the annular aperture attenuates undiffracted light, which greatly increases contrast between diffracted light and undiffracted light (Figure 16). This allows imaging of transparent cells which would otherwise be difficult to discern in an optical

microscope [48, 49]. Frits Zernike was awarded the Nobel prize in physics in 1953 for the development of the phase contrast method [50].

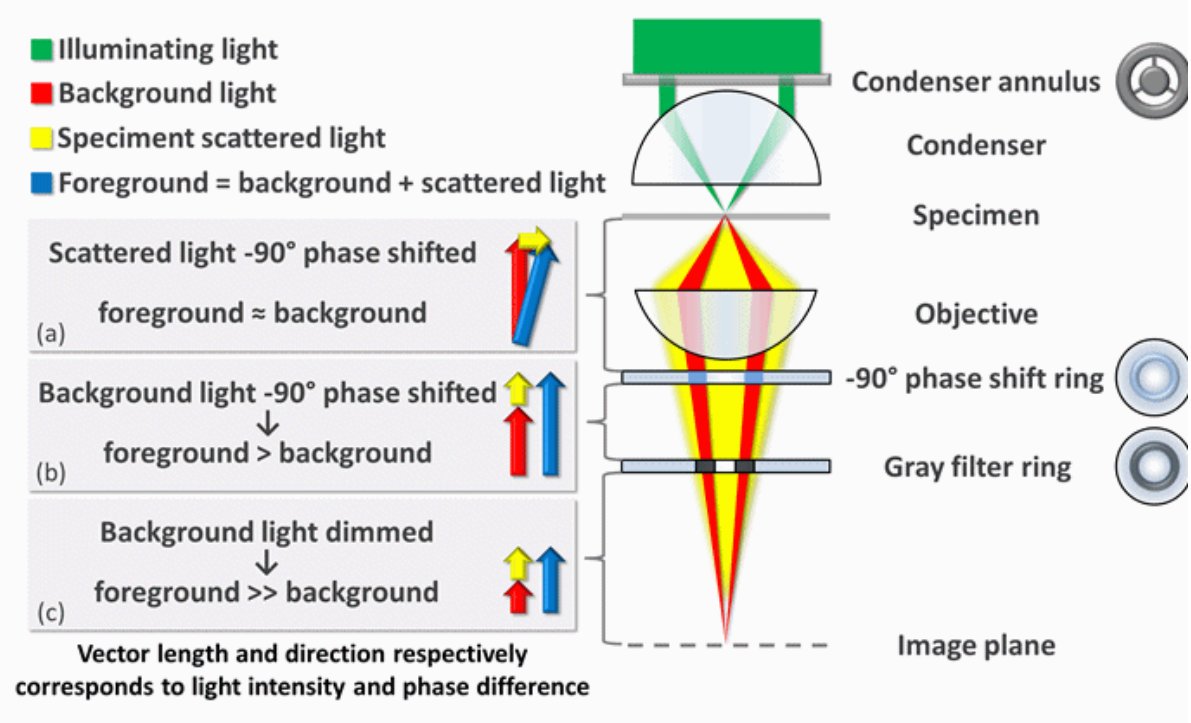

Figure 16 - Working principle of phase contrast microscope. From [51].

2.3.2.5 Centrifuge

A centrifuge is used to separate cells in suspension from the medium. The cell suspension is placed in vials and centrifuged at e.g. 10 000 revolutions / minute. The difference in density between the cells and the medium causes the cells to sink to the bottom of the centrifuge vials. After centrifuging, the cells may stick together and may need re-pipetting to obtain single cells.

2.3.3 Cell Attachment

Many types of cells need to attach to a surface or other cells to survive and thrive. These *attachment-dependent* cells, also called *anchorage-dependent* or *substrate-dependent*, include many cell types that are normally part of a tissue, e.g. muscle, nerve, bone, or skin tissue. Non-attachment-dependent cells include free-floating cells, e.g. blood cells. Monolayer attachment-dependent cells will usually spread in one layer to the limits of the substrate and then stop spreading. Multilayer attachment-dependent cells will both spread along the substrate and build on top of each other.

Cells in suspension can be treated as spheres, as an approximation to simplify analysis and calculations. Their actual shapes vary with cell type. If doing a simulation and the cells have dendrites or other protrusions, it may be necessary to include those in the simulation model.

When cells attach to a surface, e.g. the culture vessel substrate, their shape changes from a spheroid shape to a disk-like shape, increasing the contact area with the substrate and hence the impedance of the system (Figure 17) [52].

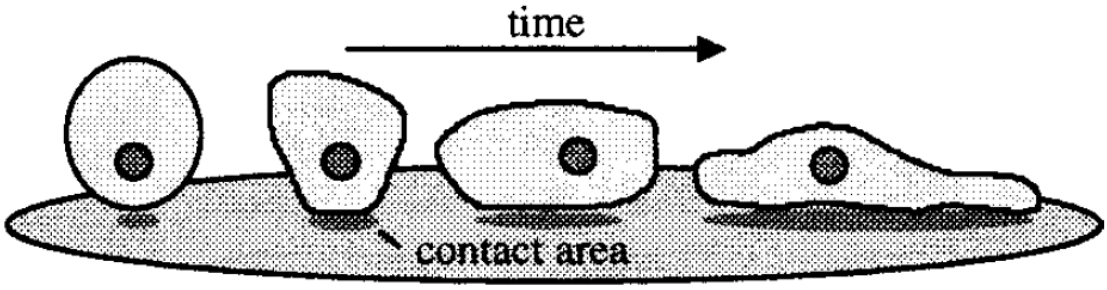

Figure 17 - Cells changing shape over time as they attach to the substrate, increasing area of contact with the substrate (shaded). From [52].

2.3.4 Immortalised Versus Normal Cells

Cells in culture may spontaneously or by applying certain culture techniques become immortal, i.e. a continuous cell line. Most normal cells can only divide a limited number of times before they reach senescence and stop dividing. Immortal cells do not share this limitation. In some ways, immortalized cells share some attributes with cancer cells, who also display unlimited cell division[5] [46].

2.3.5 Retinal Pigment Epithelium

This thesis is focused on human retinal pigment epithelium (RPE) cells (Figure 18), which are attachment-dependent monolayer cells, forming the innermost layer or the retina. The RPE is located between the photoreceptors of the retina and the Bruch's membrane. The latter is adjacent to the choroid, which is a highly vascularised layer that attaches to the sclera, the outermost and dense connective tissue layer of the eye - the "white of the eye". The RPE serves as the base for the photoreceptor cells, thereby providing nutrients and absorbing light, among other functions [53] (Figure 19).

[5] One of the functions of programmed cell death, or apoptosis, is to act as one of the body's defense mechanisms against cancer. When combined with uncontrolled cell division, absence of programmed cell death may result in a cancer.

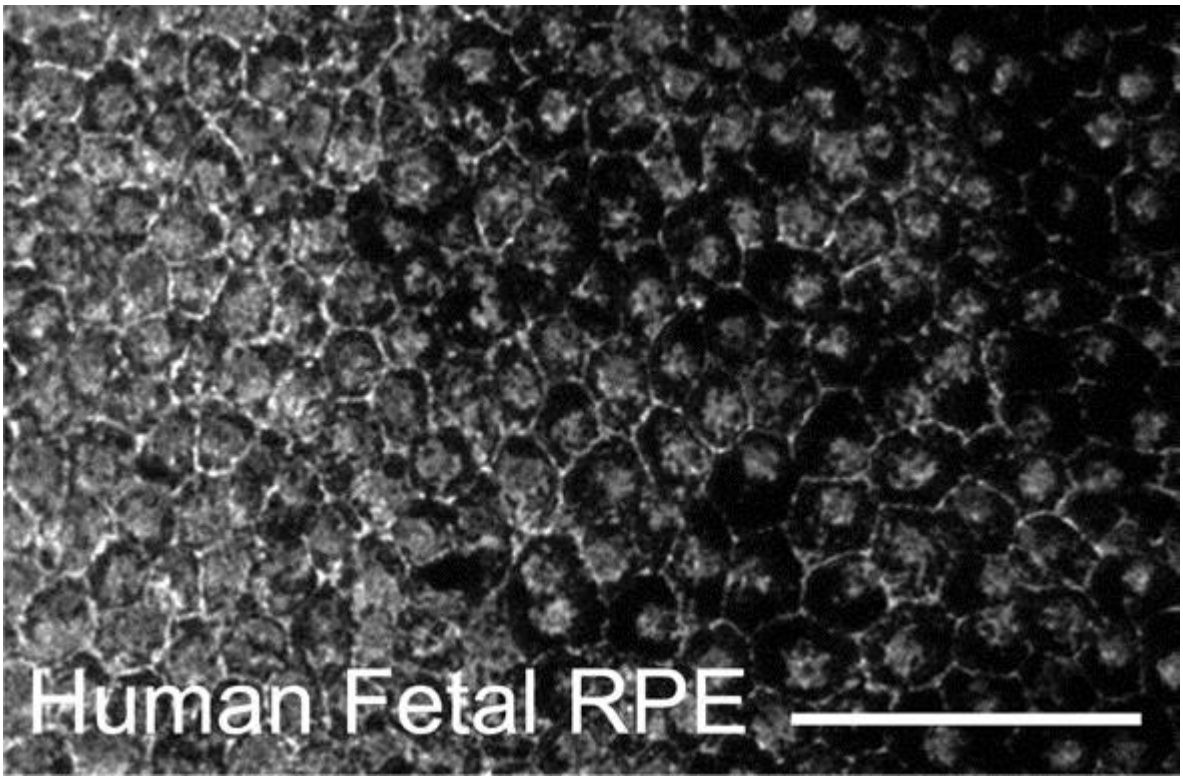

Figure 18 - Confluent layer of human fetal RPE cells. The scale bar is 50 µm. From [54].

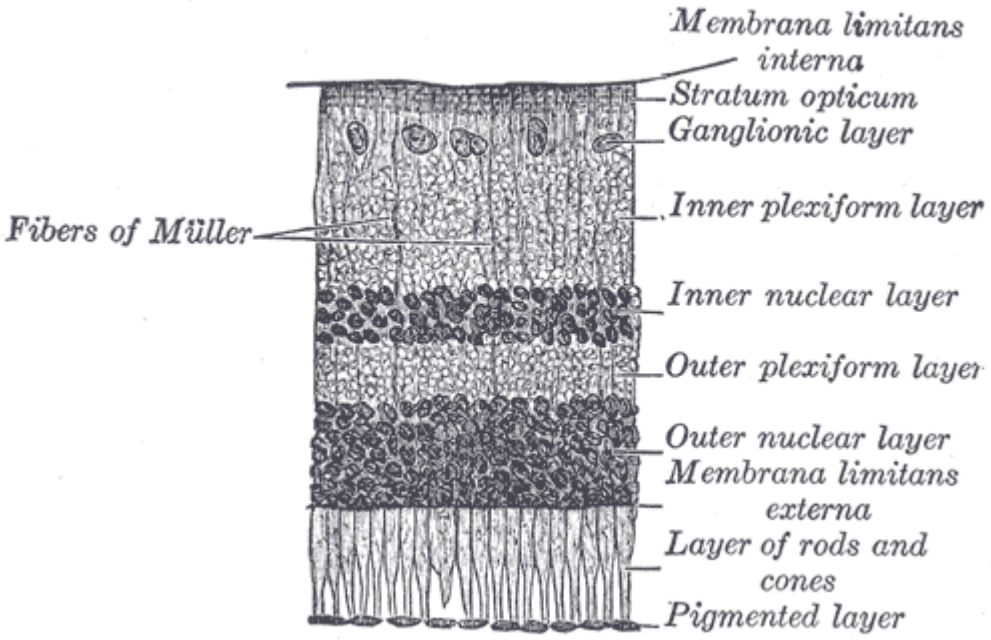

Figure 19 - Cross-section of a human retina. The RPE cells are indicated at the bottom, as "Pigmented Layer". From [55].

The appropriate culture conditions for RPE cells include a temperature of 37 °C, cell growth medium with the necessary attributes as outlined in section 2.3.7, and a biocompatible,

preferably polar substrate. Many other types of substrate are acceptable; for example, cells will grow on a gold surface.

The cells used in this thesis are ARPE-19 cells, a cell line derived from cells harvested from a 19 year old male who died from head trauma in a traffic accident in 1995 [56]. It is an immortalised cell line, so the culture can in theory be split and kept going indefinitely if taken properly care of, as described in section 2.3.8.

2.3.6 Culture Substrate

Substrate chemistry and topography are both important factors in how cells in culture live, proliferate and die. Exactly which factors promote what is hard to pinpoint, but it seems that hydrophilic materials promote cell attachment and proliferation [35].

Of special interest to the current topic is the effect of ITO as a substrate material, which is covered in its own section, and the effects of the topography of the substrate.

If no attachment-promoting film is used, the cells produce an attachment layer themselves; this layer is created within minutes or even seconds of the cells coming into contact with the substrate. The attachment layer contains integrins, i.e. proteins that promote adhesion or chemotaxis (chemically induced movement), and function as ligands for the cells' receptors. Integrins cluster together in focal contacts, areas between 0.5 and 10 μm across. Focal contacts are common in cultured cells, but less prominent *in vivo*. The cell's proximity to the substrate is closest at the focal contacts, where the substrate-cell distance is in the order of 10 nm [35]. Focal contacts occur especially in stationary cells, including epithelial cells and fibroblasts [57]. In other areas of the cell-substrate contact, the distances between cell and substrate are typically larger, and may surpass 100 nm [58].

2.3.6.1 Substrate Topography

Fine grooves in the substrate can affect cells in numerous ways. Melanocytes were shown to be guided by substrate grooves with height larger than 50 nm and width less than 4 μm, resulting in cells aligning along the grooves [59].

Grooves may affect cell morphology without affecting proliferation. Endothelial cells were shown to be guided to some degree by grooves with depths down to 200 nm, and elongation of the cells occurred increasingly when the groove depth increased towards 1 μm [60]. Grooves may also affect cell migration direction and orientation, although cells may still spread to some degree across grooves 3 μm deep; cell shape and contact area with the substrate may also be affected, as cells on grooved substrates may adopt a more elliptical shape, and may have smaller contact area with the substrate, i.e. they may be less flat [61]. Surface topography and chemistry may even affect apoptosis (programmed cell death) [62] or gene expression [63].

All in all, surface topography may affect numerous properties and behaviours of cells, and exactly how a particular cell type will be affected by a particular type of topography is hard

to predict without specific research into the cells and substrates in question. For the purpose of this thesis, we assume that a grooved topography may affect the cells' behaviour and properties, but we will keep this parameter as fixed as possible to not affect other parameters under study.

2.3.6.2 Substrate Chemistry

Plastics and glass are widely used as cell culture substrates, often covered with some form of attachment-promoting layer. Attempts are often made to make this layer resemble the ECM to some degree, in order to approximate the natural habitat of the cell and thus normalise cell behaviour to approximate their behaviour in a living organism. Collagen, a major constituent of the ECM [36], is widely used.

Hydrophilic, polar substrates seem, in general, to promote cell attachment. Otherwise, there are no consistent models that describe accurately the connection between chemical bonding structure and biocompatibility. Biocompatibility comparisons between materials sometimes yield surprising results (Figure 20) [35].

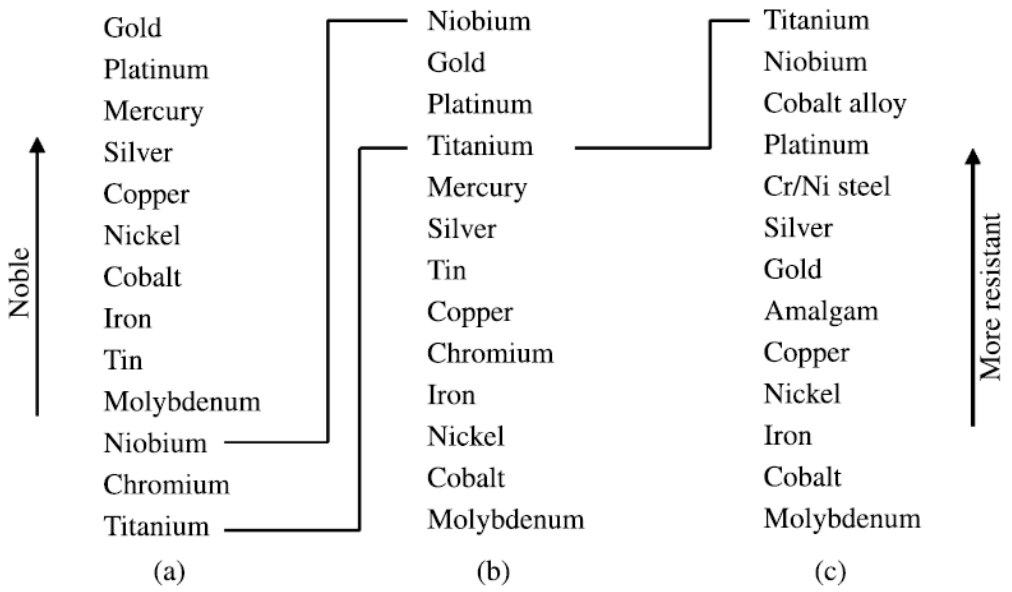

Figure 20 - Theoretical and experimental resistance for metals in the oral cavity. a) theoretical biocompatibility scale, b) general passivation effect of the metals, c) *in vivo* tested materials in the oral cavity. From [35].

Various inorganic materials have been employed as cell growth substrate [35]. Titanium is well established as a biocompatible material for implants, and both gold and ITO have been favourably used for cell culture impedance sensing [38].

2.3.7 Culture Media

Cells in cultures need a culture medium to survive and thrive. The medium needs to replicate as closely as possible the environment the cells would experience if they were in their natural habitat, as part of a body. Standard components of the medium includes salts, nutrients, pH

buffers and indicators, growth factors, amino acids, carbohydrates, proteins, lipids, trace elements, and possibly antibiotics. Different cells have different requirements, and most require animal serum, i.e. blood fluids from animals, in their culture medium [35]. The culture medium will invariably contain ions, which may include Na^+, K^+, Ca^{2+}, Mg^{2+}, Cl^-, and SO_4^{2-}[64].

2.3.8 Maintaining a Cell Line

2.3.8.1 Cell Environment

The cells only survive *in vitro* if their environment supports it. The medium must have the required constituents, described in section 2.3.7. The medium temperature must be suitable for the specific cells; for mammalian cells this temperature is usually 37 °C. As the cells process nutrients and proliferate, the pH of the medium will change unless there is some mechanism to regulate it. The pH in the medium is regulated by pH buffers, which may or may not be dependent on atmospheric CO_2 inside the incubator.

Over time, the cells expend the nutrients in the medium. To maintain the cell culture, the medium must either contain a high enough concentration of nutrients to last the whole timespan of the culture, or it must be replenished before it is depleted of nutrients, lest the cells die. This can either be achieved by an automatic system which periodically replenishes the medium, or by manual exchange of medium, e.g. by pipette. It is important that the cells are allowed to condition their environment, and therefore that the medium is not changed too often [46]. For the ARPE-19 cell line a cycle of 2-3 days is recommended.

Having a suitable amount of medium covering the cells is also important, as the medium acts as a buffer for oxygen diffusion from the surface, which the cells are dependenton. A recommended volume of medium is 0.2 to 0.3 ml per cm^3 of substrate[46], which translates to a medium depth of 2-3 mm.

2.3.8.2 Splitting the Cell Culture

Splitting an attachment-dependent cell culture entails detaching the cells from their substrate, thereby obtaining a cell suspension, and then seeding them in another culture vessel. For safety reasons and to protect the culture from infection, the process takes place in a class II microbiological safety cabinet.

Sterilisation of the flow hood is often done by wiping off surfaces with disinfectant and turning on its fan 15 minutes prior to use to ensure the air inside it is sterile. Ethanol is often used as disinfectant. To avoid inflicting temperature shock on the cells, the cell culture medium and buffer solution are removed from refrigerator units and left to warm up to room. Alternatively, suitable amounts of medium and buffer may be transferred to vessels and heated in the incubator to match their temperature to the culture requirements. Disinfected latex gloves are used.

To detach cells and create a cell suspension, trypsin is used. Trypsin is a serine protease, i.e. an enzyme that cleaves peptide bonds, and thereby cleaving the proteins attaching the cells to the culture substrate. If attachment-dependent cells are exposed to trypsin for too long, they die.

Serum used in culture medium inactivates trypsin [65]. If serum-free medium is used, a trypsin neutraliser is needed.

When pipetting, care must be taken not to scrape the cell culture substrate, as this may damage the cells. Formation of bubbles must also be avoided, as this may create harmful aerosols.

This protocol is used for splitting attachment-dependent mammalian cell cultures [46].

1. Wear gloves. Disinfect hands and work surface(s). Perform procedure in Class II microbiological flow safety cabinet.
2. Remove medium from the culture vessel by pipette and discard it in suitable bio-waste container.
3. Add buffer solution to wash the cells, taking care that the entire culture substrate is wetted and rinsed.
4. Remove buffer solution by pipette.
5. Add trypsin. Enough trypsin should be used to cover the whole cell surface. The time needed for detachment is dependent on the cell type, but the cells normally need at least 5 minutes to detach.
6. Observe the cell culture with a phase contrast optical microscope to check whether they have detached from the substrate. If they haven't detached, wait a couple of minutes and check again. Alternatively, the flask can be given a sharp jolt by hand to assist detachment.
7. When cell detachment is confirmed, introduce serum-containing medium into the trypsin/cell suspension, at least at a 5:1 ratio, as well as accommodating the medium needs of the cell culture for medium amount. The serum inactivates the trypsin.
8. Put culture vessels in incubator.
9. Disinfect equipment and work surfaces, discard single use equipment.

Centrifuging can be used to separate cells from the trypsin/medium solution, but isn't strictly necessary if the trypsin is properly inactivated. Omitting centrifuging from the procedure and introducing the cell suspension into cell culture vessels without being centrifuged reduces the risk of cell clustering, but means that inactivated trypsin will be present in the culture until the next medium change.

Detaching, splitting and re-attaching a culture is called subculturing or passing, and its passage number is the number of times the cells have been subcultured. If the passage number gets too high, the cells may undergo genetic drift.

2.3.8.3 Exchanging Cell Culture Medium

As described in section 2.3.8.1, the cell culture medium must be exchange periodically to enable proliferation and continued survival of the cell culture.

This protocol reflects the splitting procedure in section 2.3.8.2, but skips all steps pertaining to detachment, cell suspension and culture dilution.

1. Remove medium from culture vessel by pipette and discard it in suitable bio-waste container.
2. Add buffer solution to wash the cells, taking care that the entire culture substrate is wetted and rinsed.
3. Remove buffer solution by pipette.
4. Add required amount of medium to the culture(s), i.e. approximately 0.25 ml / cm^2 of the cell culture substrate, as indicated in section 2.3.8.1.
5. Put culture vessel in incubator.
6. Disinfect equipment and work surfaces, discard single use equipment.

2.3.9 Monitoring

Monitoring may be divided into in-line, on-line, at-line and off-line techniques. In-line techniques are integrated in the process, e.g. as a probe directly measuring the properties of the cell culture medium immediately surrounding the cells, or as a substrate sensor monitoring properties like heat or conductivity. On-line techniques are integrated into the production system, though not in the immediate vicinity of the cells; rather, they would monitor the stream of medium to the cell culture vessels, or the oxygen and CO_2 content of the air in the incubator. At-line techniques rely on removing a sample from the process and analysing it, but the analysis would take place in the same area as the production; detaching cells from the substrate to run them through a cell counter is an example of at-line techniques. Off-line analysis would include removing a sample and analysing it in a separate laboratory [33].

In-line and on-line techniques offer continuous and automatic data retrieval, while at-line and off-line monitoring techniques and analysis take longer, and requires an operator. At-line and, especially, off-line analysis do enable a more thorough analysis than in-line and on-line methods.

In-line measurement is an important tool in this regard, as it gives immediate data on changes and processes in the samples. The most prevalent methods for in-line analysis of tissue culture depend on optical measurement and image processing. Those methods are vulnerable to sample heterogeneity and medium turbidity. In attached cell tissue culture, the cells are not necessarily distributed evenly; they will usually grow in islands or lumps, at least until confluence is reached. Impedance sensing by substrate electrodes, e.g. the electrodes used in this thesis, may be employed as an in-line monitoring technique.

An alternative technique suited for in-line monitoring is the use of a quartz crystal microbalance (QCM) with dissipation monitoring. This is an acoustic technique where the energy dissipation of the cell culture is measured: an attached cell culture dissipates more energy than a suspended one [66].

2.4 Indium Tin Oxide

For this thesis, indium tin oxide (ITO) was chosen as electrode material. It has high biocompatibility, and it promotes cell growth and attachment of proteins [38]. It is also a fairly good transparent conductor with 80 % transparency to light in the visible range, while it is reflective in the infrared range.

ITO is a semiconductor with a band gap of around 3.7 eV, and is produced by doping In_2O_3 with up to 6.5 % Sn^{4+} ions, resulting in a heavily doped n-type semiconductor (Figure 21).

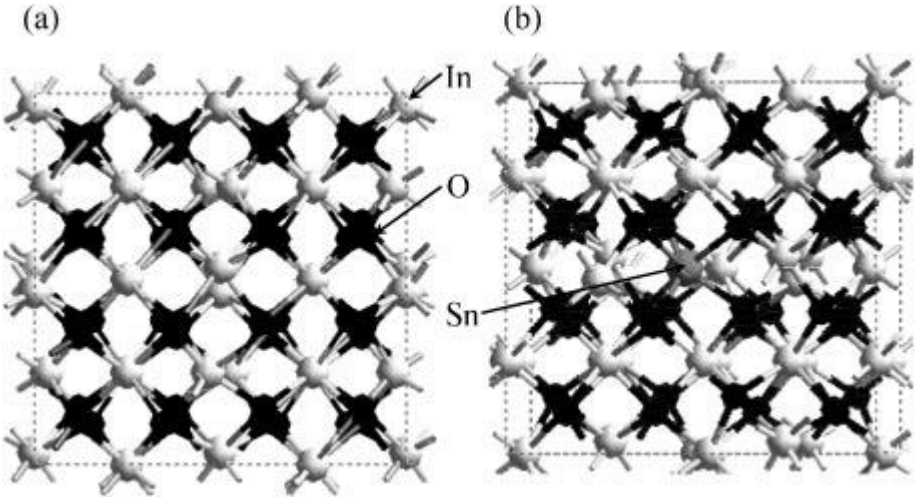

Figure 21 - a) In_2O_3 structure with 48 O^{2-} and 32 In^{3+} b) ITO structure with 48 O^{2-}, 30 In^{3+} and 2 S^{n4}+. From [67].

Its special and relatively rare combination of properties – transparency and conduction – has promoted its use in several areas of technology, e.g. covering on flat screen displays, as anode in organic light-emitting diodes (OLEDs) [68], conductive layer on capacitive touch screens [69], and defrosting layer on windscreens. Its reflexive properties in the IR range also enable its use as infrared reflector. Luckily, its high biocompatibility enables its use as cell culture substrate as well.

ITO has been reported to dissolve in strong acids and lose its conductive properties when used as electrode in a basic solution [40]. The acids and bases that had these effects had pH values of 1 and pH 14, so the effect of a cell growth medium with pH between 7.0 and 7.5, though rich in ions, may be considerably less. For the longer exposure times expected in this thesis, it should still be kept in mind, and control experiments should be attempted.

For transparent conductive material, ITO has been the industry material of choice, but other materials show promise as well, including $SrVO_3$ and $CaVO_3$ [70], who both have better conductive properties than ITO while being transparent in the visible spectrum. They are not readily commercially available as films yet, and biocompatibility tests would have to be done.

2.5 Atomic Layer Deposition

Atomic layer deposition (ALD) is a variant of chemical vapour deposition (CVD), i.e. a process where a vapour or gas is introduced to a chamber where the desired substrate is placed. The vapour reacts with active sites on the surface of the substrate, leaving a monolayer of adsorbed molecules, whereas by-products are flushed out of the system. In contrast to "ordinary" CVD, where the film is deposited in a continuous process, the materials being deposited in an ALD process will not react with or attach to themselves, only to each other (and the substrate, in the case of the first deposition), thus resulting in a self-terminated reaction.

The technique requires at least two reactants, where a two-reactant ALD cycle can be described as follows:

1. Reactant #1 is pulsed into the chamber, and reacts with and deposits product #1 on the surface of the substrate until all available reaction sites are used.
2. Reactant #1 is purged from the reactor chamber, e.g. with N_2 gas.
3. Reactant #2 is pulsed into the chamber, and reacts with and deposits product #2 on the surface of the substrate until completion.
4. Reactant #2 is purged from the reactor chamber.

This cycle is repeated as many times as desired, and builds a film one monolayer at a time, which facilitates control over the thickness and composition of the film. The thickness of the film is linearly dependent on the number of cycles performed.

The vapour is generated by heating *precursors*: compounds that vaporise and reacts at the substrate to produce the desired material. The precursor can be liquid or solid. The degree of heating depends on the precursor. The substrate is also usually heated, to facilitate reactions and building an even layer. If the substrate surface is cold, the deposited material may be uneven or porous.

The reactants are supplied through the vapour phase where its partial pressure is controlled by the temperature it is heated to. The reaction temperature is kept above the precursor temperature to avoid condensation of the precursor. The growth is generally insensitive to variations in the deposition temperature, although variations may occur. This insensitivity gives rise to the commonly called "ALD-window" in process parameters where the film is largely insensitive to any variation. Temperatures outside the ALD-window may result in incomplete deposition, inclusion of unwanted materials in the film, porosity or rough surface,

due to desorption, unwanted reactions, or low kinetics. The technique has been extensively reviewed where we can recommend Refs. [71], [72], and [73] for further information.

2.6 Spectroscopic Ellipsometry

Spectroscopic ellipsometry is a thin film characterisation technique measuring the change in polarisation and phase of reflected radiation, typically a light beam, and fitting the measurement to an existing model. It can determine film thickness, complex refractive index, complex permittivity, and conductivity, among other material properties.

A linearly polarised light beam from the ellipsometer light source hits the sample at a non-perpendicular angle and undergoes specular reflection (incident and reflected angles are equal). The reflected light beam is collected in the detector (Figure 22). The polarisation state of incident, polarised light, can be decomposed into components *s* and *p*[6], normal to each other and the beam direction. The reflection changes the phase and the respective amplitudes of the *s* and *p* components and thus the complex Fresnel coefficients $\mathbf{r_s}$ and $\mathbf{r_p}$, of the components; the ellipsometer measures the complex reflection ratio $\boldsymbol{\rho}$ between them,

$$\boldsymbol{\rho} = \frac{\mathbf{r_p}}{\mathbf{r_s}} = \tan(\boldsymbol{\Psi}) e^{i\Delta} \tag{6}$$

Where $\boldsymbol{\Psi}$ is the amplitude component of $\boldsymbol{\rho}$ and Δ is the phase shift.

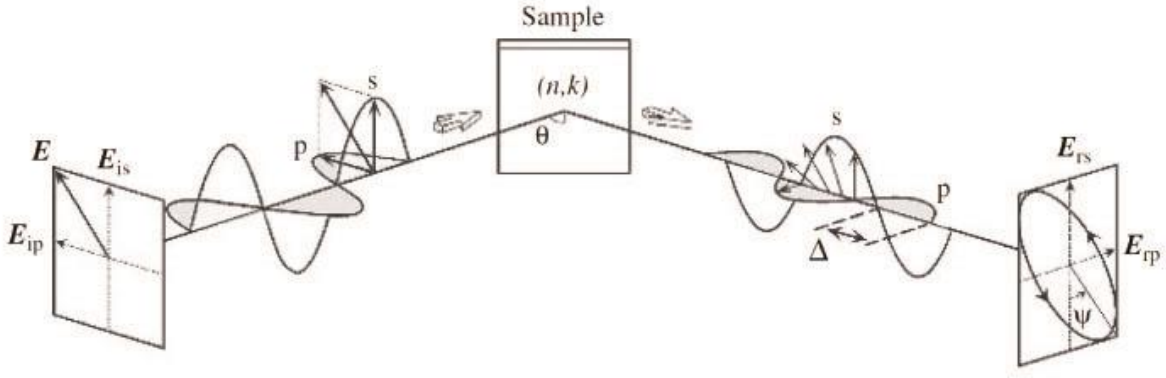

Figure 22 - Schematic of ellipsometric technique. From [74].

The values are fitted to a model, which for dielectrics often follow the Cauchy equation

$$n(\lambda) = A + \frac{B}{\lambda^2} + \frac{C}{\lambda^4} + \cdots \tag{7}$$

[6] The incident beam, the reflected beam, and the normal to the reflective surface are all coincident with the *plane of incidence*. The *p* component is parallel to this plane, while the *s* component is perpendicular to it.

where n is the refractive index, λ is the wavelength, and A, B, and C are experimentally determined coefficients.

3 Analysis, Design and Experiments

This chapter describes the initial analysis of the system, with equivalent circuit calculations and numeric simulation, describes the experiments conducted, and lastly presents the measurements that were made.

3.1 Elements of the Electrode / Cell Culture System

In broad terms, the system consists of the following elements (Figure 23):

- The soda-lime glass substrate.
- The ITO electrodes on the surface of the soda-lime glass substrate.
- The ECM layer generated by the cells.
- The cells.
- The cell culture medium.

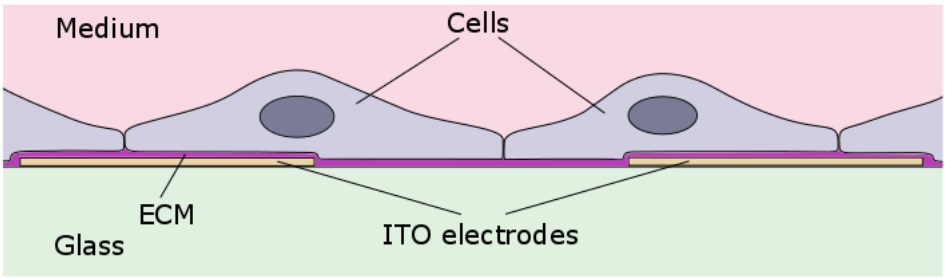

Figure 23 - The cell sensing system. The attachment-dependent cells rest on a cushion of ECM, on top of the ITO electrodes and glass substrate. Dimensions are not to scale. The ECM is approximately 75 nm thick, while the cells are 5 to 50 µm wide.

3.1.1 Current Paths

Bearing in mind that the materials to be sensed are largely volume conductors and currents pass through the entire volumes, Figure 24 is a simplified representation of the different current paths from one electrode to the other:

A. Through the ECM and medium, and between cells.
B. Through the ECM and medium, and through cells.
C. Through the ECM and cell layer.
D. Through the ECM.
E. Through the substrate.

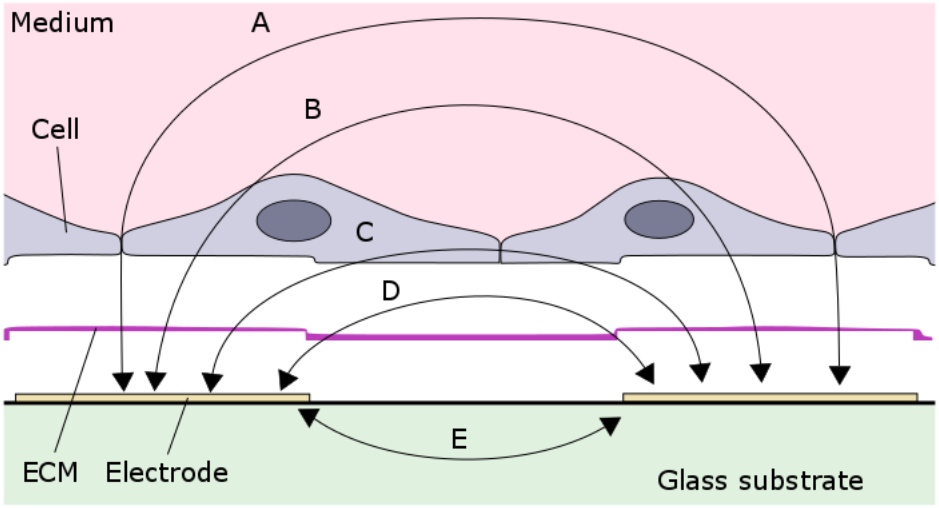

Figure 24 - Simplified cell sensing system, exploded view, with current paths, for a confluent cell layer. A: through ECM and medium, between cells. B: Through ECM, cell(s) and medium. C: Through ECM and cell(s). D: Through ECM. E: Through glass substrate. Combinations of the paths are left out for clarity. A path between electrodes only traveling through medium is not available when the cell layer is confluent, as the cells cover the entire surface of the electrodes.

To simulate the system, an equivalent electrical circuit is conceived to represent it. “Equivalent” is used with some laxity; the system is complex, and the circuit is a simplification.

As an approximation, the number of paths can be reduced for the model by considering that the medium and ECM have almost the same conductivity and can be considered to be the same for the purpose of this model, and that in a confluent culture, the current will only negligibly travel through the medium and cells without also travelling through the ECM as well. The glass has a high resistivity and a relatively low permittivity compared to the ECM and medium, and can be ignored. The list of paths then simplifies to:

1. Through the medium/ECM under the cells.
2. Through the medium/ECM and through or between the cells.

When the cell layer is confluent, there is no free path through the bulk medium only; the current has to travel either through the cells, in the narrow gaps between them or through the ECM layer underneath them. The cell membrane is insulating and effectively blocks DC, at least at current magnitudes too low to disrupt the membrane.

3.2 Modelling the System

The system can be modelled by considering a simplified electrical circuit that represents the different elements and phenomena in the system. This is often called an equivalent circuit, though the simplification necessarily means that some elements or phenomena are omitted. The desire, as in most simplification, is finding a model simple enough to analyze but complex enough to simulate the significant elements and phenomena in the circuit.

3.2.1 Electrical Properties of the System

3.2.1.1 Electrode Electrical Properties

An approximation of the capacitance of the electrodes can be made with equation 3 in section 2.2.1.4. For interdigitated electrodes with digit width w = 24 µm, digit spacing s = 24 µm, periodicity $a = w + s$, digit length p = 6 mm, overall width q = 6 mm, and with medium relative permittivity $\varepsilon_r \approx 80$ [4], resulting in a permittivity $\varepsilon = \varepsilon_r \varepsilon_0 \approx 80 \cdot 8.854 \cdot 10^{-12}$ F·m^{-1} ≈ $7.08 \cdot 10^{-10}$, the capacitance C is approximately

$$C \approx pq \frac{4}{\pi a} \varepsilon \sum_{n=1}^{\infty} \frac{1}{2n-1} J_0^2 \left(\frac{(2n-1)\pi s}{2a} \right) = 0.531 \text{ nF} \quad (8)$$

The evaluation of this expression was done in Maplesoft's computer algebra system Maple. Incidentally, Maple was unable to evaluate the expression directly, because the series doesn't converge fast enough for the program to realise that the sum is finite.

To work around the problem, the series $\sum_{n=1}^{\infty} \frac{1}{2n-1} J_0 \left(\frac{(2n-1)\pi s}{2a} \right)$ was split into two series with the indexes n substituted with 2n and 2n – 1 [75]:

```
> fingercap := proc (p, q, w, s, e);
     a := w+s;
     F := unapply(BesselJ(0, (1/2)*(2*n-1)*Pi*s/a)^2/(2*n-1),
n);
     evalf(4*q*p*e*8.854187817*(Sum(F(2*n)+F(2*n-1), n = 1 ..
infinity))/(10^12*Pi*a)) ;
end proc;
> fingercap(0.006, 0.006, 0.000024, 0.000024, 80)
                                5.315584183 10^-10
```

The capacitance of the interdigitated electrodes will vary with the number of digits, since the area of the capacitor's conductive material in effect increases with an increasing number of digits. Applying the equation for capacitance on various numbers of digits, but with the same overall electrode width and length, both 6 mm, shows that the capacitance ranges from 6.37 nF for 2 µm digit width/spacing, to 25.5 pF for 500 µm digit width/spacing (Figure 25).

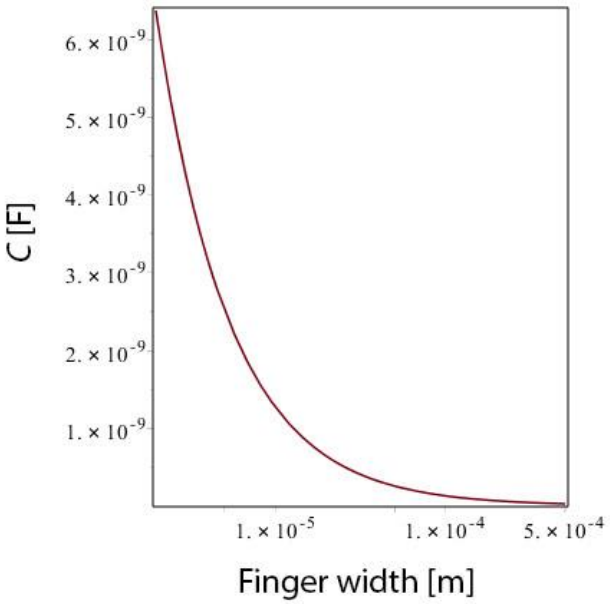

Figure 25 - Capacitance vs. digit width/spacing for a pair of interdigitated electrodes width interdigitated area of 6 x 6 mm. The minimum width, 2µm, corresponds to 750 digits per electrode, while the maximum, 500 µm, corresponds to 3.

The resistance of the ITO nanofilm is declared by the manufacturer to be approximately 35 Ω/square, which was confirmed by ohmmeter measurements at 35 ± 4 Ω. Here, a "square" is any square area, i.e. with 4 equal sides, fitted so that the ITO-covered area in question contains the smallest number of squares possible between the two measuring points. This was confirmed by measuring oblong pieces of ITO-covered glass.

To account for the electrode's geometry, it therefore has to be divided into squares. The significant non-digit area of the electrodes can be represented by 1 square per electrode (Figure 26). There are 62 digits on a 6 mm wide electrode with 24 µm wide digits. The digits are 6 mm long and 24 µm wide, which will take $\frac{6\ mm}{24\ \mu m} = 250$ squares of 24 µm width per digit. Since the current will travel on average halfway down the digit, this number can be cut in half to 125 per digit, in parallel with the other 61 digits on the electrode. The resistance R_d for 1 digit is then $R_d = 35\ \Omega \cdot 125 = 4.375\ \text{k}\Omega \approx 0.229\ \text{mS}$. The resistance R_{dtot} of 62 digits in parallel is then $R_{dtot} = \frac{1}{G_{tot}} = \frac{1}{G_1+G_2+\cdots+G_{62}} = \frac{1}{62 \cdot 0.229\ \text{mS}} \approx 70\ \Omega$. For 2 electrodes in series, with 1 square each for the contact area of the electrode and 2 sets of digits, the expected total resistance of the pair of electrodes is $2 \cdot 35\ \Omega + 2 \cdot 70\Omega = 210\Omega$.

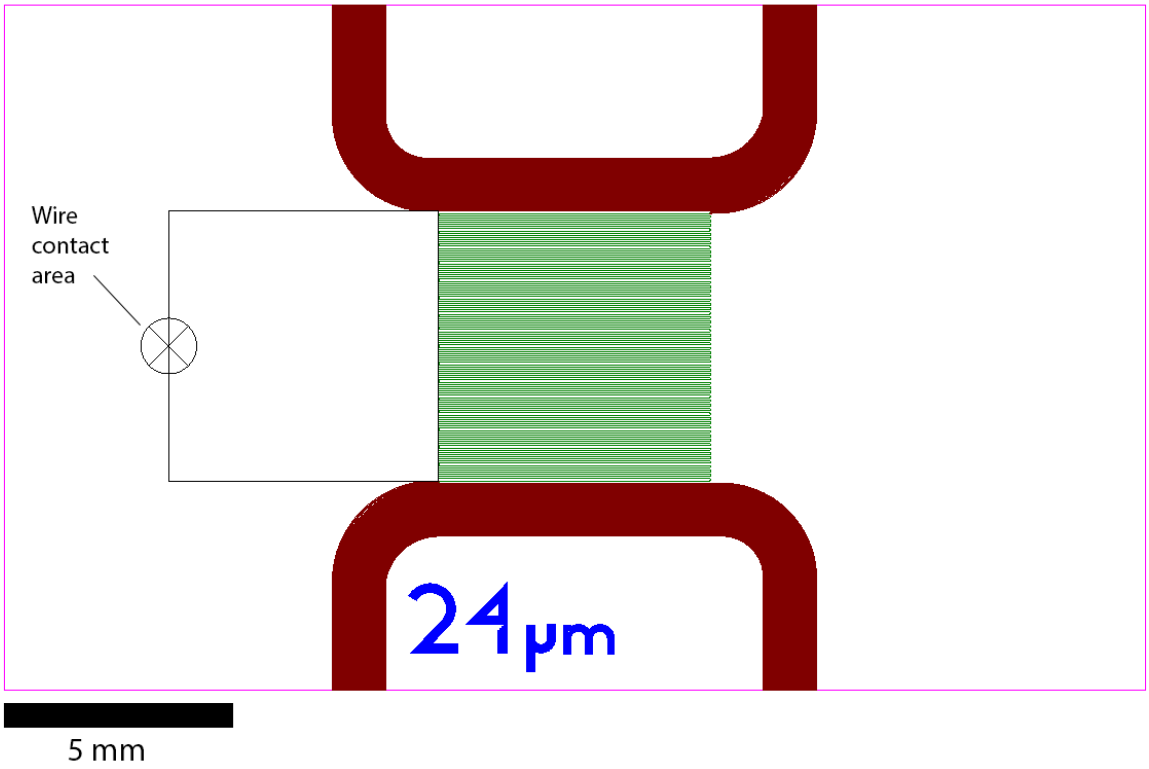

Figure 26 - Laser scribing pattern with square and wire contact indicated. Different colours indicate different draft layers. The black layer is present only for demonstration purposes, and is not part of the scribing pattern.

For a given width w_d and length l_d of electrode digits, an overall width of the digited area of wd_{tot}, and as long as w_d and the spacing between the digits are the same, and the shape of the electrode apart from the digits is invariant, this resistance R_{el} is the same for any number of electrode digits n_d, since

$$R_{el} = R_c + R_d = 2 \cdot n_{sb} \cdot 35\ \Omega + \frac{1}{\left(n_d \cdot \frac{1}{35\ \Omega \cdot n_{sd}}\right)} = n_{sb} \cdot 70\ \Omega + \frac{4 \cdot 35\ \Omega \cdot l_d}{w_{dtot}} \quad (9)$$

where n_{sb} is the number of squares in the main electrode body (excepting digits) and n_{sd} is the number of squares in one electrode digit. W_d cancels out and it R is only dependent on the total width w_{dtot} and length l_d of the digited area. In this case, where $w_{dtot} = l_d$, they cancel out as well and we are left with

$$R = n_{sb} \cdot 70\ \Omega + 140\ \Omega$$

When analysing an electrolytic system, electrode equilibrium potential (EP) and electrode polarisation may be significant. As mentioned in section 2.2.1.1, the equilibrium potential of

ITO has been measured to be in the range + 0.37 V to + 0.42 V. However, since both electrodes are ITO, the EP is equalised and will not generate currents in the sensing device.

Electrode polarisation may influence the system significantly. Data for ITO electrodes were not found, and a measurement to attempt to quantify system impedance without cells will have to be made. These measurements will then include electrode polarisation, and the values can be subtracted from measurement data to glean changes in cell impedance.

3.2.1.2 ECM Electrical Properties

The thickness of the ECM layer between the substrate and the cells is probably somewhere in the range 10-100 nm [57], depending on cell type and variations in ECM thickness for each cell, e.g. due to focal contacts. The worst-case scenario for this system is one with a large distance, where less resistance is encountered underneath the cells, reducing the current density through or between the cells.

The ECM adapts similar conductive properties to the cell growth medium [36], which has a conductivity of approximately 1 S/m and relative permittivity of approximately 80 [4], as mentioned in section 2.1.1.

The ECM layer has variable thickness, but for simplicity, in this thesis, it will be considered to be h = 100 nm. The current paths along the glass surface between the electrode digits corresponds to a conduction distance of l = 24 µm and a combined length of the edges of the electrode digits of p_{tot} = (6mm + 24 nm * π /2) * 63.5 digits ≈ 38.3 cm, so that the total cross-section between the electrodes is $A = p_{\text{tot}} \cdot h$. The resistance R_{hor} (for "horizontal resistance") in this direction is

$$R_{\text{hor}} = \rho \cdot \frac{l}{A} = \frac{l}{\sigma \cdot p_{\text{tot}} \cdot h} \approx 630\ \Omega \tag{10}$$

where ρ is resistivity and σ is conductivity. This is a rough estimate at best, albeit one which might serve as a pointer to how the system might behave.

Equation 10 implies that if the distance between substrate and cell layer decreases, the resistance of the ECM under the cells will increase, inversely proportional to the ECM thickness.

The resistance R of the ECM layer with respect to current traveling from the electrodes to the cell layer and vice versa would be determined by the conduction distance from the electrode to the cells, l = 100 nm and the area of the electrode digits $A = 2 \cdot 63.5 \cdot 24\ \mu\text{m} \cdot 6\ \text{mm} = 1.8 \cdot 10^{-5}\ \text{m}^2$, resulting in a resistance R_{ver} (for "vertical resistance") of

$$R_{\text{ver}} = \rho \cdot \frac{l}{A} = \frac{l}{\sigma \cdot A} = 5.5\ \text{m}\Omega \tag{11}$$

In view of the other resistance values for the system, R_{ver} is negligible and can be omitted from the calculations; it would certainly be indiscernible due to electrical noise in the system. The low resistance implies that the capacitance is also negligible.

3.2.1.3 Cell Layer Electrical Properties

Values for the resistance of an ARPE-19 cell layer has been reported between 10.3 ± 4 and 116.4 ± 57.2 Ω · cm^2 [76] [77] [78] [79], and the capacitance has been reported as 0.8 µF/cm^2 [76]. Capacitances for other cell types have been reported between 0.5 and 3.2 µF/cm^2 [80]. For a circular cell layer with 6.5 mm diameter and a resulting area of $\pi \cdot (0.00325\ \text{m})^2 = 3.3 \cdot 10^{-5}\ \text{m}^2 = 0.33\ \text{cm}^2$, the resistance would be between $9.9\ \Omega \cdot \text{cm}^2 / 0.33\ \text{cm}^2 = 30\ \Omega$ (worst case) and $173.6\ \Omega \cdot \text{cm}^2 / 0.33\ \text{cm}^2 = 526\ \Omega$. (best case). This would have to be doubled in calculations for interdigitated electrodes, as the path of least resistance for the current through the cells from the electrode would be up between the cells, through the bulk medium, and down between the cells again. A path entering a cell, traveling through cells before exiting and connecting to the electrode again would have considerably higher resistance.

The capacitance for the same ARPE-19 cell layer, if in accordance with Onnela *et al*.'s article [76], would be $0.8\ \mu\text{F}/\text{cm}^2 \cdot 0.33\text{cm}^2 = 0.264\ \mu\text{F}$. This capacitance is, however, frequency-dependent and an expression has to be found for it to treat the system analytically.

An equation for the *frequency-dependent* impedance of the cell layer can be approximated from these impedance plots by considering equation 4, repeated here for convenience:

$$\mathbf{Z} = R_\infty + \frac{\Delta R}{1 + (j\omega\tau_Z)^\alpha} \quad [\Omega]$$

α will have to be calculated based on impedance values measured. As R_0 and R_∞ vary in articles as described in ref. [76], making an accurate prediction is difficult. The variable needs to be adjusted after measurements have been made. But as a guidance we can use one of the sets of values from the article published by Onnela *et al*. [76] and shown in Figure 27, where the f_c of the cell layer (the frequency of the peak of *Z"* in the Nyquist plot) was 19555 Hz, R_0 is approximately 10 Ω, and R_∞ seems to be approximately 2 Ω. The cell layer α-dispersion stretches from approximately 3 kHz to 400 kHz. At the characteristic frequency f_c, Re(**Z**) = 6 Ω and Im(**Z**) ≈ -4 Ω.

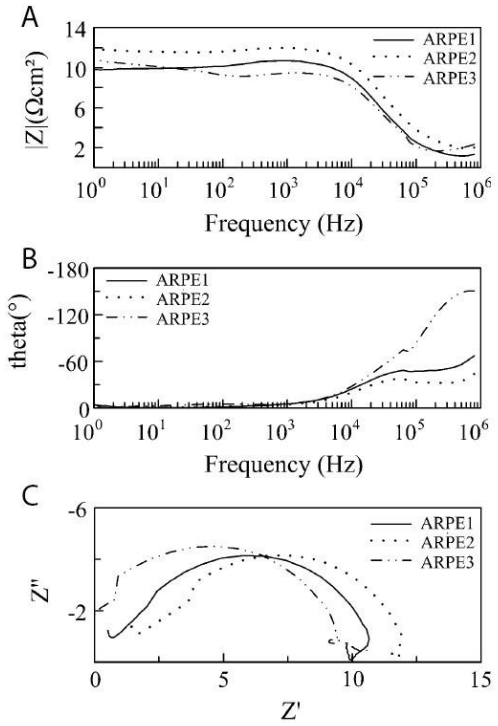

Figure 27 - Impedance measurements of ARPE-19 cells. A: Bode plot, absolute value of impedance |Z| vs frequency f. B: Phase angle θ vs frequency f. C: Nyquist plot, real part of impedance Z' vs imaginary part of impedance Z''. Based on [76]

Substituting the values from plot A in Figure 27 in equation 4 and performing some trial and error analysis for estimating the value for α by visually comparing plots with Figure 27, suggests that $\alpha \approx 0.9$, resulting in the equation

$$\mathbf{Z} = R_\infty + \frac{\Delta R}{1 + (j\omega\tau_Z)^\alpha} = 3\,\Omega + \frac{27\,\Omega}{1 + (j\omega\frac{1}{19555\,Hz})^{0.9}} \qquad (12)$$

Plotting $|\mathbf{Z}|$ in Maple results in the graph in Figure 28. The plot agrees fairly well with Onnela *et al*.'s impedance plot; well enough for an approximation.

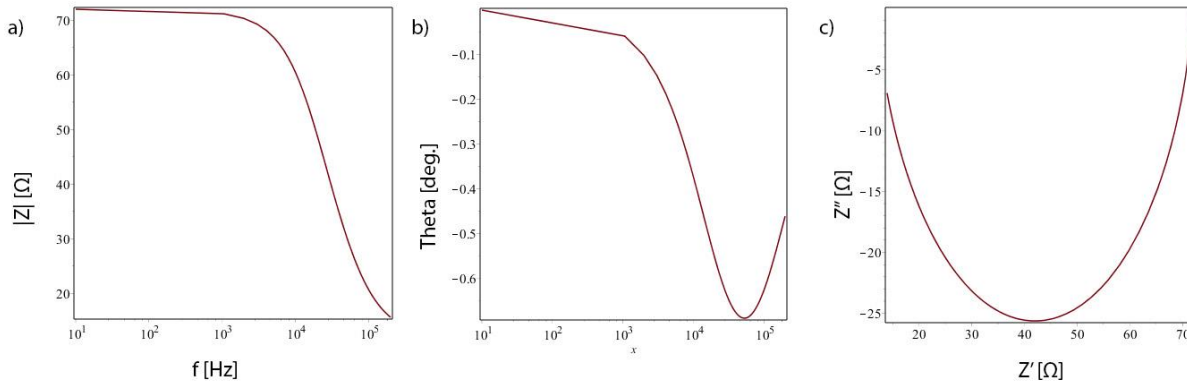

Figure 28 - Impedance plot of ARPE-19 cell layer based on values from Onnela *et al.* [76]. Bode plot a)|Z| vs frequency, and b) phase angle theta vs frequency. c) Nyquist plot, *Z" vs Z'*.

3.2.1.4 Medium Electrical Properties

For comparison, making an estimate of how the system will behave without the cell layer can be useful. The cell growth medium has an expected conductivity of $\sigma \approx 1$ S/m and a relative permittivity of $\varepsilon_r \approx 80$ [4], which result in a resistivity of $\rho = 1/\sigma \approx 1\ \Omega \cdot \mathrm{m}$. The resistance of the medium can be estimated by considering that significant current will travel through the medium above the electrodes and not just between them. A reasonable estimate might involve using the interdigital distance as an approximation for the upper edge of the volume the current will travel through, i.e. an assumption that most of the current will travel below 24 µm above the electrodes. The resistance R_m is then

$$R_m = \rho \cdot l/A \approx 2.6\ \Omega \tag{13}$$

This calculation involves educated guesswork and approximations, but might give a pointer to what order of magnitude the resistance will have. This resistance is expected to be frequency independent up to 10 MHz [4]. The resistance is significantly less than what is expected when a confluent cell layer is covering the electrodes. When the cell layer is incomplete, this should be apparent by a significantly lower resistance than when it is confluent.

The capacitance of the electrode-medium system is estimated in section 3.2.1.1 to be approximately 2.7 nF. The double layer effects at the electrode/medium and the cell/medium interfaces is included in the culture layer capacitance calculations [76].

3.2.1.5 Nanofilm Electric Properties

One of the goals of the project is to see whether it is feasible to cover the substrate and electrodes of the sensing device with a thin film and see whether measurements are still feasible. Intuitively, it should be, since an electrode with cells attached is automatically covered with ECM, which in essence is an organic thin film.

The thin film has to be an insulator, or at least a bad enough conductor that the current doesn't travel through the thin film instead of the ECM, cells and medium. $CaCO_3$ is an insulator with a band gap of 7 eV [81] and a relative permittivity of between 8 and 9 [82]. Presumably, its insulating properties will stop DC unless the $CaCO_3$ film undergoes dielectric breakdown. Its dielectric properties should allow it to contribute to the capacitance of the electrode system. The $CaCO_3$ permittivity is about 9 % of the cell growth medium, and it is solid at room temperature and has no electrolytic conductance, so its permittivity should be frequency-independent to at least the GHz range; see section 2.1.1 . The capacitance of the $CaCO_3$ thin film will effectively be in series with the capacitive system of the electrodes, ECM, medium and cells, and the capacitance for a capacitor with two different dielectrics in parallel is given by the relation

$$\frac{1}{C_{tot}} = \frac{1}{C_1} + \frac{1}{C_2} \Leftrightarrow C_{tot} = \frac{C_1 + C_2}{C_1 C_2} \tag{14}$$

Regarded together with the electrodes and ECM layer only, the $CaCO_3$ thin film is in parallel with the ECM, and according to equation 3, the capacitance of the interdigitated electrodes with 24 µm digit width and spacing, and 6mm digit area width and length, is 531 pF and the capacitance for a capacitor with two different dielectrics in parallel is

$$C_{tot} = \frac{C_1 C_2}{C_1 + C_2} \tag{15}$$

Since $CaCO_3$ is soluble in water, the conductive properties of the system should be monitored over time.

Electrical properties of the TTIP/glycine film were not attainable prior to the experiments.

3.2.1.6 Glass Substrate Electrical Properties

The glass type used as substrate for the ITO thin film is soda lime glass, which typically has a composition of approx. 85 mole % SiO_2 and 15 mole % Na_2O. The permittivity varies with temperature and frequency: at room temperature, with AC frequencies increasing from 9 kHz to 90 MHz, the real part of the permittivity decreases from 6.56 to 6.08, while the phase angle decreases from 0.31 to 0.11 radians [83]. The measured DC resistance of the uncoated glass substrate (the reverse side) exceeded 20 MΩ.

3.2.2 Equivalent Electrical Circuit

The system can be analysed by considering a circuit composed of ideal electrical components, in this case resistors and capacitors, to simulate the different elements of the cell culture and electrodes (Figure 29). None of the elements involved are considered to be inductive to any significant degree. If the cell layer on the electrodes is confluent, there is no free path from electrode to electrode through the medium only, and the bulk medium resistance R_b can be eliminated from the circuit. The resistance R_{ECM} represents the resistance of the direct path between the electrodes under the cells. The resistance R_c represents the

resistance of the cell layer, though in effect this is the resistance of the ECM in the tight space between the cells.

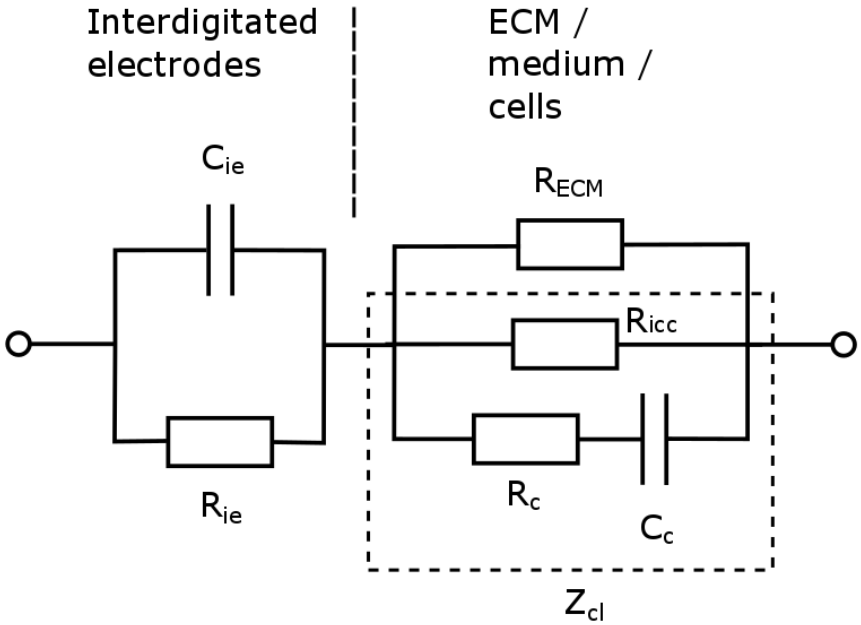

Figure 29 - Simplified equivalent circuit of the cell sensing system for attached, confluent cells. Impedance of the wires and bulk medium have been eliminated as they are expected to be negligible. Subscript "ie" refers to interdigitated electrodes. Subscript "ECM" refers to extracellular matrix. Subscript "icc" refers to intercellular channels. Subscript "c" refers to cells. Subscript "cl" refers to the collective properties of the cell layer. Z_{cl} is a Cole CPE. Cfr Figure 13.

In the circuit in Figure 29, all electrode electric effects are lumped into the two electrode-representing circuit elements C_{ie} and R_{ie}. While electrode polarisation, surface effects, shape-dependent capacitance, and material impedance could have been modelled with separate elements modelled. In this case, a simple representation was deemed sufficient, which also simplifies calculations.

Approximate values for the properties of these equivalent circuit elements have been calculated sections 3.2.1.1, 3.2.1.2, and 3.2.1.3., and are presented in Table 1.

Table 1 – Approximate electrical properties of elements of the equivalent circuit. Subscripts indicate frequency of current. R_∞ is represented by the expected resistance, constant up to 10 MHz.

Element	R_0 [Ω]	R_∞ [Ω]	C [µF]
Electrodes	35	35	$2.66 \cdot 10^{-4}$
ECM	630	630	(included in electrode capacitance)
Cell layer	10	1	0.264 µF
Bulk medium	2.6	2.6	(included in electrode capacitance)

In the circuit, the parallel elements of the electrodes is connected in series with the parallel and series elements of the cell/medium subsystem. If we consider the permittivity of the

electrodes and medium to be invariant, i.e. we disregard frequencies above 10 MHz, then the only frequency-dependent permittivity in the system is that of the cell/double layer element. The calculation below is limited to the one dispersion documented by Onnela *et al*. [76], and shown in section 3.2.1.3.

The impedance of the system is the combined impedances of the elements in Figure 29:

$$\mathbf{Z}_{\mathrm{tot}} = \mathbf{Z}_{\mathrm{el}} + \frac{1}{\frac{1}{\mathbf{Z}_{\mathrm{c}}} + \frac{1}{\mathbf{Z}_{\mathrm{ECM}}}} = \frac{R_{\mathrm{el}}}{1 + R_{\mathrm{el}} j\omega C_{\mathrm{el}}} + \frac{\mathbf{Z}_{\mathrm{c}} R_{\mathrm{ECM}}}{\mathbf{Z}_{\mathrm{c}} + R_{\mathrm{ECM}}} \tag{16}$$

where the subscripts el, c and ECM indicates electrodes, cells and ECM, and $\mathbf{Z}_{\mathrm{c}}$ is taken from Equation 12 in section 3.3.3. Substitution with values from Table 1 and Equation 12 in a Maple plot results in the graphs in Figure 30. This analysis and consequently the plots are expected to be adjusted when measurements have been made and an estimate of electrode polarisation has been made.

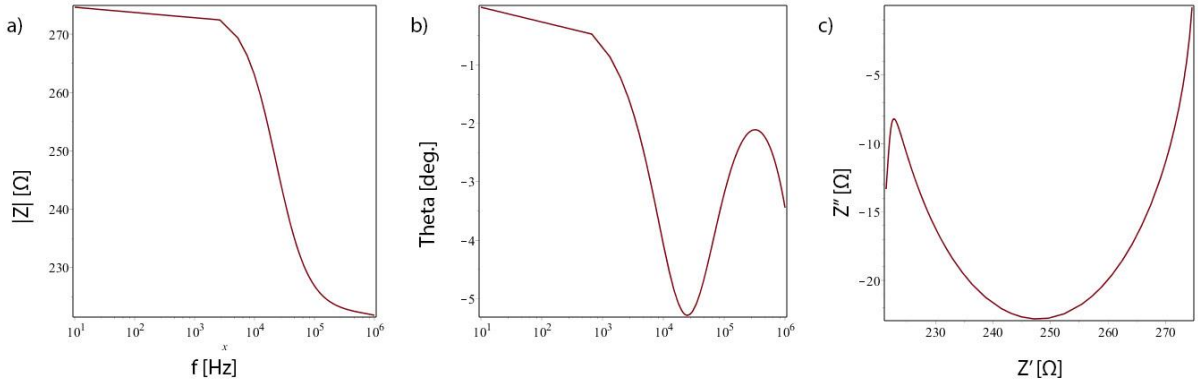

Figure 30 - Impedance plot of sensing system with ARPE-19 cells confluent on interdigitated electrodes in cell growth medium. Bode plot a)|Z| vs frequency, and b) Phase angle theta vs frequency. c) Nyquist plot, *Z" vs Z'*.

In the circuit representation, the following approximations have been made:

- The inductance of the system is regarded as negligible and has been ignored.
- The resistance and capacitance of the wires are negligible and have been ignored.
- The conductivity of the medium is approximately the same as the ECM [36] and uniform, about 1 S/m [4] (see section 2.1.2). It is also regarded as frequency-independent up to 10 MHz [4].
- The relative permittivity of the medium is approximately 80 [4].
- The cells insulate their interior completely, and function as a capacitor together with the double layer around them.
- For currents traveling underneath the cells between the electrodes, the resistance of the ECM is relatively large. Current along this path is therefore ignored.

The ECM's permittivity is uncertain, but according to Bagnaninchi *et al.*, it is much lower than the combined medium-cell-ECM system [84]. The impedance of the ECM for current traveling from the electrodes towards the cells is viewed as purely resistive.

3.2.3 Finite Element Method

To visualise how the current density may be distributed, a model and FEM mesh was produced in COMSOL Multiphysics (COMSOL) (Figure 31). The geometry was chosen to match the dimensions of the laser-scribed electrodes; ITO electrode digits, 350 nm high, 24 µm wide and 6 mm long (in z direction normal to the image); ECM covering the glass and electrodes, 75 nm thick; cell layer resting on the ECM, 2 µm thick; culture medium covering the cell layer. To conserve computing power, the cell layer was modelled as a uniform layer with the impedance parameters found in Onnela *et al*.'s article [76] and the model was simplified to a 2D representation. All other material parameters were used as built-in in COMSOL Multiphysics. Corners were rounded to avoid infinitely sharp geometry, which can cause problems with the current density calculations in the software. As can be seen from the current density detail plot (Figure 31 f), the current density is highest at the electrode edges.

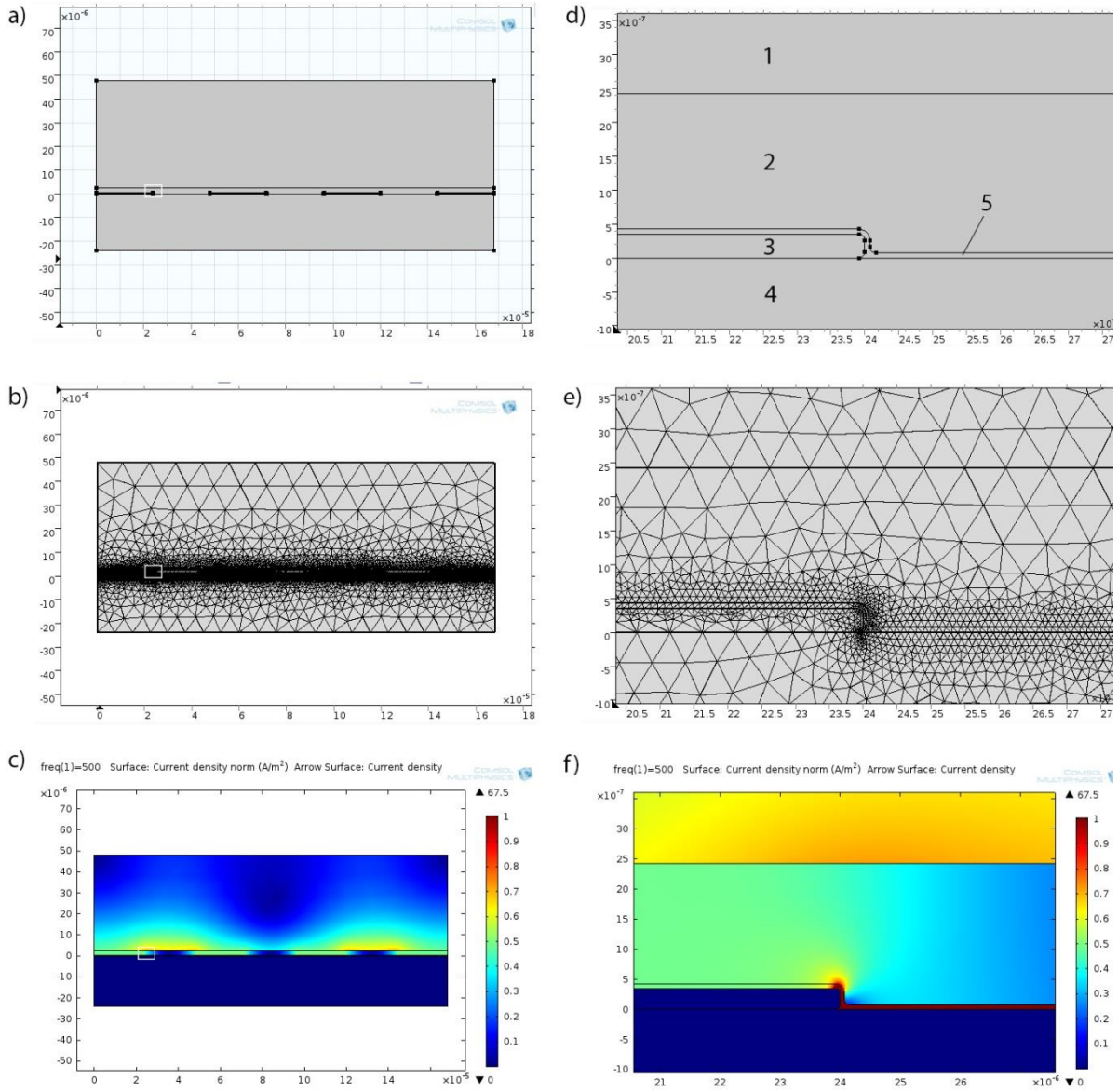

Figure 31 - Finite element method simulation of 4 ITO electrode digits on glass substrate, covered with ECM, a cell layer, and cell culture medium. The white rectangles indicate magnification area. All images generated in COMSOL software.

a) Wireframe. b) Mesh. c) Current density plot. d) Wireframe, detail. 1: culture medium. 2: Cell layer. 3: ITO electrode. 4: glass substrate. 5: ECM. e) Mesh, detail. f) Current density plot, detail.

3.3 Design of Cell Culture Impedance Sensing Device

One of the concerns in the design process was the contact between the ITO electrodes and the wires used for measurement, and that this contact should not wear away the ITO layer. Crocodile clips were considered too abrasive, with a significant possibility of quickly wearing off the ITO layer at the contact sites. Soldering was attempted but proved unsuccessful; the metal would not stick to the ITO surface. Spring-loaded, rounded gold contacts were eventually chosen. The contact between the ITO layer and the wires was good, and the ITO layer was not damaged significantly by the contacts.

3.3.1 Considerations Influencing the Device Design

The proliferation of ARPE-19 cells in the sensing device is dependent on the environment in which they are seeded and maintained. Although inspiration and characteristics were drawn from existing cell growth systems, the need for attaching both a cell growth well and a pair of electrodes to the glass slide poses some specific challenges.

The different requirements that shaped the design and the sensing device were:

- **Galvanic contact.** The contact between the wires and the ITO layer needed to be reliable, constant and sustainable.
- **The strength of the glass plate.** The spring-loaded contacts exert a considerable pressure on the 1 mm thick glass plate, and the device needs to be assembled and used without the pressure from the springs cracking the glass.
- **Oxygen / CO_2 exchange.** The gap between the cell growth well and its lid has to be large enough for gas exchange.
- **Evaporation**. The gap between the cell growth well and its lid also has to be tight enough to limit evaporation. Evaporation concerns dictate that the lid also has to have a "curtain" extending down past the rim of the well on its outside.
- **Leakage**. The cell well and substrate, as well as the interface between them, must be watertight to hold the cell growth medium inside the culture well.
- **Toxicity.** The materials in contact with the cell growth medium should not release substances harmful to the cells. The cell growth well has to be attached to the ITO/glass plate with no leakage.
- **Ease of assembly.** The device should be assembled without damaging the components.
- **Robustness.** The device should withstand use over time without leaking, breaking or otherwise changing properties.

Suitable ventilation proved vital to both ensure oxygen circulation and limit evaporation. The final device had a 1 cm high cylindrical SiO_2 glass well with inner diameter 6.5 mm and outer diameter of 9 mm, attached to the scribed ITO/glass slide on top of the digits of the interdigitated electrodes with aquarium silicone. The well was capped by a glass lid which rested on 0.5 mm high knobs and had a 0.5 mm margin between the inner diameter of the lid wall and the outer diameter of the well, creating an overall gap of 0.5 mm around the well for ventilation and extending 6 mm below the rim of the well on its outside.

The slide was assembled with the wires and contacts in an ABS plastic mount and two ABS plastic clamps. The cell culture well was separate from the wire contact mounts to eliminate the need for a strong adhesive for the culture well, and the glass plate had support from the plastic clamps at its back side to counteract the pressure exerted on the glass slide by the spring-loaded contacts.

The materials of the cell well and the lid must be watertight to prevent leakage and evaporation. They must also be non-toxic to the cells. Parts of the devices are 3d-printed using ABS plastic, which is resistant to the humidity and temperature inside the incubator, but since most 3d-printed materials are porous and not watertight, the inside wall of the well must either be lined with a watertight material like silicone, or be made from a different material, e.g. glass, which was used eventually.

Any adhesive in contact with the cells or cell growth medium must be non-toxic. As many glues and fillers like silicone contain fungicides to prevent mould, they are unsuitable for cell culture vessels. Aquarium glue and aquarium silicone both proved sufficiently non-toxic to allow cell proliferation. The varieties tested were Universal Adhesive aquarium glue from JBL Haru, and Parasilico silicone from DL Chemicals. Silicone was used in the sensing devices for its transparency – the aquarium glue is opaque black. Several different glues were tried, but most did not permit cell growth, presumably due to leakage of toxins into the cell growth well. Eventually, aquarium silicone was used, and cells attached and proliferated, albeit at a lower rate than in commercially obtained culture vessels. See section 3.4.6.1.3 for a description of the toxicity tests.

3.3.2 3D Model

The design underwent several iterations after the device was put into use, to accommodate necessary changes during the progression of the thesis. See Appendix A for an overview of the different iterations. The 3D model was produced in Dassault Systemes' computer assisted design (CAD) software Solidworks (Figure 32).

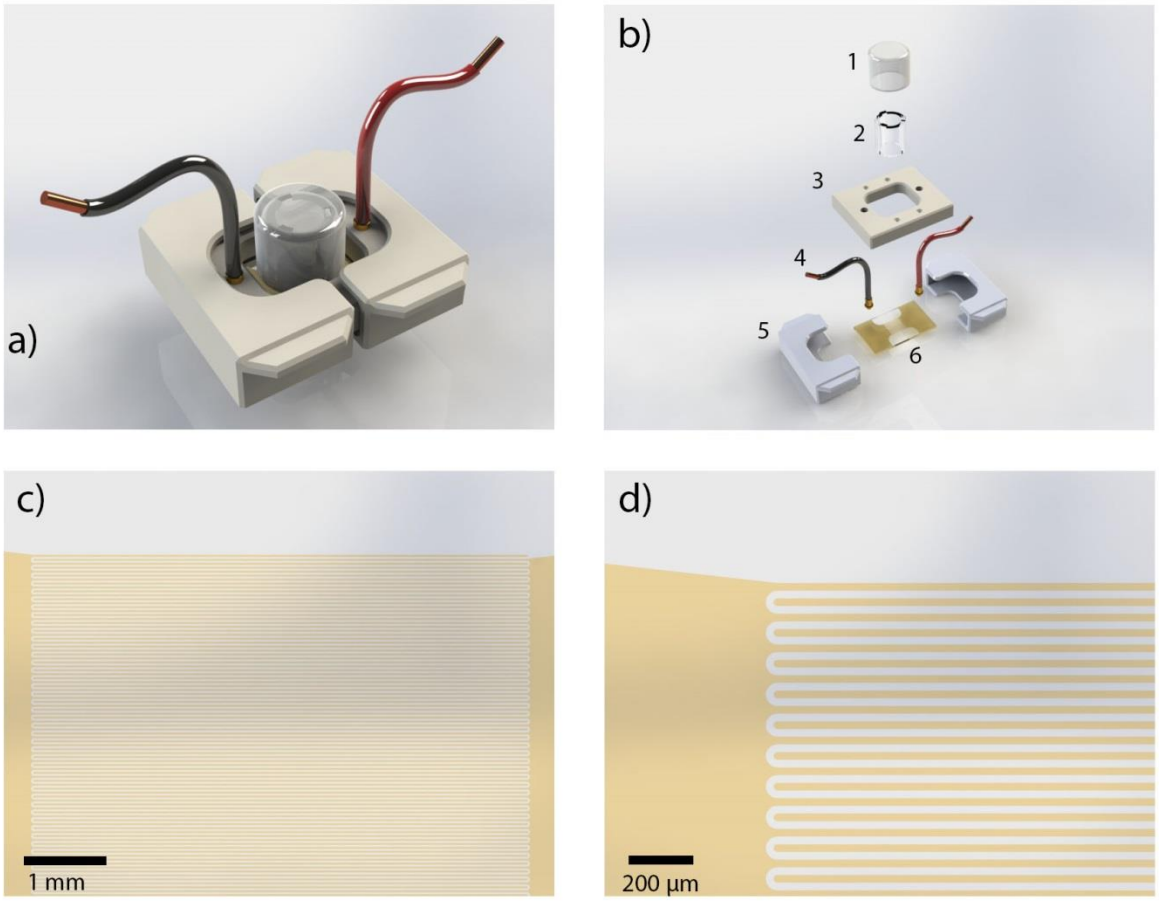

Figure 32 - Renders of the final design for the cell culture impedance sensing device. a) Assembled view; b) Exploded view. 1: Glass cap. 2: Glass well. 3: ABS slide/wire mount. 4: Copper wires with spring-loaded gold contacts. 5: ABS clamps. 6: Etched ITO-covered soda glass plate with interdigitated electrode area seen in the middle. c) Close-up detail of electrode pair. d) Very close up of electrode digits.

A 2D technical drawing was used for visualising parts for workshops when requesting parts. Figure 33 is an example with size requirements for the cell well and lid shown in context with the sensing device. The draft was generated and developed in Solidworks' technical drawing functionality.

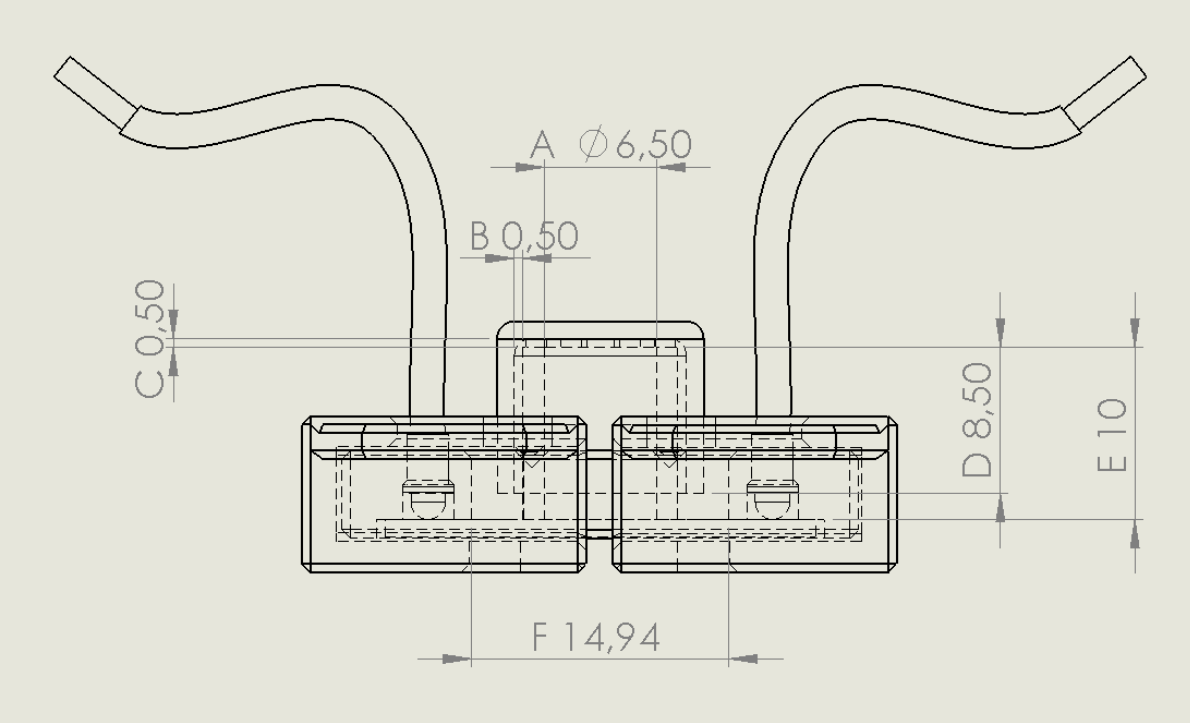

Figure 33 – Draft with side view of the cell culture impedance sensing device. A: inner diameter of the culture well, B; gap between outer circumference of the culture well and the inner circumference of the well lid; C: gap between upper rim of the culture well and the ceiling of the well lid; D: height from upper rim of the culture well to bottom rim of well lid; E: height of the cell culture well; F: width of the space around the well lid.

3.3.3 Scribing Pattern

The interdigitated geometry of the electrodes (Figure 8) was chosen in an effort to make the sensitivity of the electrodes as uniform as could be achieved over the growth surface, so that the locations of attaching cells would influence the impedance reading to a minimal degree. The current density is highest at the electrode edges (see Figure 31), so the higher the density of electrode edges, the higher the probability will be that any particular cell will be situated on top of an electrode edge and sensed. The electrode digits and the gaps between them were therefore chosen to be as slim as the scribing laser would allow them to be, i.e. roughly 25 µm, to maximise the number of cells that would be picked up by the electrodes.

As described in section 2.3.2.5, the cells rest on an ECM-like substance, approximately 75 nm above the substrate. The cell distance from the substrate is a factor; if this distance is comparable to or larger than the distance between the electrodes, the sensitivity through the cells may be inconveniently weak. With a distance between the cells and substrate of 75 nm, the electrode width and interdistance of 24 µm would not be a problem in this regard.

With a digit width of 24-192 µm, a digit length and electrode width of 6 mm, the conditions for using equation 3 in section 2.2.1.4 should be fulfilled by the sensing device constructed for this thesis. How large the number of parallel strips need to be is unclear from the article,

but as long as the condition $a << p$ and $a << q$, the conditions should be fulfilled; this is arguably the case for all the electrodes produced for this thesis, as the widest electrode digits have a digit width and interdistance of 192 µm and a digit length and overall electrode width of approximately 6 mm.

The scribing pattern (Figure 34, Figure 35) was made in Dassault Systémes' drafting software DraftSight. Where the ITO was to be ablated in a wider area than the scribing width, i.e. around the electrodes, the scribing lines had to be drawn with a small enough distance between them to make sure they always overlapped. This distance turns out to be about 12 µm, due to the unevenness of the scribed lines. The laser has a scribing width of roughly 24 µm, so electrode digit interdistance was difficult to reduce below this. The drafting and scribing programs offer a hatching feature, which fills an area with parallel lines, but this feature failed and hatched areas where it wasn't designated, possibly because of the high detail of the drawing.

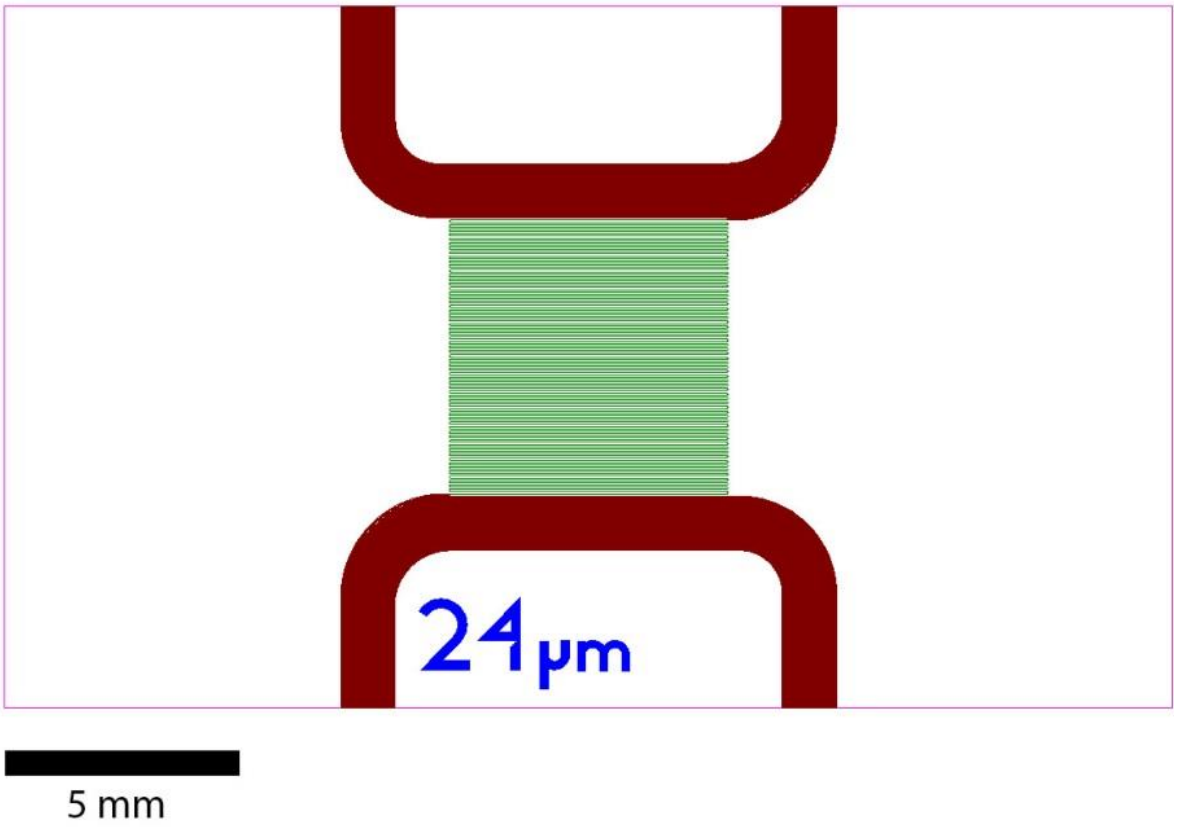

Figure 34 - The scribing pattern for a glass plate with 2 interdigitated electrodes. The different colours indicate different layers of the drawing file. The dimensions of the plate is 25 x 15 mm. The white areas are not scribed, leaving the ITO layer intact. The electrodes consist of the ITO left on the plate after ablation. The scribing design is a negative image of the electrodes. The brown areas are lines with 12 µm distance, ensuring overlap between the lines, to insulate the ITO electrodes from each other. The green area consists of zig-zag lines with 24 µm interdistance, removing the ITO between the electrode digits, creating electrode digits 24 µm wide and with 24 µm spacing. The blue lettering serves as an identifier for the spacing of the lines and for which side of the glass the ITO layer and electrodes are situated.

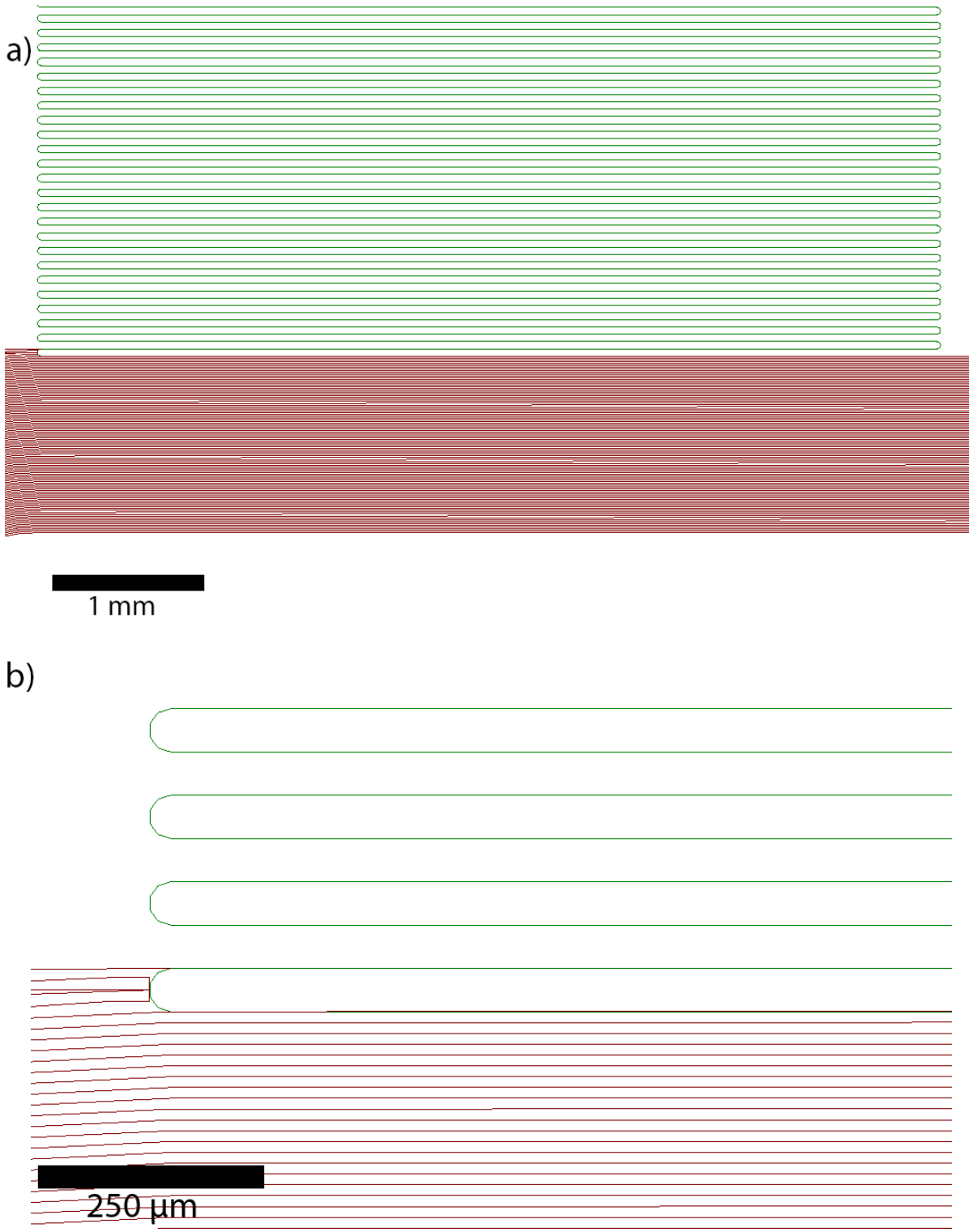

Figure 35 – Details of electrode scribing pattern at various degrees of magnification. a) The green lines defines a zig-zag pattern which ablates the ITO between the electrode digits. The line width in the figure is not indicative of the width of the laser beam. b) The brown lines ablate a continuous area which isolates the electrodes from each other.

An alternative version with 192 µm digits width and interdistance was also produced, to investigate the influence of varying digit dimensions (Figure 36).

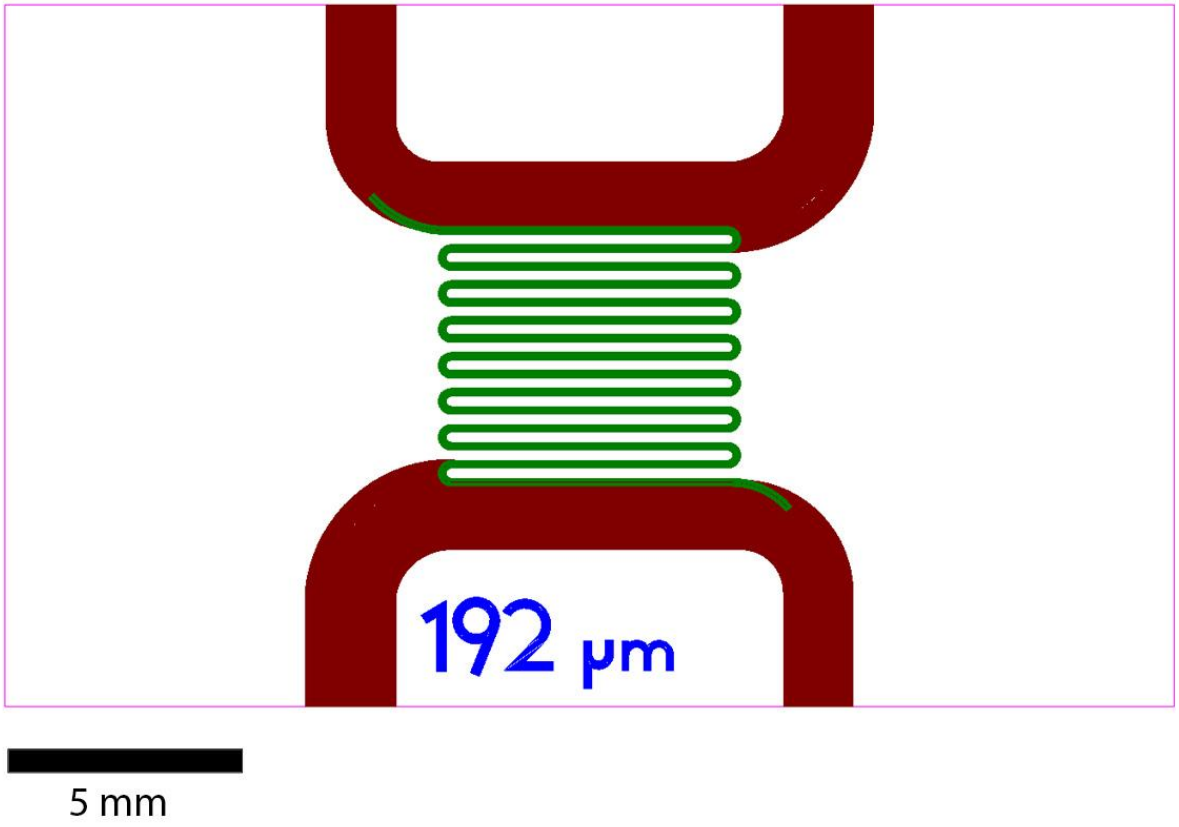

Figure 36 - Scribing pattern for a pair of interdigitated electrodes with 192 m digit width and interdistance.

3.4 Experiments

The experiments can be divided into the following parts:

- Designing and manufacturing the cell culture impedance sensing devices.
- Conducting impedance measurements on cells in the sensing devices.

The ALD-coated ITO electrode slides were characterised by spectroscopic ellipsometry.

3.4.1 ITO Electrodes

A 1 mm thick soda lime glass plate coated with a 350 nm sputtered layer of ITO [85] was procured from SPI Supplies. The ITO sheet had a measured resistance of 35 ± 3 Ω per square.

3.4.1.1 Laser Scribing

Račiukaitis *et al*. reported an ablation threshold fluence for a 120 nm ITO film as 2.57 J/cm^2, when using a laser wavelength of 532 nm, scribing diameter of 24 µm, a distance between consecutive pulses of 2 µm, pulse frequency 250 Hz, and pulse duration of 60 ps. The ablation threshold for glass was reported as 4.66 J/cm^2 [86]. A pulse distance of 2 µm with a 24 µm diameter incident laser beam means that 12 pulses will overlap to some degree, although less so towards the edges of the scribed line.

The laser used in this thesis, a ROFIN PowerLine E Laser Cutter, has a maximum power output of 16 W, but this is not directly adjustable in the laser's settings. Rather, the current is set to the desired level. The maximum current available in the laser scribing software is 32 A, which then presumably corresponds to the maximum output of 16 W. The manufacturer was not responsive when asked for confirmation of this.

Experimentation determined an ablation threshold of 16 A for the 350 nm ITO film. The glass remained intact at this level. At 32 A, corresponding to 16 W, the glass was ablated as well. Since $P = I^2R$, it's reasonable to assume that a current of 16 A corresponds to an output of 4 W.

The incident laser beam is circular with a diameter 24 µm, resulting in a scribing area is $A_{beam} = 4.52 \cdot 10^{-6}$ cm^2. The pulse duration is 1 µs. A power of 4 W yields an energy of $W = P \cdot t = 4 \cdot 10^{-6}$ J per pulse, in turn resulting in a fluence of $H_e = W / A = 0.88$ J/cm^2 per pulse. The incident laser beam spot has a speed of 50 mm / second, meaning the pulses arrive with a 1.5 µm distance between their centres and that the areas of 16 laser pulses overlap to some degree. Multiplying the fluence with the number of pulses overlapping gives a total fluence of 14.1 J/cm^2 along the centreline of the scribed line, decreasing towards the edge, where the fluence is 0.88 J/cm^2. These values are different from those reported by Račiukaitis *et al*., though the 350 nm film used in this thesis should be expected to need more energy to be ablated.

One technique which was attempted involved defocusing the laser to increase the beam diameter at the ablation surface, and thus increases the area scribed by the beam. It also decreases the energy density of the beam at the surface. With the current increased to maximum, the width of the beam should be able to be increased considerably while still ablating the ITO. While the technique indeed ablated a wider area, the technique was unsuccessful in combination with lines scribed with the focus point aligned to the substrate. The reason for this seems to be that the laser beam tilts to follow the lines of the pattern. The focus point is adjusted correspondingly, but when the beam is defocused, a mismatch occurs between the focus height, ablation area and the beam tilt, so the scribed lines are offset, and increasingly so the further the line is positioned from the centre of the scribing area (Figure 37).

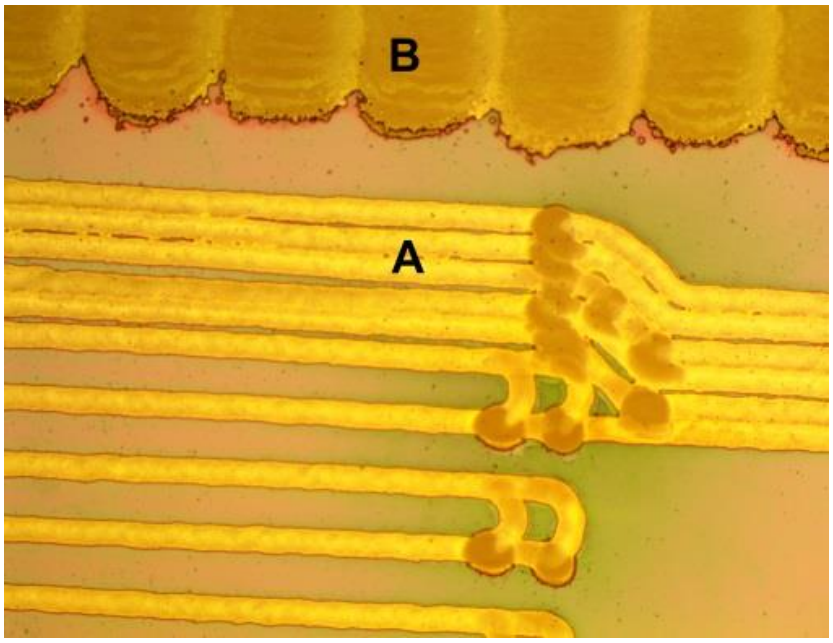

Figure 37 - A: Scribed lines from focused laser beam B: Scribed area from defocused laser beam. In the design, there was no distance between area A and B, but when the scribing is performed, a considerable gap results because of the tilt of the laser is not compensated for properly to align adjacent lines.

The scribing patterns presented in 3.3.3 were imported to Rofin's proprietary Visual Laser Marker program. The pattern (Figure 34) took approximately 3 minutes to execute, varying according to how many executions were needed of the cutting lines; this number varied between 75 and 240.

Initial attempts at scribing the electrodes with 15 A current were only partly successful; the scribing was incomplete for 2 out of 4 electrodes, evident when observed with an optical microscope (Figure 38). Resistance measurements for the electrode sets gave results ranging from 300 Ω to the 100 kΩ range, depending on degree of success for the individual scribing processes. Successfully scribed electrode had DC resistance values in the 100 kΩ range, while unsuccessful electrodes were in the 100 Ω – 1 kΩ range. Resistance values in the 100 kΩ range may be acceptable for measurements of cells and cell growth medium, where the expected resistance is several degrees of magnitude lower. When the laser current was increased to 16 A, the inter-electrode resistance was consistently in the 100 kΩ range or above, and the electrode structure looked successfully scribed when inspected in an optical microscope (Figure 39).

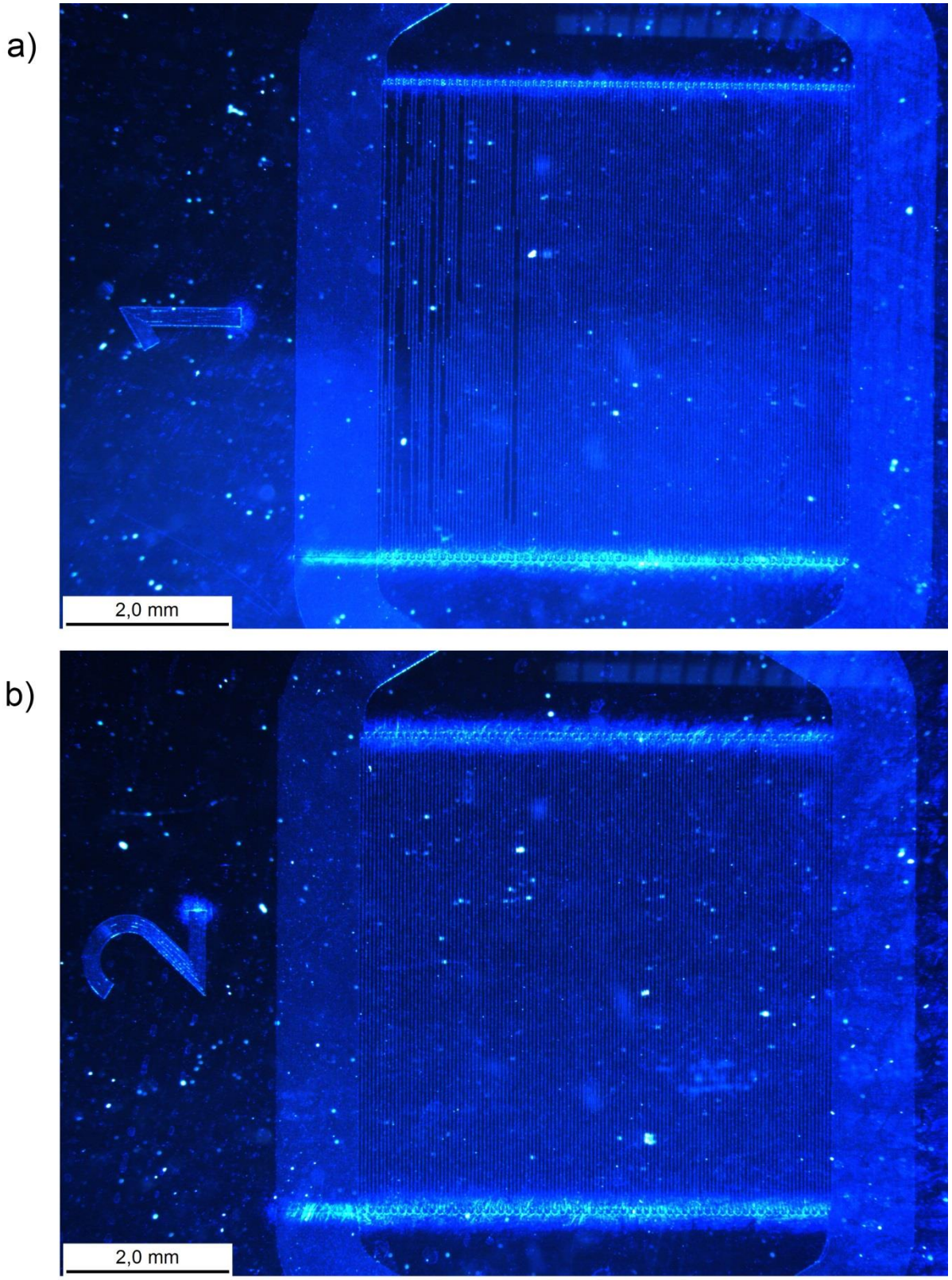

Figure 38 - Electrodes scribed with 15 A current. Incompletely scribed electrode digit spacing results in contact between the electrodes. a) Electrode set 1 is incomplete; the wider dark lines at the left side of the digit area indicate intact ITO layer. b) Electrode set 2 is successfully scribed.

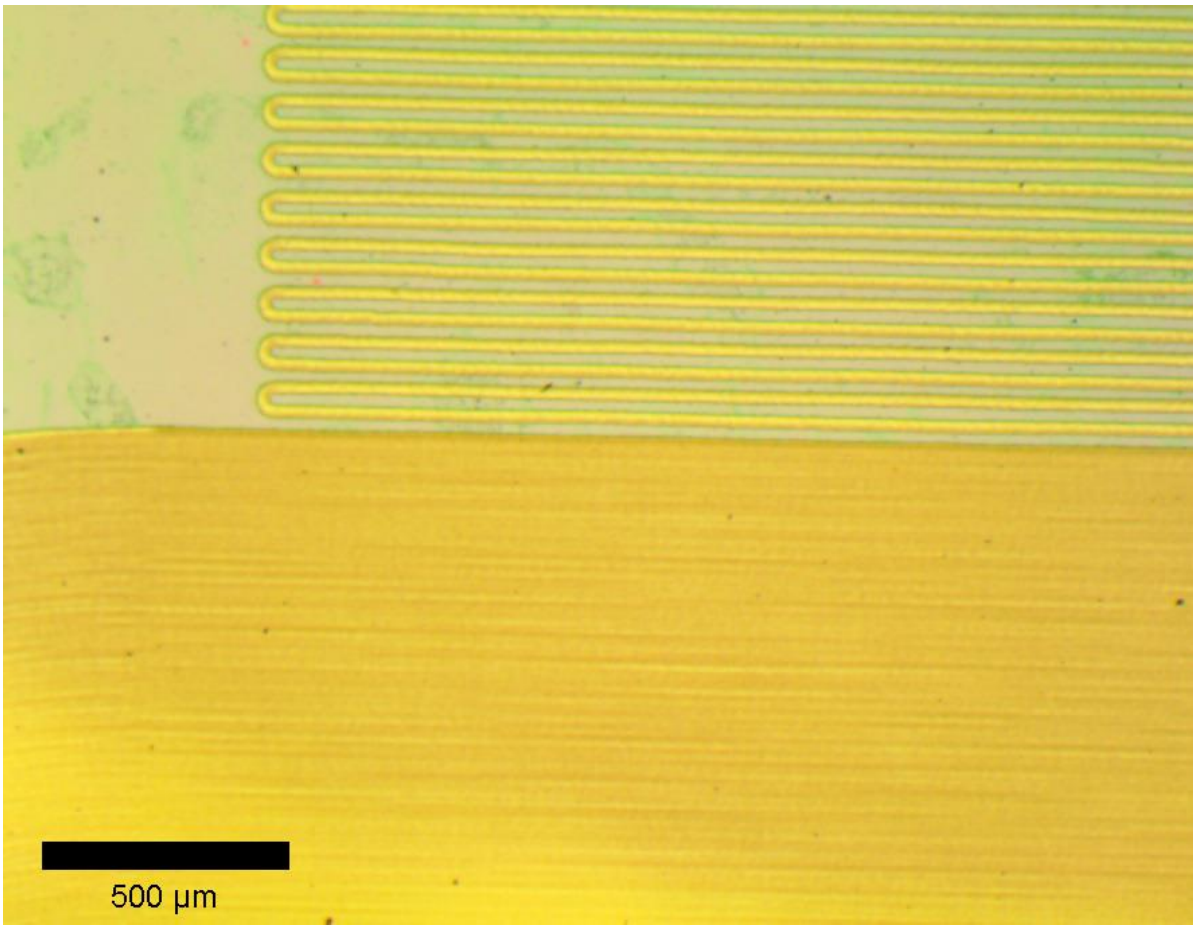

Figure 39 - Detail of interdigitated ITO electrode scribed by laser ablation from 350 nm ITO film on glass.

3.4.2 Atomic Layer Deposition

TTIP / glycine and $CaCO_3$ films were deposited on glass slides with ITO electrodes by ALD technique in an ASM Microchemistry F - 120 Sat reactor. They were chosen to attempt to enhance biocompatibility, make the substrate surface uniform, and for the convenience of using materials tried, tested, and available in the ALD laboratory – the TTIP/glycine procedure has been extensively explored by Leva Momtazi in her ongoing PhD work. Hybrid films made from TTIP and lysine have been demonstrated as being biocompatible and facilitate cell growth [87]; glycine is similar to lysine and was expected to enable cell growth similarly as well as retaining the biocompatibility. The biocompatibility of $CaCO_3$ has been demonstrated in regards to bone cells [88], as well as its natural occurrence as the main ingredient in shells of sea shells and snails.

The ALD cycle of TTIP/glycine:

1. TTIP and N_2 carrier gas pulse, 1.5 seconds.
2. TTIP purge / N_2 flush, 1 s.
3. Glycine pulse, 2 s.
4. Glycine purge / N_2 flush, 1 s.

The reaction chamber held a temperature of 225 °C and a pressure of 3 mbar, and 400 cycles were performed.

The ALD cycle of $CaCO_3$ deposition:

1. $Ca(thd)_2$ pulse, 1.5 s.
2. $Ca(thd)_2$ purge / N_2 flush, 1 s.
3. O_3 pulse, 2 s.
4. O_3 purge, / N_2 flush, 1 s.
5. CO_2 pulse, 2 s.
6. CO_2 purge, / N_2 flush, 1 s.

The reaction chamber held a temperature of 250 °C and a pressure of 3 mbar, and 1000 cycles were performed.

After the measurements of the $CaCO_3$ film were complete, two additional ALD treatments were done on electrode slides to investigate the effect of O_3 and heat treatment. The first of these ran the $CaCO_3$ deposition program, with the $Ca(thd)_2$ and CO_2 supplies blocked, i.e. only the O_3 pulses were performed. The second ran the $CaCO_3$ deposition program with all supplies shut off. Both treatments included the heat treatment of the program.

The films were measured with a J. A. Woollam spectroscopic ellipsometer, model alpha-SE, using a model based on the Cauchy function to extract thickness, by placing small slides of Si near the electrode slides in the ALD chamber, and measuring the films on the Si slides.

3.4.3 3D Printing

Plastic parts for the different design iteration were produced in ABS plastic with an Ultimaker 2+ 3D printer using 100 µm print lines. 3D printed plastic is porous and not waterproof, so the plastic was not suitable as cell culture well or lid; when it was used for the well, medium leaked out, and when used for the lid, the medium evaporated rapidly.

3.4.4 Glassware

The culture well and well lid of the sensing device were produced at the UiO Chemistry Department glassblower's workshop. The well was cut to 10 mm length from a 9 mm SiO_2 glass tube with 6.5 mm inner diameter. The lid was cut from a 13 mm SiO_2 glass tube with inner diameter of 10 mm, and closed off at one end.

3.4.5 Assembly

The sensing device (Figure 40, Figure 41) was easy to assemble without breaking anything, and was held together mechanically in all places except where the cell culture well was fixed to the electrode glass slide with silicone.

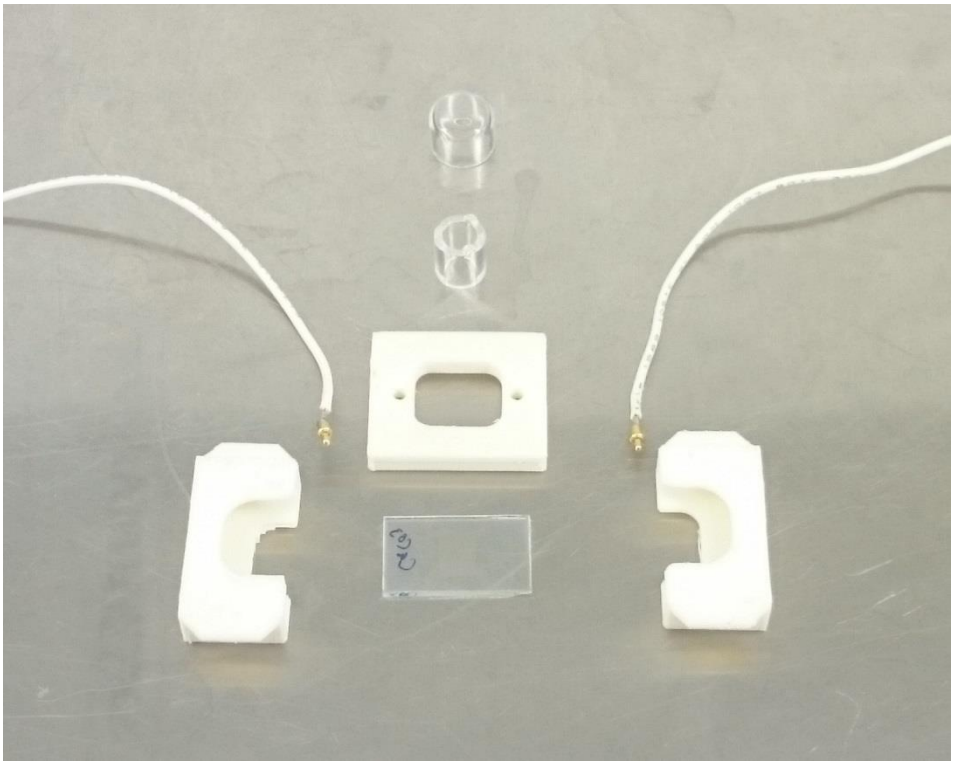

Figure 40 - Cell culture impedance sensing device, before assembly. Compare with 3D model in Figure 32.

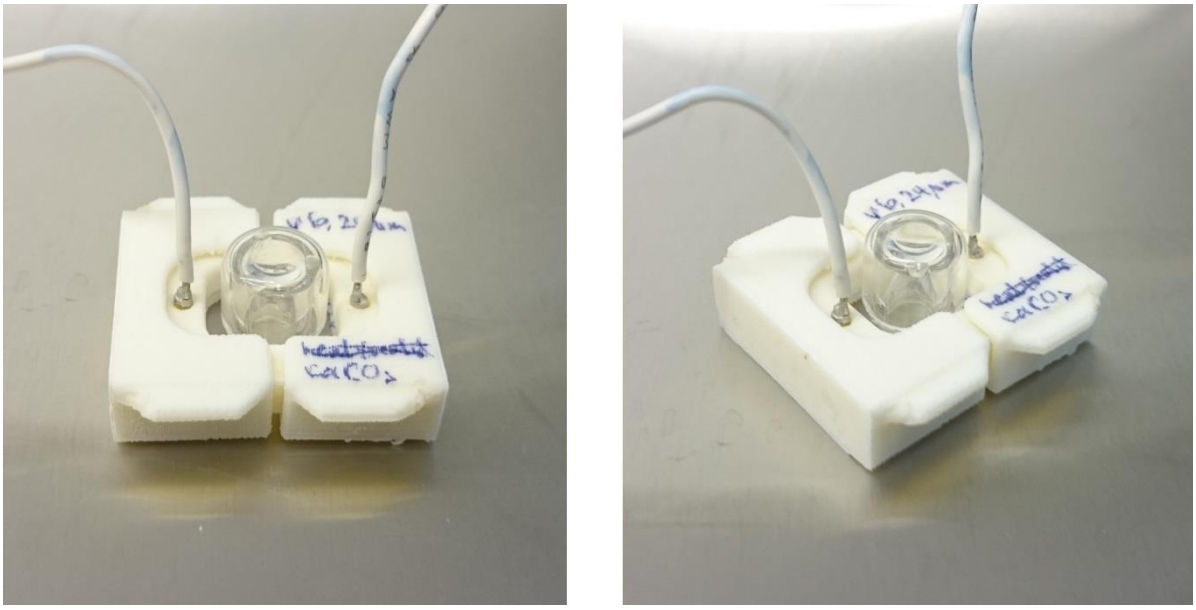

Figure 41 - Cell culture impedance sensing device, assembled. Compare with 3D model in Figure 32.

3.4.6 Cell Culture

The cells used in this project are from the ARPE-19 line, provided by Oslo University Hospital. All work with the cells was performed in a Kojair KR-105 Class II microbilogical safety cabinet.

The culture was maintained in Thermo Scientific Nunc^{TM} filter cap EasYFlasks of 75 cm^2 and 25 cm^2, which were kept in a ThermoForma Series II Water Jacketed CO_2 Incubator at 37 °C and 5 % CO_2. The area value of the EasYFlasks indicates the area available for cell culture in the flask, i.e. the flat bottom of the flask when it is lying down. One 75 cm^2 flask contained a culture which was kept going continuously as a backup culture, while one 75 cm^2 flask and one 25 cm^2 flask were repeatedly trypsinated and split, according to the procedure in section 2.3.8.2, for sensing device experiments. The culture medium used was Dulbecco's modified Eagle's medium with Ham's F-12 nutrient mixture (DMEM), with 10 % fetal bovine serum (FBS) from Gibco and 1 % antibiotic P/S Solution from ScienCell, containing penicillin and streptomycin. The buffer used in medium exchange and culture splitting was Dulbecco's phosphate-buffered saline (DPBS).

Cell cultures were observed in a

3.4.6.1.1 Exchanging Cell Culture Medium

Exchange of cell culture medium was performed as described in section 2.3.8.3, using DMEM and DPBS, and was performed every 2 or 3 days, using 15 ml medium in the 75 cm^2 flasks and 5 ml in the 25 cm^2 flasks. In one instance, because of holidays, the cells were given 150 % of the normal amount of medium, i.e. the 75 cm^2 flask was given 22.5 ml medium, and the 25 cm^2 flask was given 7.5 ml, and left to themselves for 8 days; the cultures survived this.

3.4.6.1.2 Splitting the Cell Culture

The protocol in section 2.3.8.2 was followed. The cultures were split in 1:2 ratios, to facilitate quick confluence in the new cultures. According to McAteer and Davis, a 1:2 split ratio will usually result in a confluent culture after approximately 3 days [46]. Splitting was performed with 0.25 % Trypsin-EDTA (1X) from Gibco. 5 ml was used for the 75 cm^2 flasks, 2 ml for the 25 cm^2 flasks. The cells were usually confluent 3-5 days after splitting (Figure 42).

The first cultures were centrifuged in a Hettich Rotofix 32 centrifuge after splitting. The resulting cultures struggled with clustered cells. Re-pipetting was attempted, and reduction of the centrifuge time, but the clustering remained an issue. Eventually, the was changed, skipping the centrifuging and using 5 times as much medium as trypsin to neutralise the trypsin as described in section 2.3.8.2. This resulted in quickly confluent cultures with few clustering issues.

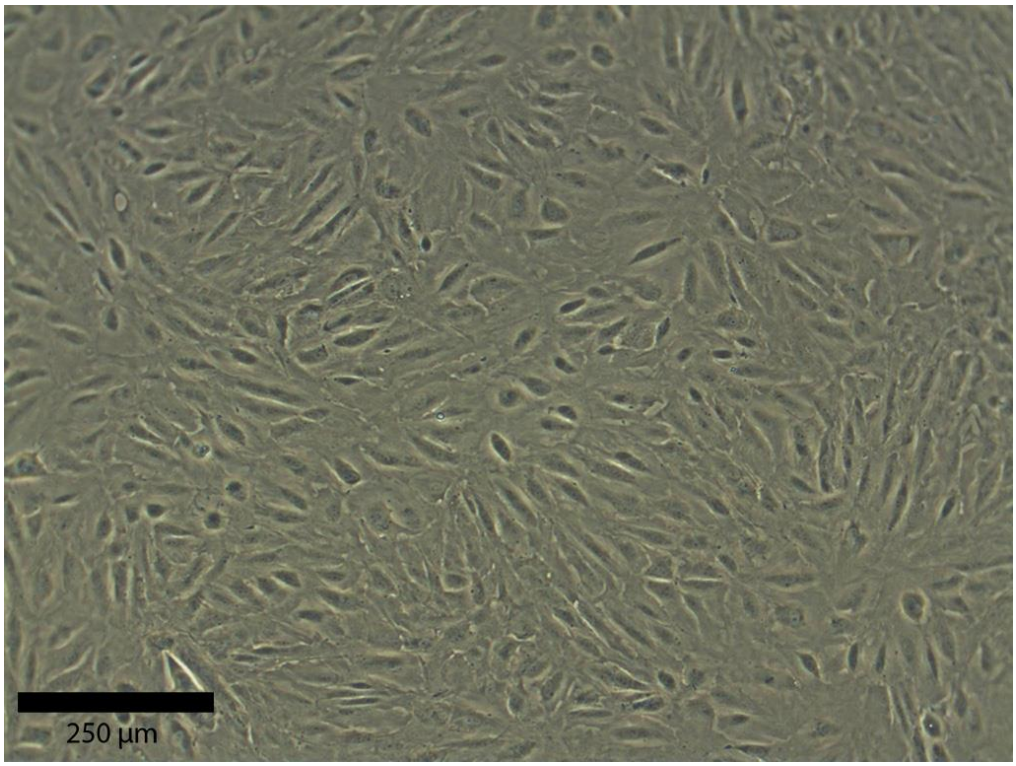

Figure 42 - Confluent ARPE-19 cells (passing #2) 4 days after culture splitting.

3.4.6.1.3 Toxicity Tests

Toxicity tests were performed for ARPE-19 culture with 5 different adhesives: Pattex "No More Nails" construction adhesive, Casco "Silikon" filler silicone, Loctite "Power Epoxy Universal" two-component adhesive, JBL Haru "Universal Adhesive" aquarium adhesive, and DL Chemicals "Parasilico" aquarium silicone. The aquarium adhesive and silicone were procured and tested after the other three products had been tested and proved inadequate.

In the first round of tests, the products from Pattex, Casco and Loctite were tested in 25 cm^2 cell growth flasks, each with a smear of one of the adhesives, cells proliferated reasonably well. A 3 cm^2 smear of epoxy or filler silicone hardly inhibited cell proliferation, while a similar spear of construction adhesive caused cells to only grow at a distance – approx. 2 cm – from the smear. A 0.5 cm^2 smear of these adhesives in the same type of flask did not affect cell proliferation significantly, and some cells even attached on top of the smears and grew there. See Appendix E for some notes on the survivability of the ARPE-19 cells over time in the toxicity tests.

When the construction adhesive, epoxy and silicone were utilised in the sensing device, cells did not attach or survive. When a 6.5 mm diameter glass well was attached to the bottom of commercially acquired plastic cell growth wells with either of those 3 adhesives, the cells did not attach, and consequently died. Control groups of cells in 6 mm diameter commercially

acquired wells proliferated well. The “smear test” was evidently not usable in this context and was discarded as a toxicity test method.

The second round of toxicity tests only included aquarium adhesive and aquarium silicone, and were performed only with glass wells fixed with adhesive or silicone to the bottom of a cell culture vessel; not with a smear inside a culture vessel. They both allowed cell attachment and proliferation both when fixed to the bottom of commercially produced cell culture vessels and when used in the sensing device.

3.4.6.1.4 Observation

The cells were observed and photographed using a Nikon Diaphot ELWD 0.3 phase contrast microscope.

3.4.7 Cell Culture in the Sensing Devices

For the cell culture wells used in this thesis, which measured 6.5 mm across, the appropriate amount of medium is $(0.25 \pm 0.05)\ \mathrm{ml/cm^2} * (0.325\ \mathrm{cm})^2 \cdot \pi = 0.083\ \pm 0.017$ ml, resulting in a medium depth of 2.5 ± 0.5 mm. 0.10 ml was used as the standard for the 6.5 mm diameter wells of the sensing device for a medium depth of 3 mm. Due to rapid evaporation of medium in early experiments, a couple of runs with double the amount was attempted, i.e. 0.20 ml, was performed, but cells would not proliferate under those conditions.

Cells were split in a 1:2 density from a confluent culture, and were seeded with this density.

3.4.8 Impedance sensing

Impedance measurements of the cell cultures were made with a Sciospec single channel impedance analyser ISX-3v2, which is capable of impedance measurements at frequencies up to 20 MHz, but proved to be unreliable above 1 MHz. It was connected via shielded cables and crocodile clips to the 10 cm wires of the cell culture impedance sensing device.

3.5 Measurements

3.5.1 ALD Coating

Both ALD deposition procedures involved in this project had 1 x 1 cm^2 Si control slides accompanying the substrates in the ALD chamber, to check the film thickness.

The thickness of the TTIP/glycine film was measured to 50.0 ± 5.0 nm, the $CaCO_3$ film to 43.2 ± 0.7 nm. The resistivity of the TTIP/glycine film was measured to 0.0085 ± 0.0025 Ω·cm.

3.5.2 Impedance Measurement Parameters

Of particular concern was noise in the system. After several failed experiments, it was evident that only short, shielded cables would be adequate in order to sufficiently reduce the signal noise level. The length of the wires connecting the sensing device to the impedance analyser was consequently reduced to a length where measurements could be performed adequately in the expected dispersion range, 3 kHz to 400 kHz.

3.5.3 Influence of Medium on Measurements

The medium composition and volume may significantly influence measurements. As time passes after a medium change, cells extract nutrients from the medium and excrete waste products into it, changing the ion content of the medium. Evaporation reduces the volume and increases the ion concentration (by reducing the water content) in the medium, both affecting the impedance of the medium. To minimise the influence of varying medium amount, measurements were performed immediately after a medium change.

3.5.4 Sensing Device Variations

All measurements were made in a cell culture well with a 6.5 mm diameter. Most experiments were unsuccessful in the sense that sufficient measurements of the cells could not be performed, for various reasons, including: the cells remained unattached and died due too inadequate ventilation or toxic adhesive; medium evaporated and cells died from dehydration and lack of sustenance; medium leaked out due to adhesive failure and cells conversely died.

The list of different electrode configurations for which experiments were conducted successfully is:

1. Electrodes with 24 µm wide digits.
2. Electrodes with 192 µm wide digits.
3. Electrodes ALD-coated with a 50 nm thick TTIP/glycine nanofilm.
4. Electrodes ALD-coated with a 40 nm thick $CaCO_3$ nanofilm.
5. Electrodes drip-coated with collagen.
6. Heat-treated electrodes, to match heat treatment during ALD process.

2 was produced using an alternative laser scribing pattern where the digit thickness and spacing were increased to 192 µm, while the overall electrode length and width was retained. # 3 and # 4 were coated by ALD technique as described in section 3.4.2. # 5 was prepared by placing a drop of collagen diluted to 1 vol. % in water on a chilled electrode plate and letting it dry. # 6 was produced by subjecting the slide to only the temperature treatment of the ALD process used for # 3 and # 4

Impedance measurements were made:

- without anything in the cell culture well.
- with only medium in the cell culture well.
- with cells, immediately after changing medium if being performed on a medium change day.

For measurements between 2 MHz and 20 MHz the impedance analyser returned phase values of below $-\pi$, which is below the phase angle of a purely capacitive system. The measurements for frequencies above 1 MHz were therefore regarded as unreliable and not included in the following plots.

3.5.5 Cell visibility

The cells were more difficult to discern on the glass/ITO surface than on the plastic surface of the EasYFlask culture vessels. Not only because of the added visual element of the ITO electrode digits, but also by a significant reduction in contrast for the cells (Figure 43). The cell cultures were maintained until their density was indiscernible from 100 % confluence, but since it is hard to discern between degrees of confluence from approximately 80 % to 100 %, a "90 % confluence" has been used in the results section.

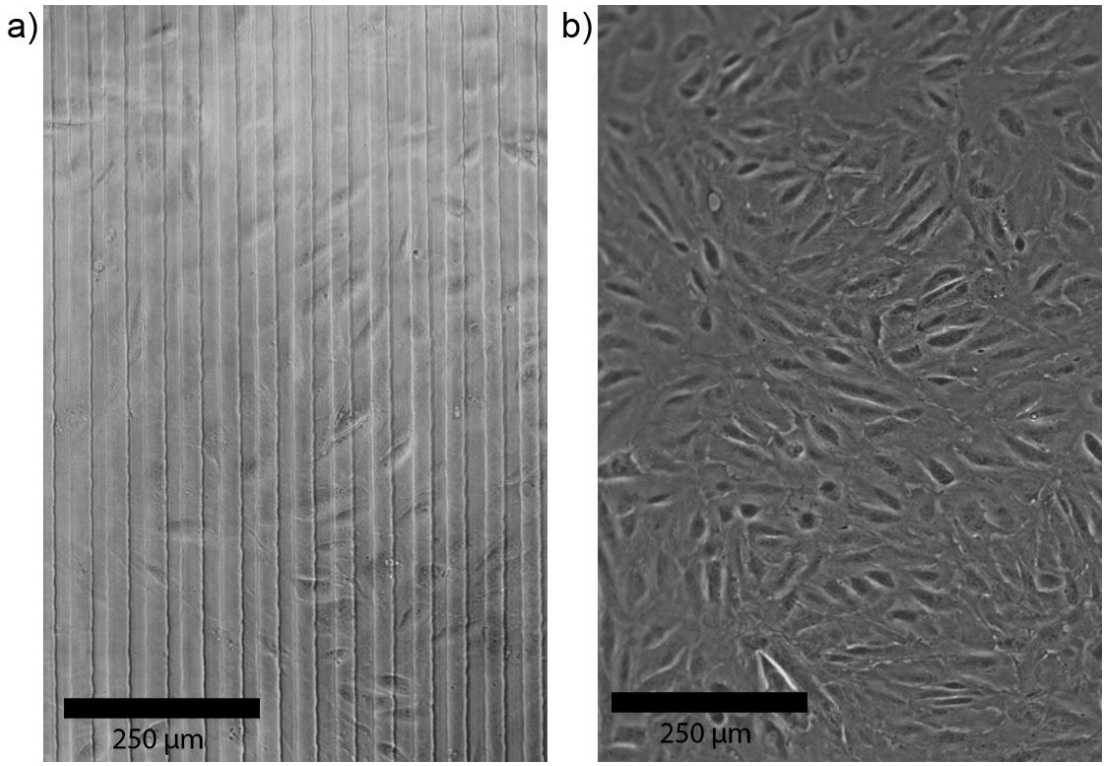

Figure 43 - Cells in a) cell culture impedance sensing device with ITO electrodes and b) EasYFlask culture vessel.

3.5.6 Impedance ARPE-19 Cells on ITO Electrodes, 24 µm digits

The culture seeded directly on ITO electrodes was measured before attachment and while proliferating, until the culture reached approximately 90 % confluence after 14 days (Figure 44), and measurements were made at the time of seeding, during growth and at the end of the

experiment run with the parameters described in section 3.5.2. Cells from the same passing, seeded in a cell culture flask, were confluent after 7 days.

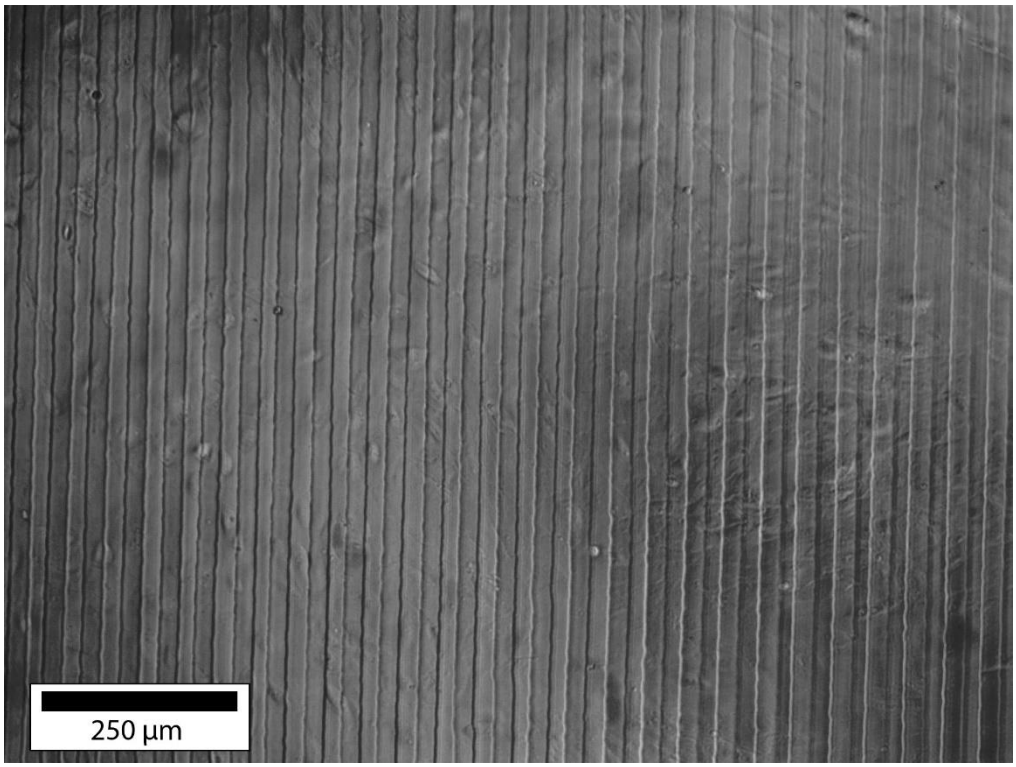

Figure 44 - ARPE-19 cells growing on interdigitated ITO electrodes on glass.

The impedance analyser measures the real and imaginary parts of the impedance[7] **Z** (Figure 45, Figure 46).

[7] When doing a series of sweeps with a time delay inbetween, the impedance analyser records |**Z**| and phase.

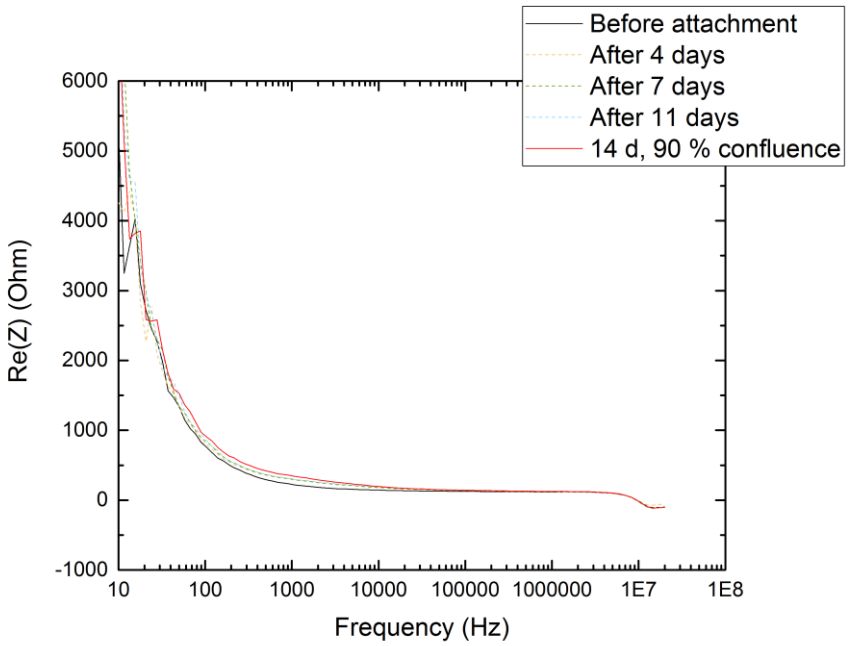

Figure 45 - Impedance measurement of ARPE-19 cells over 14 days. The real part of the impedance of the current vs its frequency.

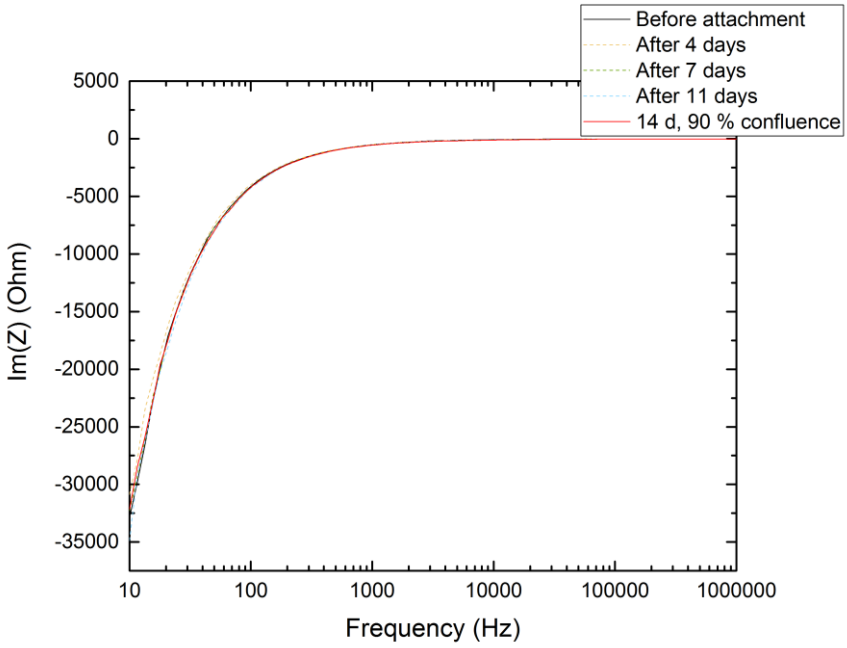

Figure 46 - Impedance measurement of ARPE-19 cells over 14 days. The imaginary part of the impedance of the current vs its frequency.

The absolute value of the impedance, $|\mathbf{Z}|$ (Figure 47), is found by the equation

$$|\mathbf{Z}| = \sqrt{(\mathrm{Re}(\mathbf{Z}))^2 + (\mathrm{Im}(\mathbf{Z}))^2} \qquad (17)$$

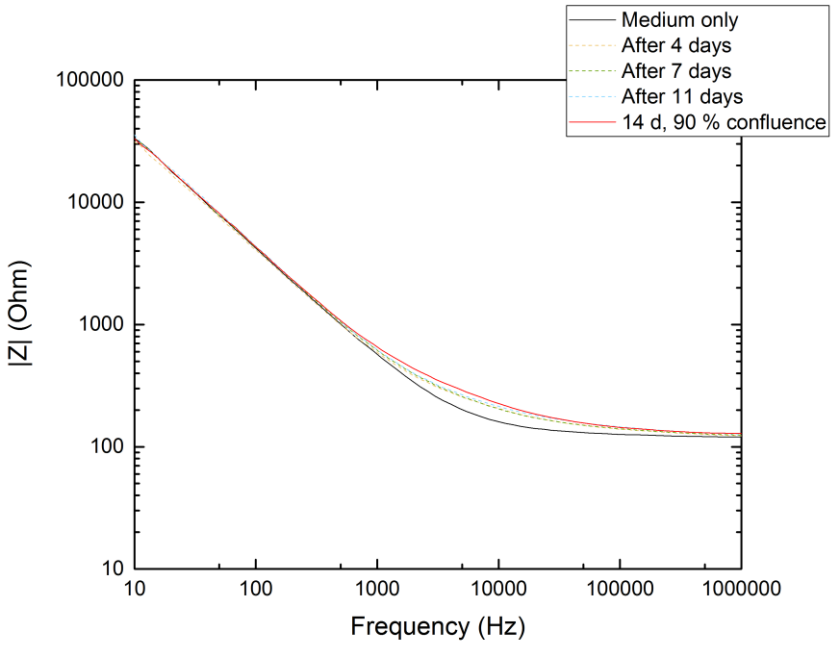

Figure 47 - Impedance measurement of ARPE-19 cells over 14 days. |Z| vs frequency.

A plot in the expected dispersion frequency range may make trends in this range more visible (Figure 48).

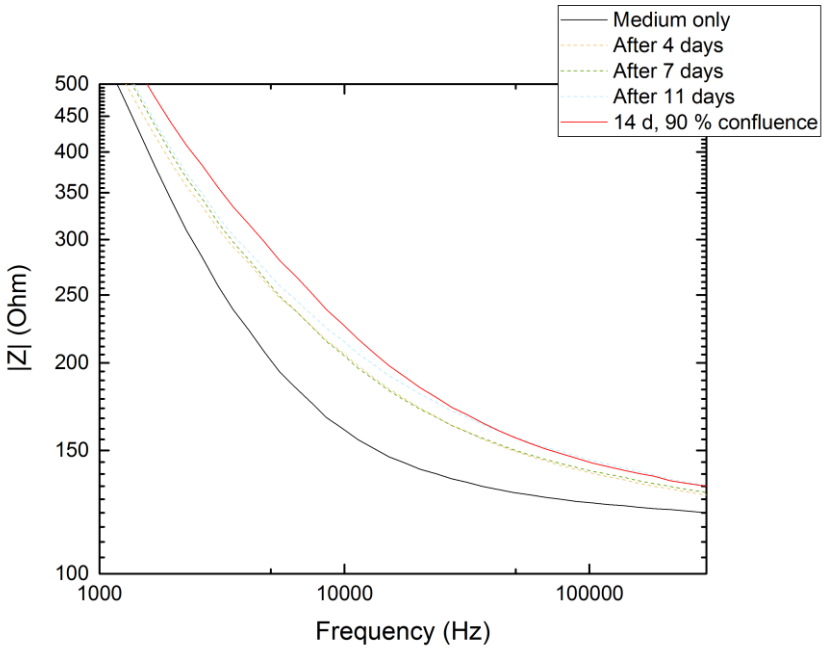

Figure 48 - Impedance measurement of ARPE-19 cells over 14 days. |Z| vs frequency in expected dispersion range.

Calculations for the difference $|\mathbf{Z}|_{diff}$ between the frequency-dependent impedance absolute values at maximum cell layer confluence $|\mathbf{Z}|_{cf}$ and for medium only $|\mathbf{Z}|_{m}$, so that

$$|\mathbf{Z}|_{\mathrm{diff}} = |\mathbf{Z}|_{\mathrm{cf}} - |\mathbf{Z}|_{\mathrm{m}} \quad (18)$$

are included for the different sensing device variations and plotted in (Figure 49).

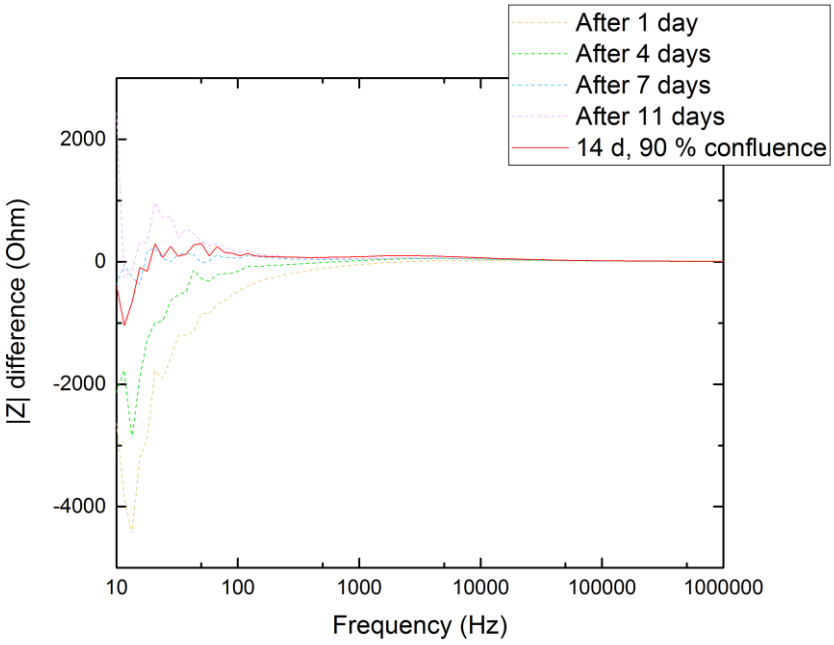

Figure 49 - |Z| difference between sensing device with and without ARPE-19 cells. Measurements below 1 kHz have large differences; the |Z| values in this frequency range were also large, cfr Figure 47.

Limiting the |**Z**| difference plot to the frequency range of the expected dispersion (section 3.2.1.3, Figure 27) might give some insight into whether an influence from the cells can be gleaned (Figure 50). In these measurements, a dispersion similar to the one found by Onnela *et al*. [76] is discernible.

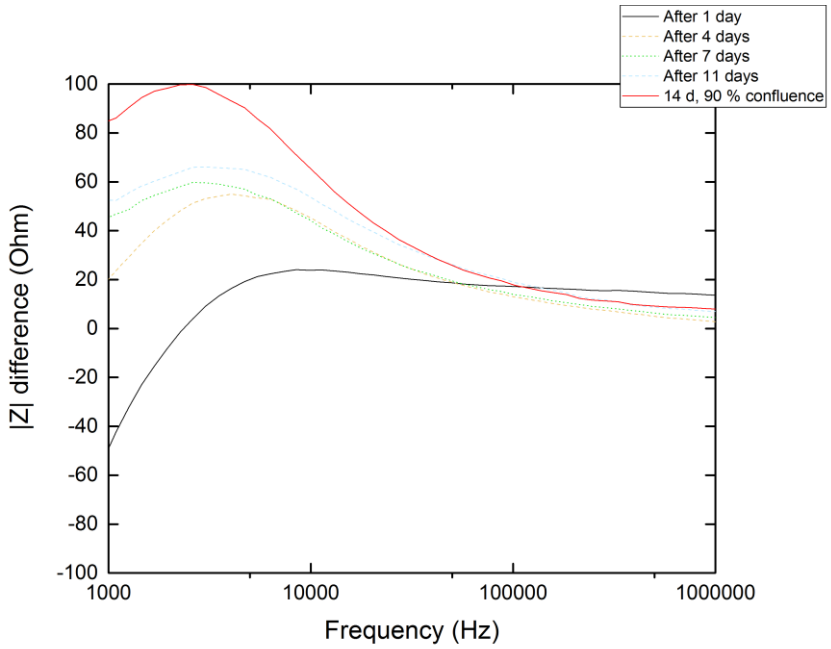

Figure 50 - Difference in |Z| between ARPE-19 cells in medium and medium only, in the expected dispersion frequency range, approximately 3 kHz to 400 kHz (Section 3.2.1.3, Figure 27).

The phase ϕ of the current (Figure 51) can give some insight into what capacitive elements are present in the system, and is found by the equation

$$\varphi = \operatorname{atan}\left(\frac{\operatorname{Im}(\mathbf{Z})}{\operatorname{Re}(\mathbf{Z})}\right) \tag{19}$$

A negative phase angle indicates that the system has a capacitive element and that this element dominates any inductive elements. A phase angle of $-\pi/2$ indicates a purely capacitive system.

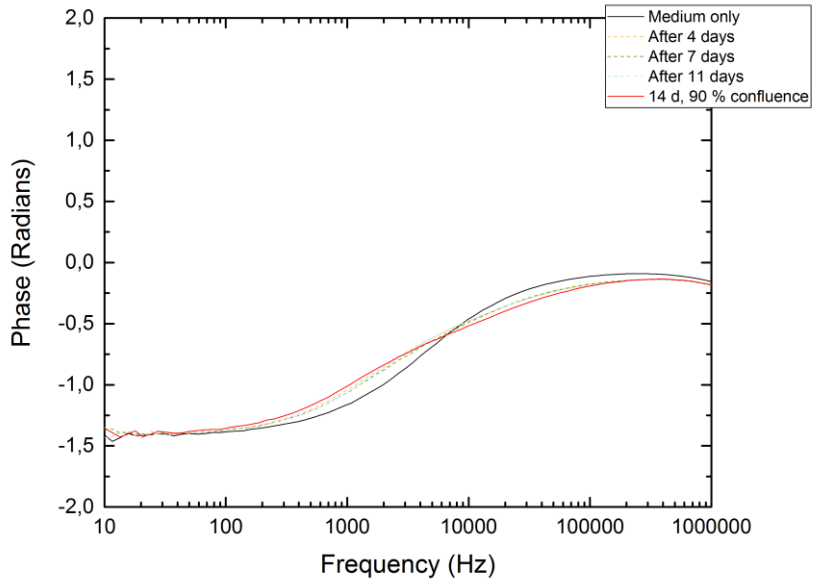

Figure 51 - Impedance measurement of ARPE-19 cells over 14 days. Phase angle vs frequency.

The phase plot indicates that when cells are present, i.e. after 14 days, when the culture was almost confluent, the capacitance of the system below 5 kHz is lower than for the un-seeded system, while at frequencies from 5 kHz to 1 MHz the capacitance is greater, but with a smaller margin when approaching the higher values.

A Nyquist plot is a logarithmic plot of Im(**Z**) vs Re(**Z**) (Figure 52):

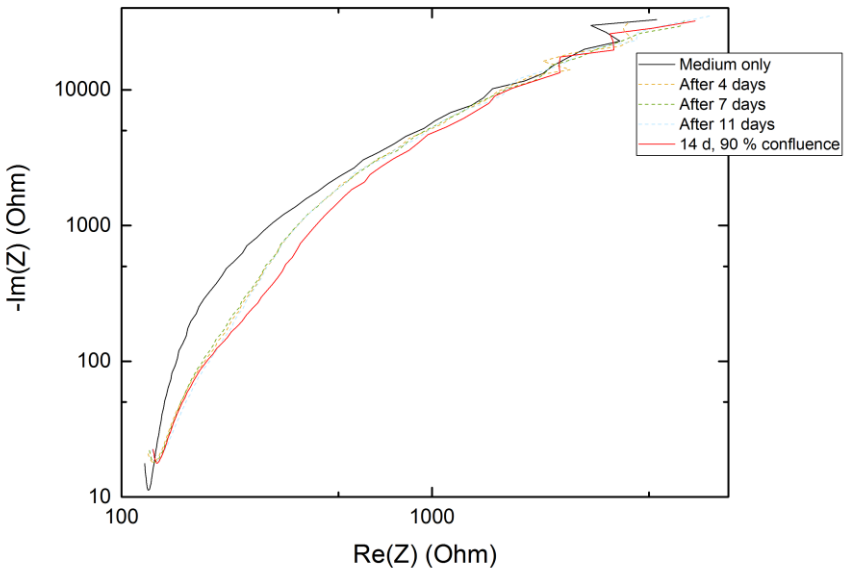

Figure 52 - Impedance measurement of ARPE-19 cells over 14 days. Nyquist plot. Note the negative axis label for Im(Z).

A Nyquist plot of the 90 % confluent cells, with values for medium only subtracted, limited to the expected dispersion frequency range, to give an idea of the characteristic frequency of the cell measurements (Figure 53).

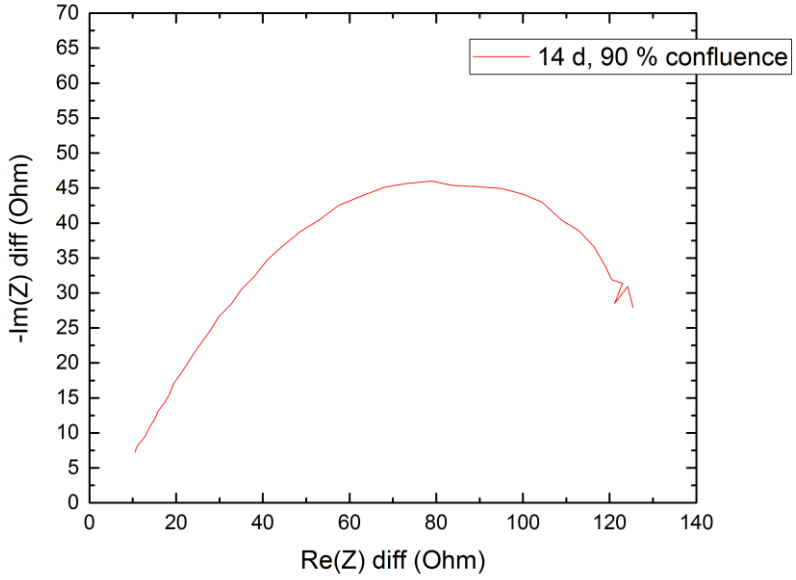

Figure 53 – Difference in impedance measurements of ARPE-19 cells between the initial-cell free measurement and the 14 days old, 90 % confluent culture. Nyquist plot. Note the negative axis label for Im(Z).

The characteristic frequency of the impedance profile, corresponding to the apex of the plot, is at 5.25 ± 1.55 kHz, significantly lower than the value of 19555 Hz reported in Onnela *et al.*'s article [76].

For reference, measurements of impedance for an ITO electrode pair is plotted below, along with the impedance of the wire contact area of one of the electrodes (Figure 54).

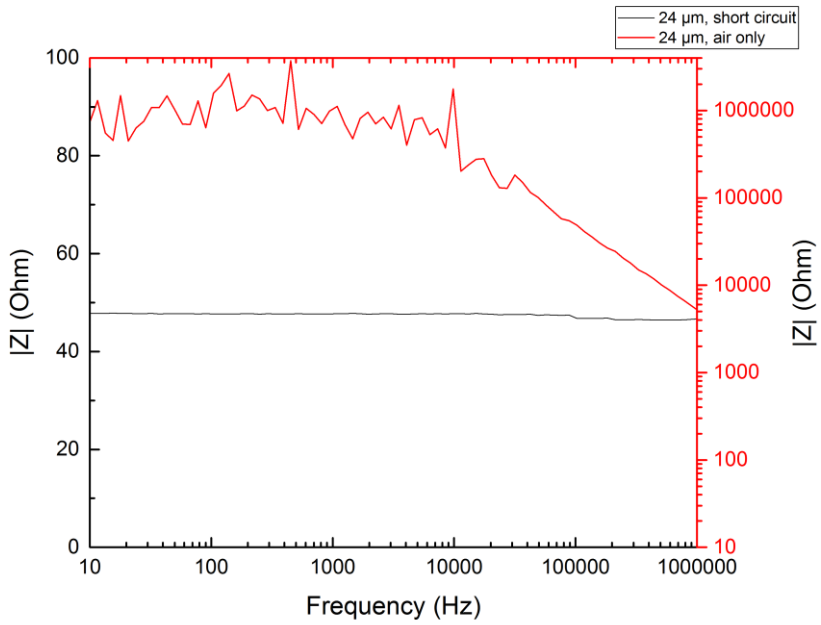

Figure 54 - Impedance of interdigitated ITO electrodes. Measurement of the wire contact area of one electrode in black, corresponding to the left, black, axis. Measurement of the impedance between the electrodes with only air in the cell culture device in red, corresponding to the right, red, axis.

A control experiment was run for another device with the same parameters as the one above (Figure 55, Figure 56).

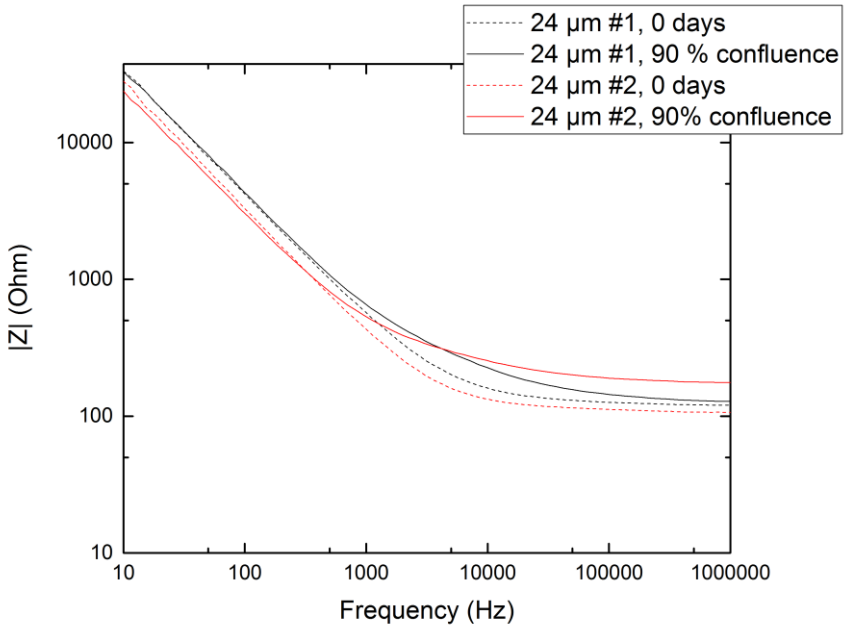

Figure 55 - Impedance measurements of ARPE-19 cells in two separate but identical devices.

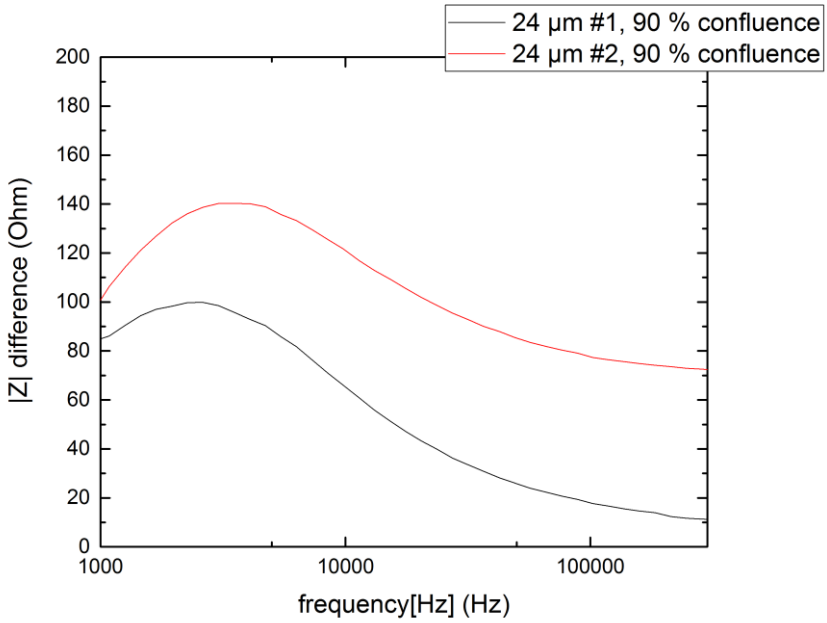

Figure 56 - Impedance measurements of ARPE-19 culture. The difference between the last and the first measurement is shown for each experiment. The axes have been limited to better display the expected dispersion range.

While values differ between the experiments, the trend is similar: a decline in |**Z**| in the expected dispersion range of 3 kHz – 400 kHz.

A comparison between the Nyquist plots for the two different 24 µm-digit electrodes sensing ARPE-19 culture is made in Figure 57.

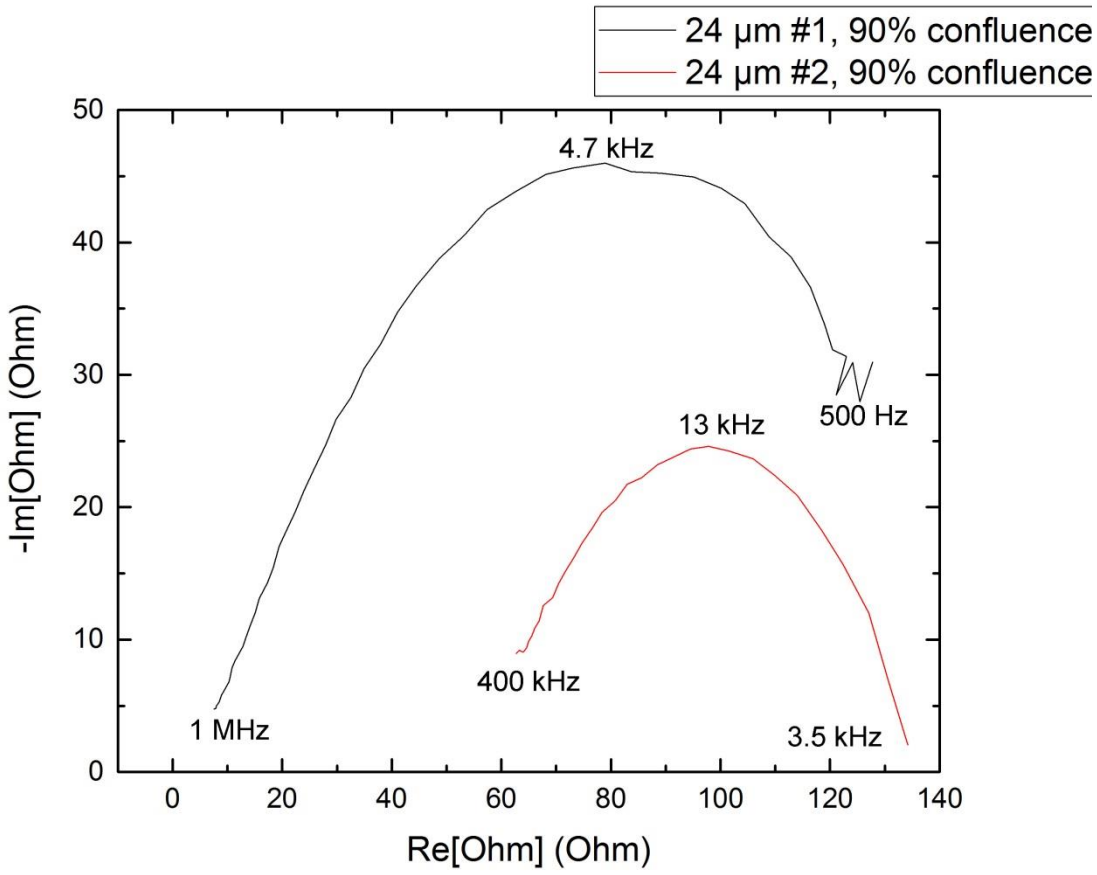

Figure 57 - Nyquist plots for ARPE-19 cell layers in two different sensing devices with 24 µm-digited ITO electrodes. Impedance values for the system (excepting ARPE-19 impedance) have been subtracted to reflect the impedance values of only the ARPE-19 layers.

The Nyquist plots both correspond to Onnela *et al.*'s reported dispersion range of ARPE-19 [76], though the dispersion for the cells in #1 is wider than reported one, as well as a characteristic frequency – 4.7 kHz – considerably lower than the reported in their article, which was 19,6 kHz. #2 shows a dispersion very similar to Onnela *et al.*'s, in almost exactly the same frequency range, but with a slightly lower characteristic frequency at 13 kHz.

3.5.7 ITO Degradation Test

Measurements of a sensing device over time with medium were made to investigate whether degradation of the ITO electrodes was affecting measurements (Figure 58, Figure 59, Figure 60, Figure 61). The Re(**Z**) and Im(**Z**) plots have been omitted from this and the next two sections for the sake of brevity.

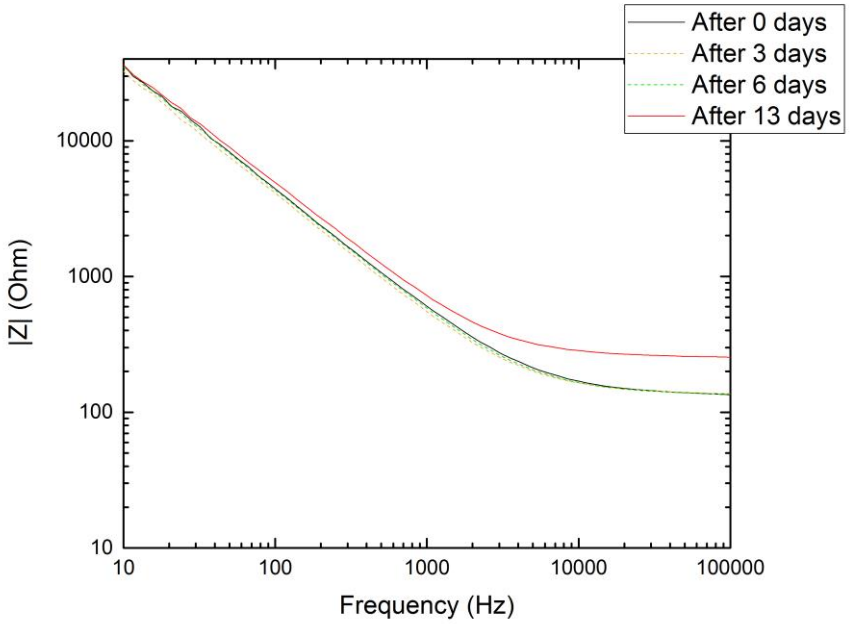

Figure 58 - Impedance measurements of 24 µm-digit interdigitated ITO electrodes with cell culture medium over time to investigate ITO degradation in cell culture medium.

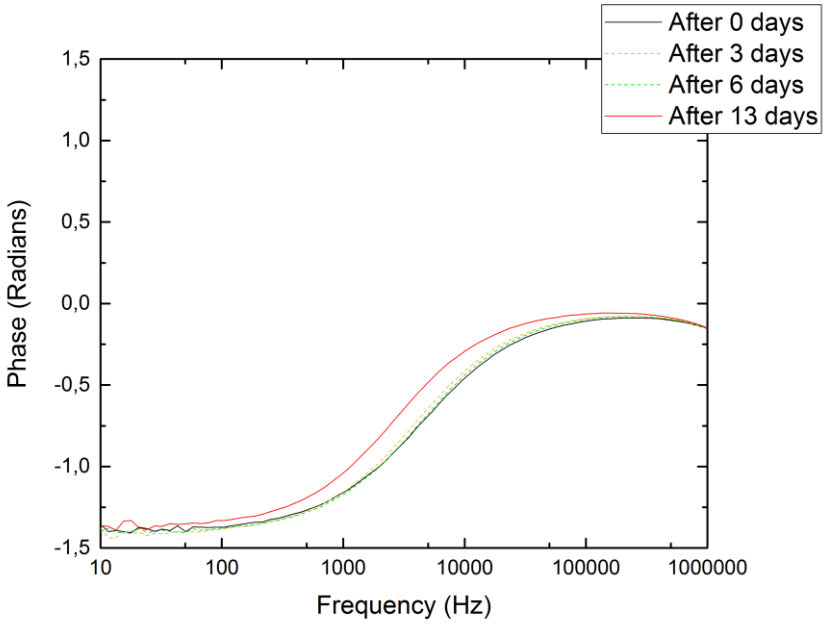

Figure 59 - Impedance measurements of 24 µm-digit interdigitated ITO electrodes with cell culture medium over time to investigate ITO degradation in cell culture medium.

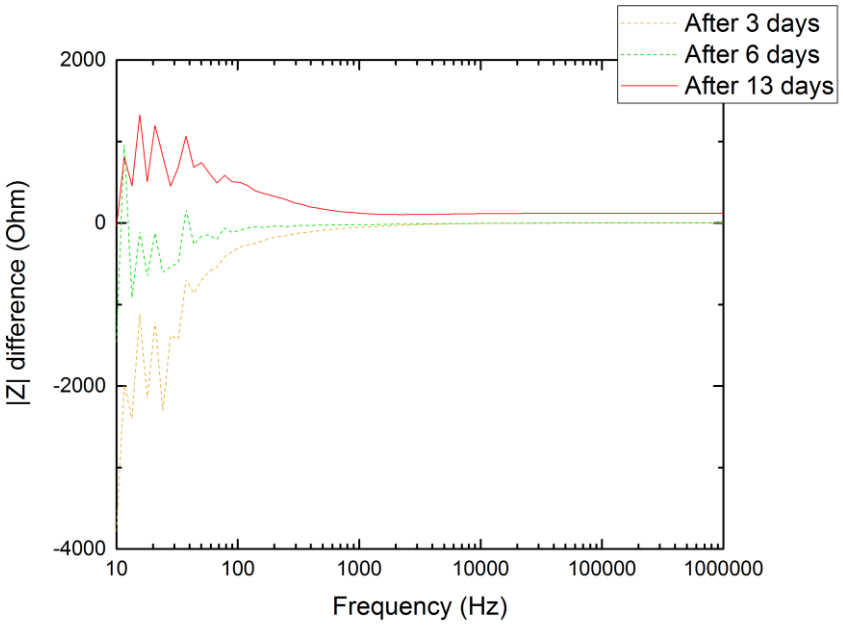

Figure 60 - Difference in |Z| over time for 24 µm-digit interdigitated electrodes with medium only.

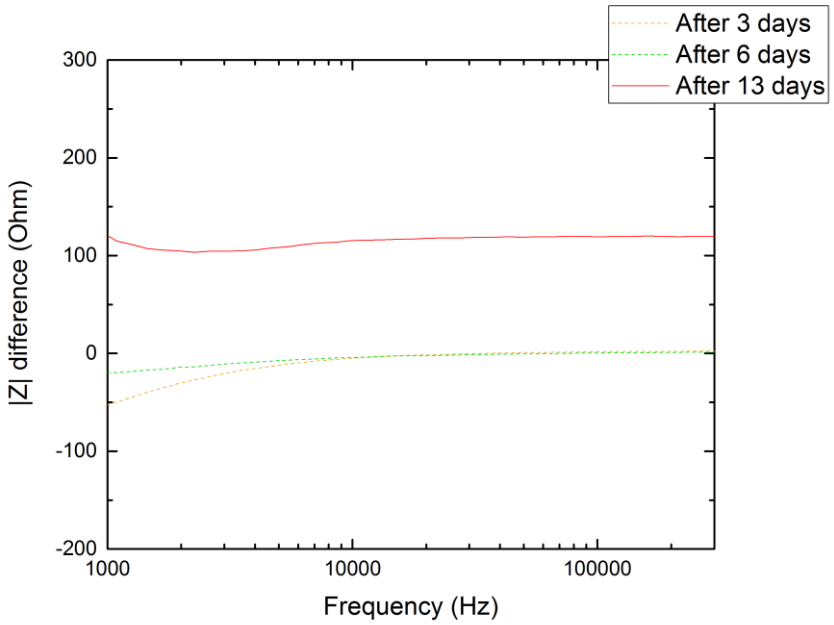

Figure 61 - Difference in |Z| over time for 24 µm-digit interdigitated ITO electrodes with medium only, in the expected dispersion frequency range for ARPE-19 cells (section 3.2.1.3, Figure 27).

Since the ITO impedance increases over time when exposed to culture medium, the increase in impedance in the culture measurements may not be attributable to the cells alone. However, the most significant finding in the $|\mathbf{Z}|_{diff}$ plots is that there is no discernible

dispersion in the expected dispersion range. This indicates that the dispersion measured with cells covering the electrodes is likely attributable to the cells.

3.5.8 Impedance of 192 µm-digit, Collagen-coated and TTIP/glycine-coated Electrodes

For comparison, a sensing device with interdigitated ITO electrodes with 192 µm digit width and spacing was constructed. Cells reached approximately 90 % confluence in 6 days (Figure 62). Another device, with 24 µm digit width and spacing, received collagen coating on the sensing area of the electrodes, and cells reached 90 % confluence after 14 days (Figure 63). Yet another device was ALD-coated with TTIP and glycine, and reached 90 % confluence after 6 days (Figure 64). Their results are combined for brevity.

Cells from the same splitting, seeded in a cell culture flask, were confluent after 4 days.

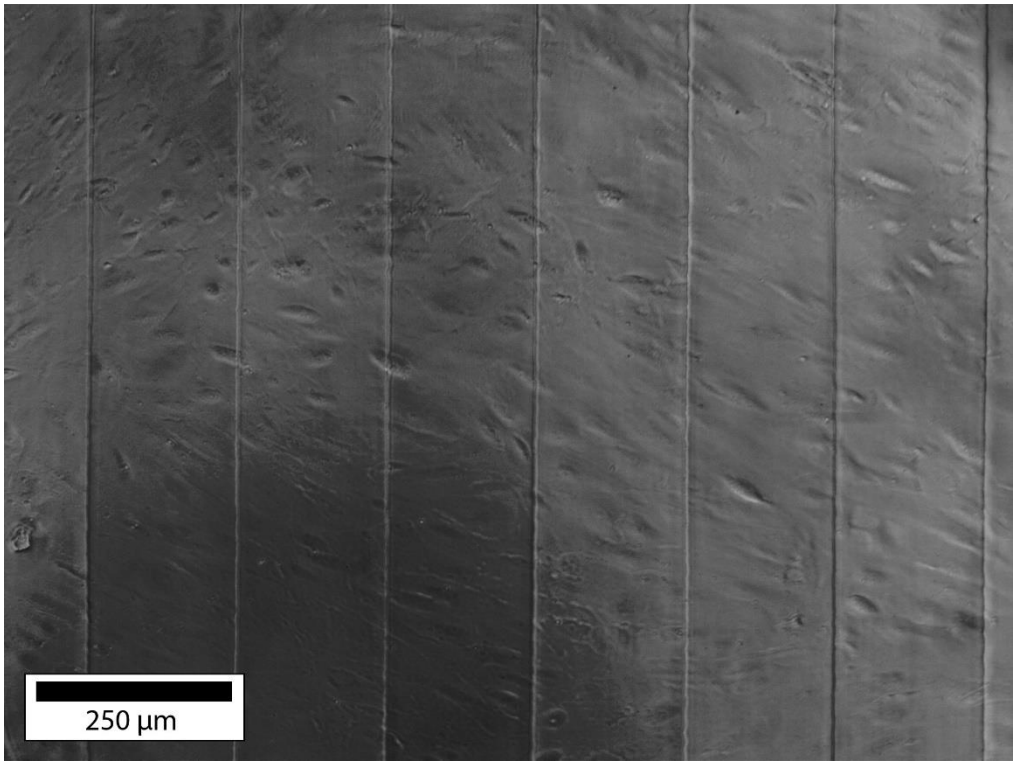

Figure 62 - ARPE-19 cells growing on ITO electrodes with width and spacing of 192 µm, 6 days after seeding.

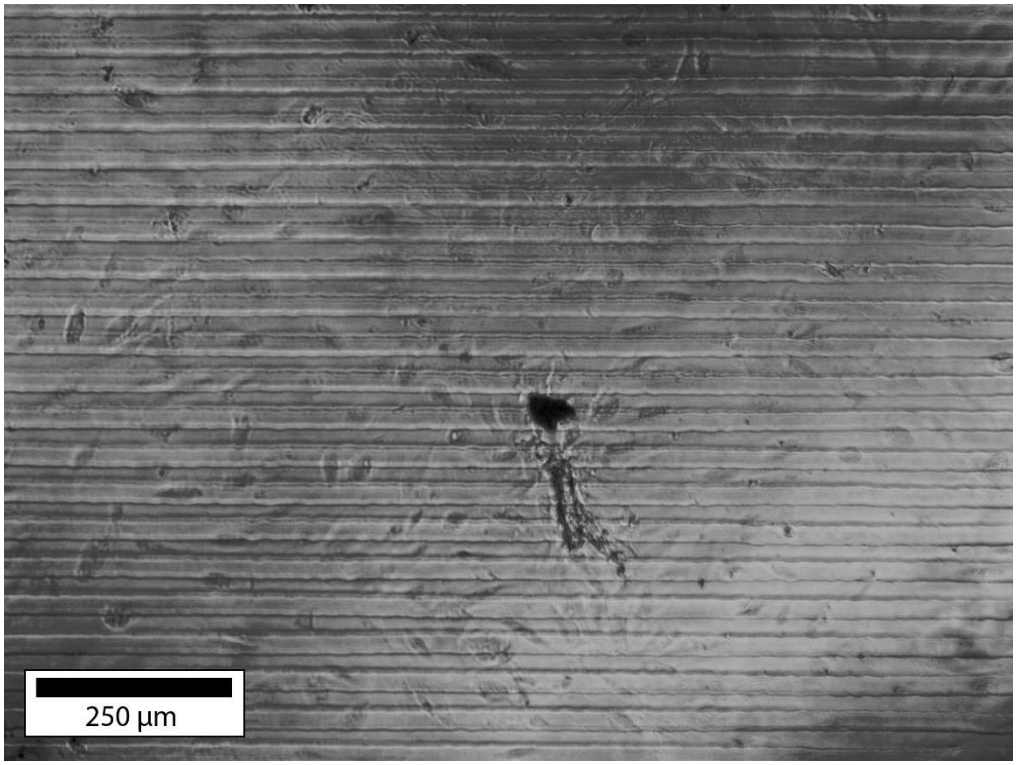

Figure 63 - ARPE-19 cells growing on ITO electrodes with width and spacing of 24 µm and coated with collagen. 14 days after seeding.

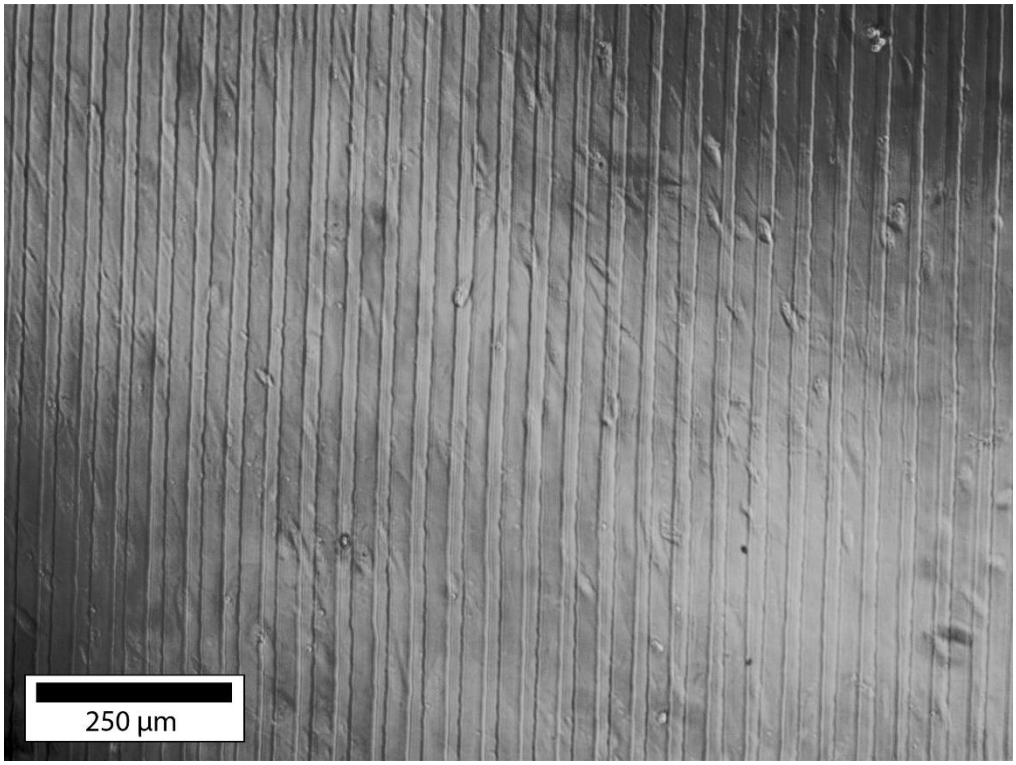

Figure 64 - ARPE-19 cells growing on ITO electrodes with width and spacing of 24 µm and coated with a 40 nm TTIP/glycine film. 6 days after seeding.

Measurements were performed with the parameters described in section 3.5.2. (Figure 65, Figure 66, Figure 67, Figure 68)

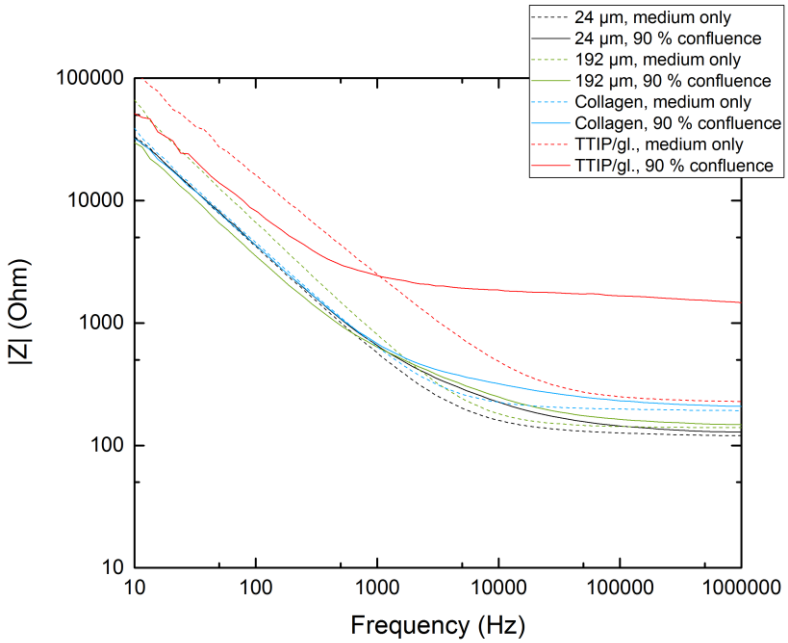

Figure 65 - Impedance measurement of the ARPE-19 culture seeded in a 192 µm-digit cell sensing device, and the 24 µm-digit devices coated with collagen and TTIP/glycine, with the uncoated 24 µm-digit device included for comparison.

For clarity, the values for $|Z|_{diff}$ for these substrates are separated into 2 plots (Figure 66 and Figure 67), since the TTIP/glycine-coated electrode $|Z|_{diff}$ values are considerably higher than for 192 µm-digit and collagen-coated electrodes.

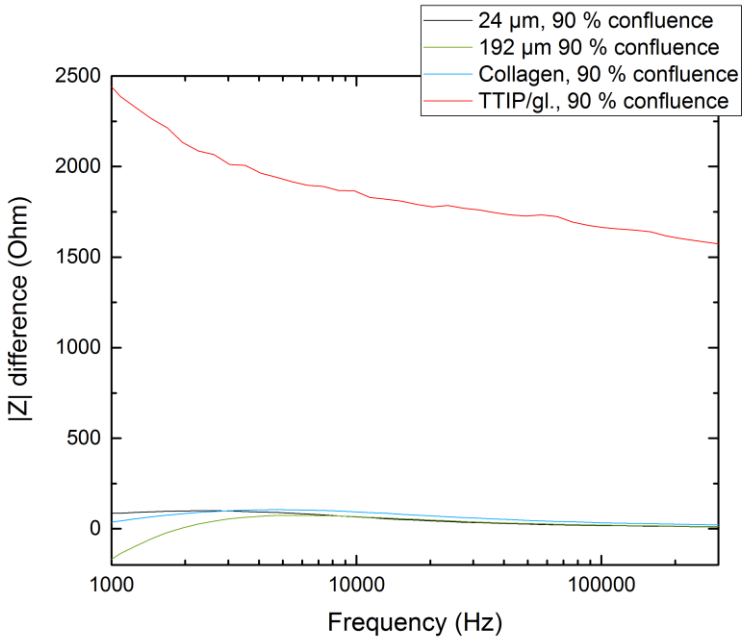

Figure 66 - Impedance measurement of ARPE-19 cultures in the TTIP/glycine-coated device, with measurements of the 192 µm-digit cell sensing device, the 24 µm-digit collagen-coated device, and the uncoated 24 µm-digit device included for comparison. Difference between |Z| values at maximum confluence of ARPE-19 cells and for medium only.

The $|\mathbf{Z}|_{diff}$ values for TTIP/glycine are considerably higher than for the others. There is a dispersion in the expected dispersion range between 3 kHz and 400 kHz, but when compared with the other measurements, the differences in $|\mathbf{Z}|$ are too large to be attributable to the cells alone, though it may be have been caused by modification of the substrate by the cells.

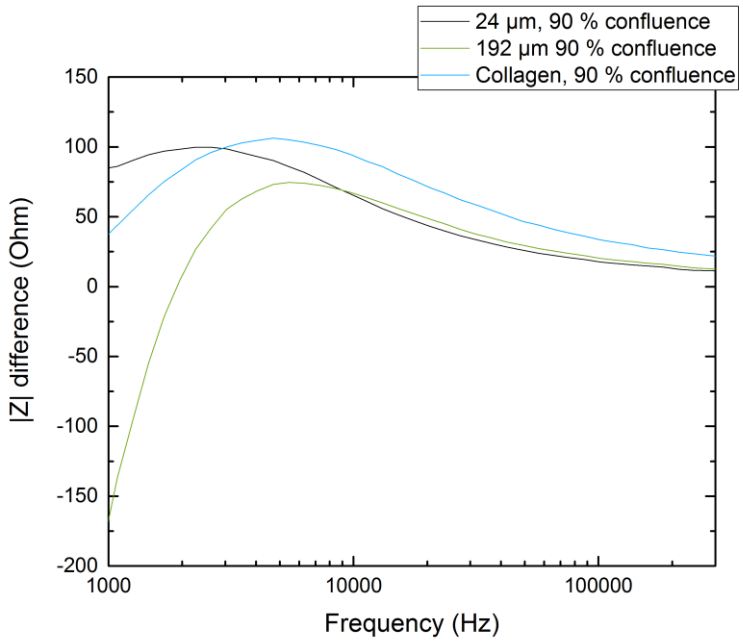

Figure 67 - Impedance measurement of ARPE-19 cultures in the 192 µm-digit cell sensing device and the 24 µm-digit collagen-coated device, with the uncoated 24 µm-digit device included for comparison. Difference between |Z| values at maximum confluence of ARPE-19 cells and for medium only.

The phase plot shows a significantly different capacitive behaviour for the TTIP/glycine-coated electrodes (Figure 68). The phase angle is larger at frequencies between 2 kHz and 900 kHz for the unseeded TTIP/glycine device, and smaller outside of this range. After 6 days of medium and cell exposure, the phase angle drops to significantly lower values for all frequencies below 900 kHz; lower than for the un-coated electrodes. This also points to some kind of modification of the substrate by the medium or the cell layer, as the medium is fresh and the cell layer has been measured to display a different impedance profile.

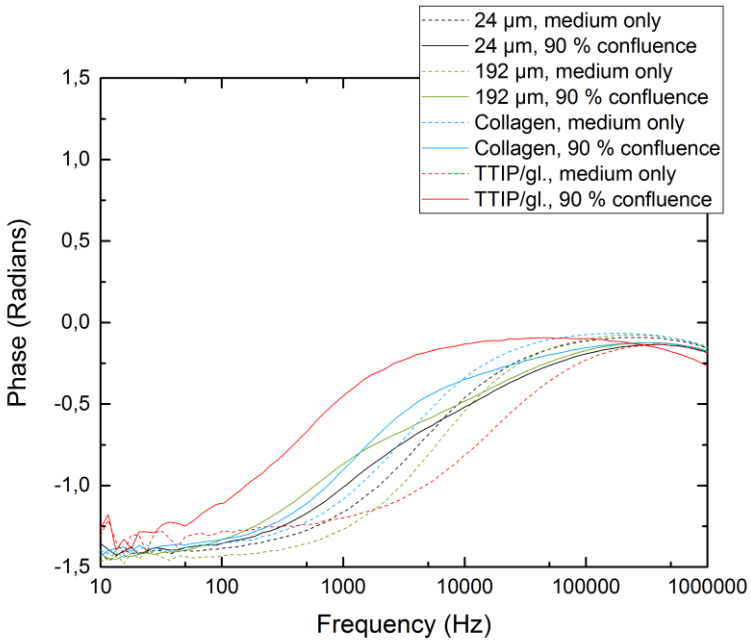

Figure 68 - Impedance measurement of ARPE-19 cultures the 192 µm-digit cell sensing device and the 24 µm-digit collagen-coated device, with the uncoated 24 µm-digit device included for comparison.

3.5.9 Impedance of $CaCO_3$-, O_3- and Heat-treated Electrodes

The ARPE-19 cells attached on the $CaCO_3$-coated electrodes reached 90 % confluence in 6 days (Figure 69) and were attempted measured as described in section 3.5.2. The measurements indicated faulty electrodes, or electrodes that had been short-circuited. The electrodes had been been checked and approved by inspection in optical microscope, and measured before ALD coating, showing a DC conductance in the higher 100 kΩ range, so the decision was made to give an ITO electrode glass slide the same heat treatment as the $CaCO_3$-coated slide, but with the valves for the precursors closed, to ascertain whether the ALD process caused the electrode failure. Inadvertently, the O_3 valve was left open, but the measurements for this slide are significant. Measurements over time of a $CaCO_3$-coated slide with only medium in the culture well were also performed to see if the film was affected by the cell culture medium over time. The results are combined in plots below (Figure 70, Figure 71, Figure 72, Figure 73). Lastly, measurements were made on a slide which had undergone the ALD process but with all valves closed, resulting in a treatment of only the ALD process temperature.

Cells of the same passage but seeded in a cell culture flask, were confluent after 4 days.

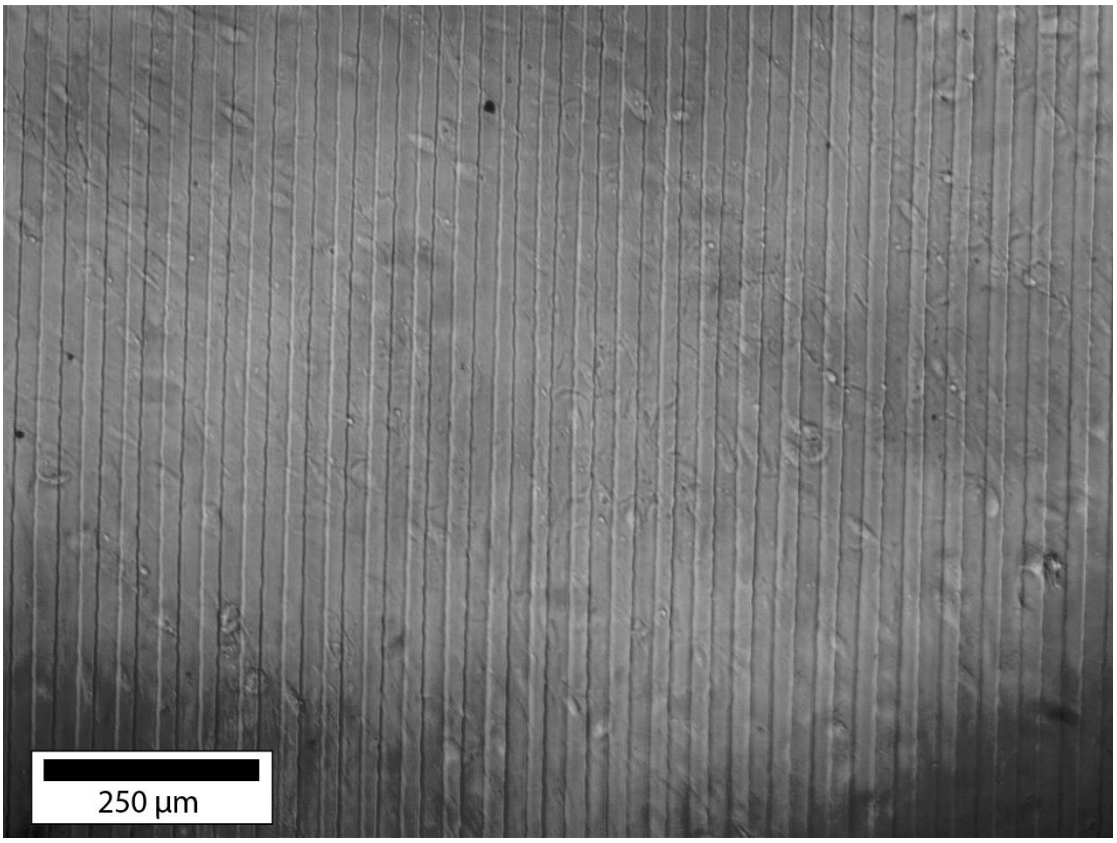

Figure 69 - ARPE-19 cells attached on ITO electrodes coated with $CaCO_3$ film.

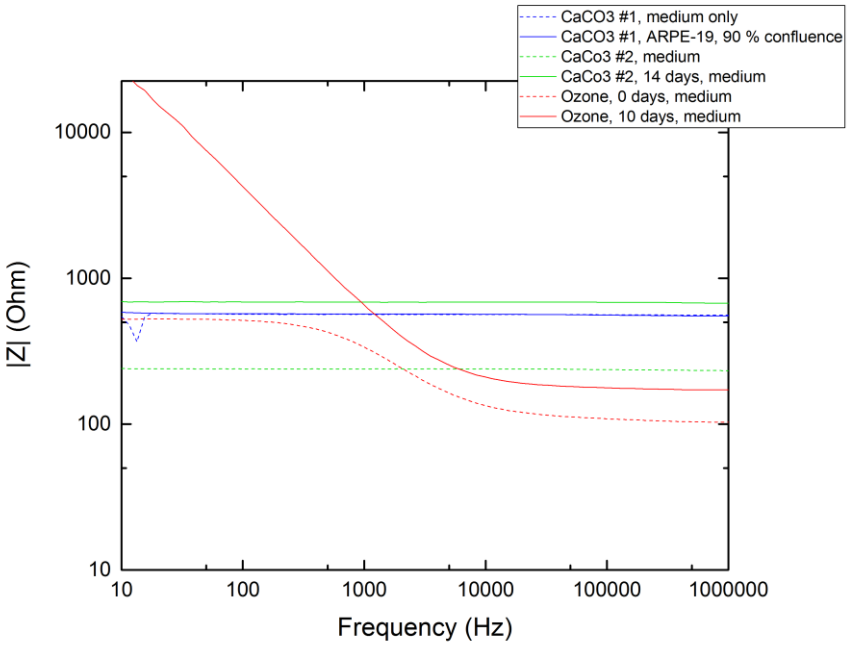

Figure 70 - Comparison of |Z| between a $CaCO_3$-coated slide with ARPE-19 cells, a $CaCO_3$-coated slide with only medium, and a slide with O_3 treatment.

The reduced influence from electrode polarisation on the $CaCO_3$- and O_3-treated slides indicates that the ALD treatment contributes significantly to the electrodes being partly short-circuited. The rise in impedance for the O_3-coated electrode after 10 days, approximating an electrode polarisation profile, indicates that any film created by the ALD process has been at least partly dissolved.

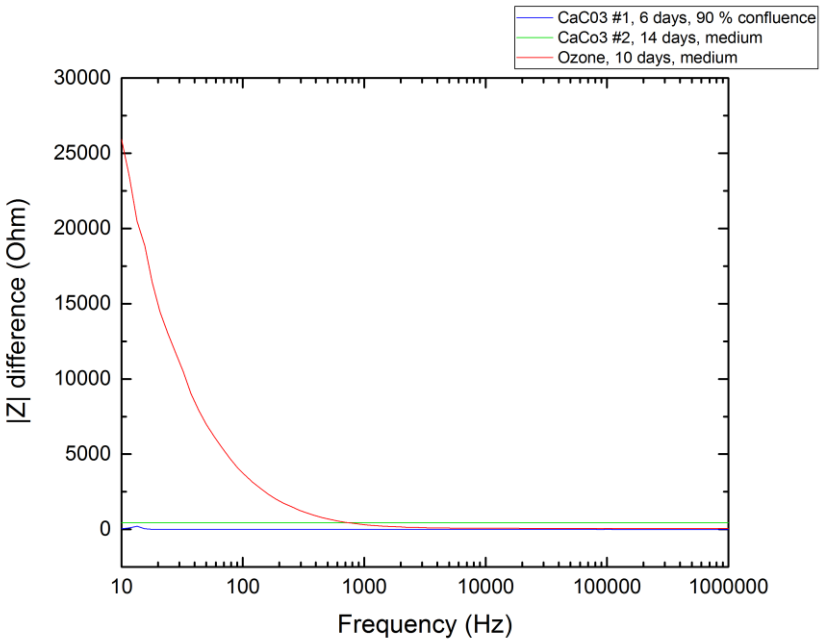

Figure 71 - Comparison of $|Z|_{diff}$ between a $CaCO_3$-coated slide with ARPE-19 cells, a CaCO3-coated slide with only medium, and an O_3-treated slide.

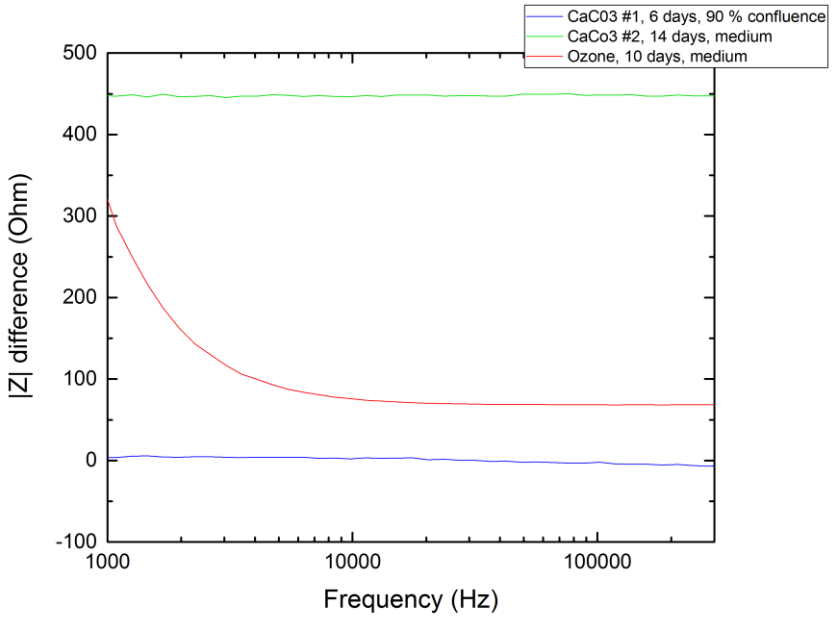

Figure 72 – Comparison of |Z| between a $CaCO_3$-coated slide with ARPE-19 cells, a $CaCO_3$-coated slide with only medium, and an O_3-treated slide. Frequency range is limited to the expected dispersion range for ARPE-19 cells.

The measurements show very little influence from the ARPE-19 cells. Over time, the impedance rises. There is no discernible electrode polarisation for the $CaCO_3$-coated cells, contrary to what would be expected if the film was dissolved.

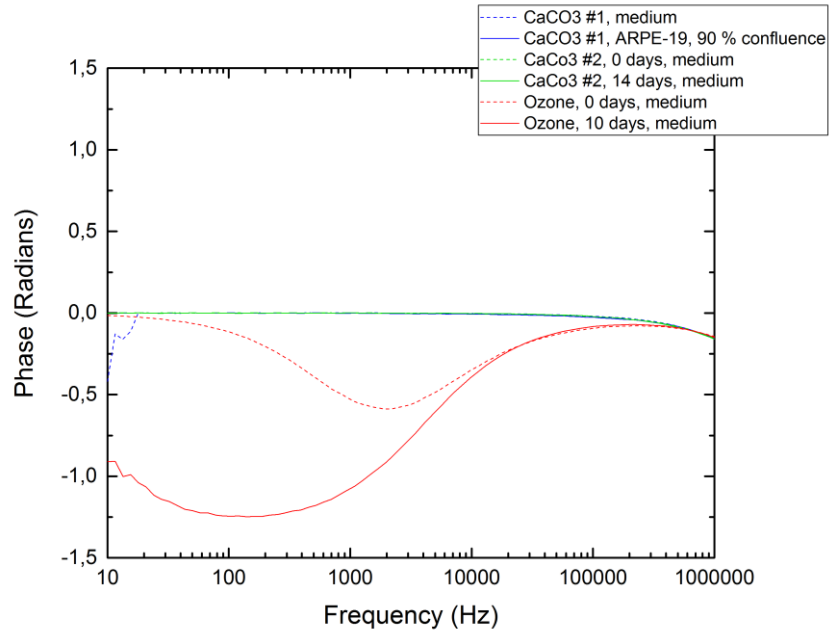

Figure 73 - Comparison of phase angle between a $CaCO_3$-coated slide with ARPE-19 cells, a $CaCO_3$-coated slide with only medium, and an O_3-treated slide.

The phase angle profile of the O_3-treated device after 10 days of medium exposure approaches the profile for an uncoated device, lending strength to the hypothesis that the substrate modification, e.g. a film, imbued by the O_3 treatment, is disappearing, likely dissolving into the medium.

Measurements to check the conduction properties of the electrodes without anything in the wells were made for one the $CaCO_3$ devices, and the O_3–treated one, on suspicion of the electrode separation having been compromised (Figure 74, Figure 75), as well as a measurement of the contact area of one electrode, to ascertain the impedance of an ITO film that has undergone ALD treatment, but excluding the influence of the electrode digits.

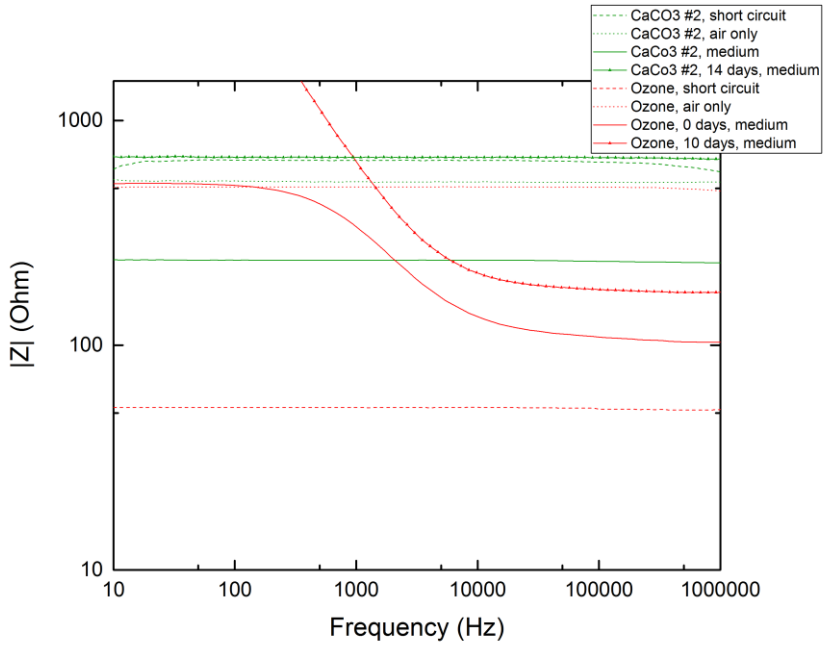

Figure 74 - Comparison of |Z| between between electrodes coated with $CaCO_3$ and O_3-treated ones. Measurements of "air" were made with the electrodes of the sensing device, with nothing in the culture well except air. Measurements of the "short circuit" were made on the wire contact area of one of the electrodes.

The measurements show a *higher* impedance for the measurements of $CaCO_3$-coated ITO film than for the electrode system with medium. This indicates either that the $CaCO_3$-coating has a very uneven distribution or that the coating degrades all over as time passes.

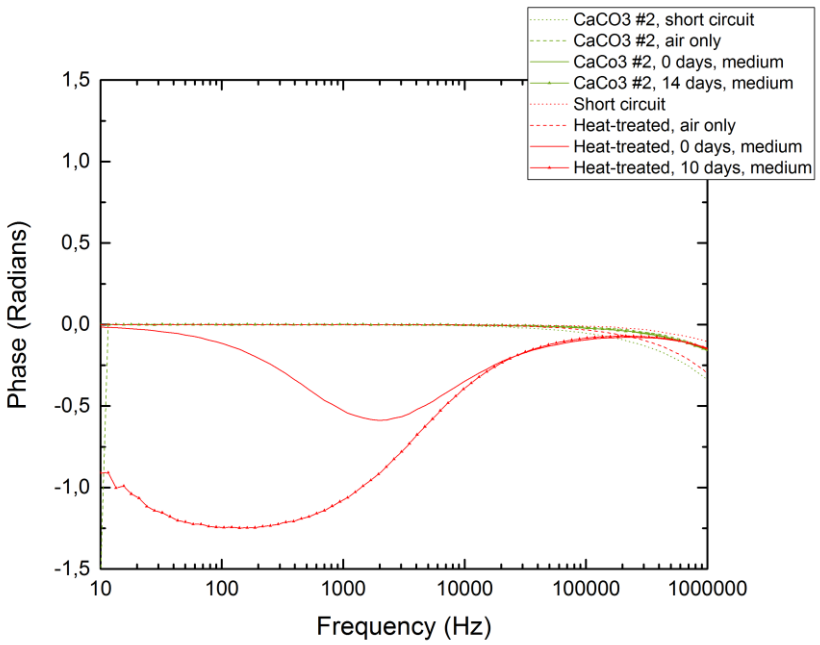

Figure 75 - Comparison of |Z| between between electrodes coated with CaCO3 and O_3-treated ones. Measurements of "air" was made with the electrodes of the sensing device, with nothing in the culture well except air. Measurements of the "short circuit" was made on the wire contact surface of the electrode.

The impedance plots above show a remarkable lack of influence from electrode polarisation

The impedance of the slide which received only the heat treatment of the $CaCO_3$ deposition program was measured (Figure 76) to ascertain whether the heat treatment alone would cause a short circuit.

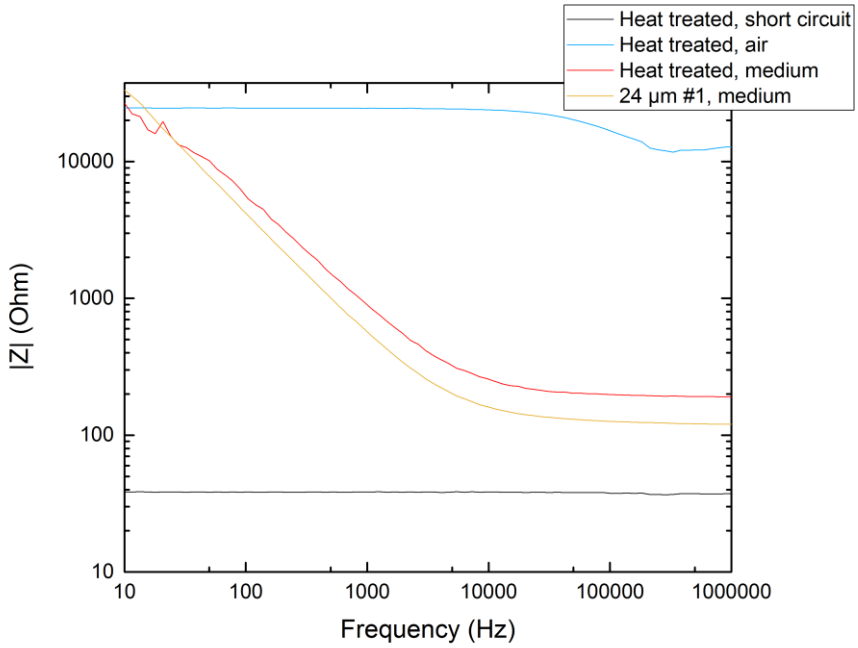

Figure 76 - |Z| for the heat-treated slide. Measurements of "air" was made with the electrodes of the sensing device, with nothing in the culture well except air. Measurements of the "short circuit" was made on the wire contact surface of the electrode. Medium-only measurement of the untreated electrode slide (from section 3.5.6) included for reference.

3.6 Impedance profile of ARPE-19 cell layer

Values derived from measurements in the different sensing devices are presented in Table 2.

To find a value for low-frequency impedance $|\mathbf{Z}|_0$ for the ARPE-19 culture, the $|\mathbf{Z}|_{diff}$ value at the end of the dispersion $|\mathbf{Z}|_{disp\_end}$ can be subtracted from the value at the start of it, $|\mathbf{Z}|_{disp\_start}$, so that $|\mathbf{Z}|_0 = |\mathbf{Z}|_{disp\_start} - |\mathbf{Z}|_{disp\_end}$.

The characteristic frequency f_c is the corresponding frequency to the apex of the Nyquist plot.

The capacitance can be calculated from $\mathrm{Im}(\mathbf{Z})$ at the characteristic frequency by the formula $\mathrm{Im}(\mathbf{Z}) = 1/\omega C$.

The dispersion frequency range is the frequency band from the point where the $|\mathbf{Z}|$ dispersion starts to where it practically evens out to a flat line.

Table 2 - Impedance characteristics of ARPE-19 culture

Device	$\|\mathbf{Z}\|_0$ (Ω)	f_c (kHz)	C (µF)	Dispersion freq. range (kHz)
24 µm #1	90	4.7	0.74	2.2 - 380
24 µm #2	69	13	0.50	3.5 - 212
192 µm	70	18	0.36	2.0 - 440
Collagen	90	13	0.34	0.8 - 300

Estimates of these values with uncertainty are then: $|\mathbf{Z}|_0 = 79.5 \pm 10.5\ \Omega$; $f_c = 11 \pm 7$ kHz; C = $0.54 \pm 0.20\ \mu$F, and the dispersion range is 2.15 ± 1.35 kHz to 228 ± 114 kHz.

4 Discussion

This chapter presents a discussion on measurement results and their implications, the suitability of the cell culture impedance sensing device, substrate biocompatibility, and a short note on RPE cultures.

4.1 Accuracy of Results

The number of successful samples in this research project is quite limited, with only one or two viable experiment runs for each type of substrate. Conclusions drawn from those experiments are made on the premise that there are multiple variables influencing the system, and both the cells and the measurements are sensitive to changes and differences in the different experimental runs, and that these differences are sometimes hard to control or register.

The temperature of the medium can have a significant effect. Though the cultures were incubated at 37 °C, they were moved out of the incubator and measured at room temperature.

A very significant effect can be seen in the time between a medium change and the measurement. As time passes, cells extract nutrients from the medium and excrete waste products into it, changing the ion content of the medium. Evaporation reduces the volume and increases the ion concentration (by reducing the water content) in the medium. In Figure 47, Figure 48, and Figure 50 this is visible as a gap between the measurement before and after medium change the 14^{th} day. Otherwise, measurements of all devices were made immediately after a medium change.

4.2 The Sensing Device

4.2.1 Substrate and Electrode Suitability for Measurements

Following is a discussion on the suitability of the different substrates for impedance measurements of ARPE-19 cell culture.

4.2.1.1 Interdigitated ITO Electrodes, 24 µm and 192 µm Digit Width / Spacing

4.2.1.1.1 $|\mathbf{Z}|$ for ARPE-19 cells

Figure 50 and Figure 67, displaying the development of $|\mathbf{Z}|_{diff}$ over time, clearly show a decrease and convergence in $|\mathbf{Z}|_{diff}$ in the expected dispersion range, between 3 kHz and 300 kHz. This is very likely due to the dispersion of the cell layer. The plots also show increasing values for $|\mathbf{Z}|_{diff}$ over time, as the culture layer density increases and approaches confluence. This is probably the clearest indication found in this project that the cells influence the measurements. The measured dispersion range match measurements made on the same type of cells by others [76]. It is reasonable therefore to conclude that cell attachment can be read from the measurements, by analysing trends in $|\mathbf{Z}|$ and $|\mathbf{Z}|_{diff}$.

The frequency range of the dispersion that was found indicates that it is a β-dispersion (cf. section 2.1.1), and attributable to cell membrane capacitance, protein molecules, and/or Maxwell-Wagner effects. Other dispersions were not discernible.

For device #1,$|\mathbf{Z}|_0$ = 90 Ω, comparing $|\mathbf{Z}|_{diff}$ at 3 kHz and 400 kHz. For device #2, in the same frequency range,$|\mathbf{Z}|_0$ = 69 Ω. For the 192 μm digit sensing device, $|\mathbf{Z}|_0$ = 70 Ω. Based on these measurement, and considering the uncertainty inherent in an experiment with only three samples, pinpointing a value for $|\mathbf{Z}|_0$ is difficult. To account for two measurements being very similar at 69 Ω and 70 Ω, it may be pertinent to choose a value nearer to these than to the last measurement at 90 Ω, for a value of $|\mathbf{Z}|_0$ = 75 ± 15 Ω. Dividing by 2 to account for the current traveling through the cell layer twice gives an estimated $|\mathbf{Z}|_0$ of the ARPE cell culture layer of 37.5 ± 7.5 Ω, which corresponds to a value of 12.2 ± 2.5 Ω, not far from Onnela *et al.*'s reported value of 10 Ω [76], also evident in the Maple plot for the ARPE-19 cell layer, modified to reflect experimental values (Figure 77).

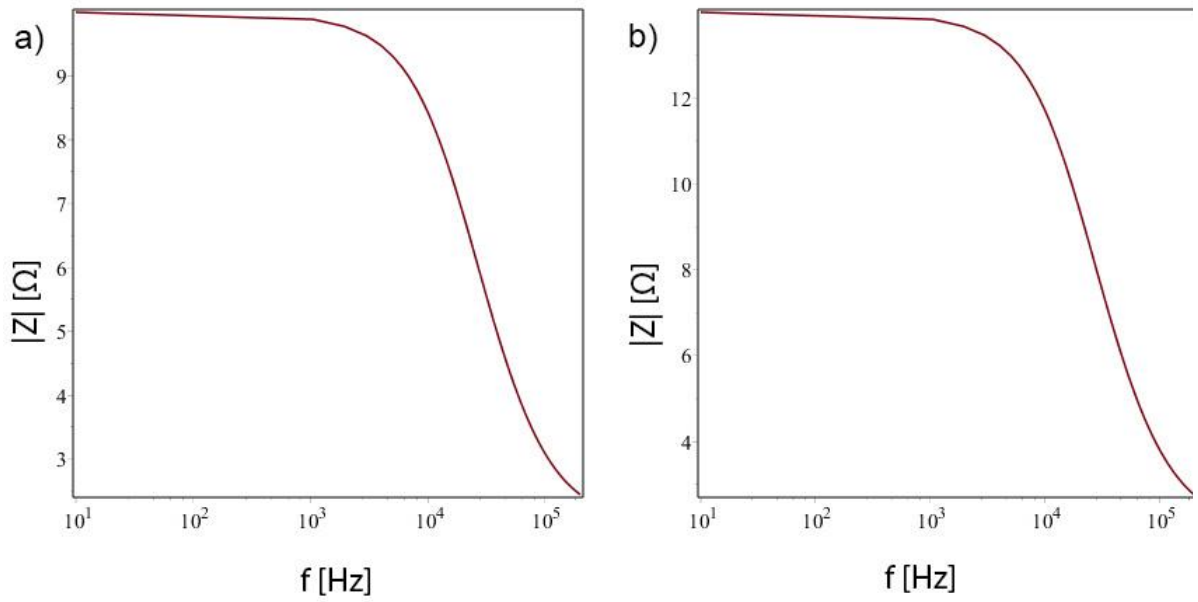

Figure 77 - Impedance plot of confluent layer of ARPE-19. a) original plot b) plot updated according to experimental values.

4.2.1.1.2 Capacitance of ARPE-19 Cells

The cell layer capacitance is indicated by the phase angle: large negative values indicate higher capacitance. In all plots where the ARPE-19 layer influences the values, presence of the cell layer correlate with a larger (negative) phase angle in the lower frequencies and a smaller (negative) angle in the higher frequencies, with some variations in where the two plots cross each other. The larger angle in lower frequencies is expected, as the impedance of the system is expected to increase with the inclusion of cells.

The derived capacitances from the measurements give a capacitance for the cell layer of 0.54 ± 0.25 µm, for a capacitance per area value of 1.6 ± 0.8 µF/cm^2. Onnela *et al*.'s capacitance measurement of 0.8 µF/cm^2 falls within the uncertainty margin of this value.

4.2.1.1.3 Electrode Sensitivity

The interdigitated ITO electrodes measured an impedance profile that matches Onnela *et al*.'s study for frequencies above 3 kHz, specifically the expected dispersion range of 3 kHz – 400 kHz [76]. Though the impedance profiles differed slightly between the 24 µm- and 192 µm-digit electrodes (Figure 65), the registered signals for the ARPE-19 cells were similar between them (Figure 67). Since both are equally suitable with respect to sensitivity to the cells, a lower digit width and spacing is probably preferrable to a higher one, to limit current density and to some degree equalize sensitivity over the substrate; the digit width shouldn't be brought too low, as they may lose sensitivity in the cell layer. A digit width of the order of magnitude of the ECM thickness, for instance, may be too narrow.

4.2.1.1.4 Electrode Polarisation

The "naked" ITO electrodes on a soda lime glass substrate imbued a high resistance in the system at lower frequencies, as can be seen in Figure 45 and Figure 47; the phase angle of almost -1.5 at lower frequencies means the system is predominantly capacitive; along with the high resistance at low frequencies, this is indicative of electrode polarisation dominating the system at those frequencies. An adjustment to Equation 16 is necessary to incorporate this electrode polarisation in the calculations.

To add electrode polarisation to the equivalent circuit, a $\mathbf{Z}_{\mathrm{ep}}$ term can be added to Equation 16 to represent it, in series with the rest of the system.

$$\mathbf{Z}_{\mathrm{tot}} = \mathbf{Z}_{\mathrm{ep}} + \mathbf{Z}_{\mathrm{el}} + \frac{1}{\frac{1}{\mathbf{Z}_{\mathrm{c}}} + \frac{1}{\mathbf{Z}_{\mathrm{ECM}}}} = R_{ep} + \frac{1}{j\omega C_{ep}} + \frac{R_{\mathrm{el}}}{1 + R_{\mathrm{el}} j\omega C_{\mathrm{el}}} + \frac{\mathbf{Z}_{\mathrm{c}} R_{\mathrm{ECM}}}{\mathbf{Z}_{\mathrm{c}} + R_{\mathrm{ECM}}} \quad (20)$$

An adjusted Maple plot, taking into consideration measurements at frequencies below 1 kHz and an update of $|\mathbf{Z}|_0$ to 75 Ω, is presented in Figure 78.

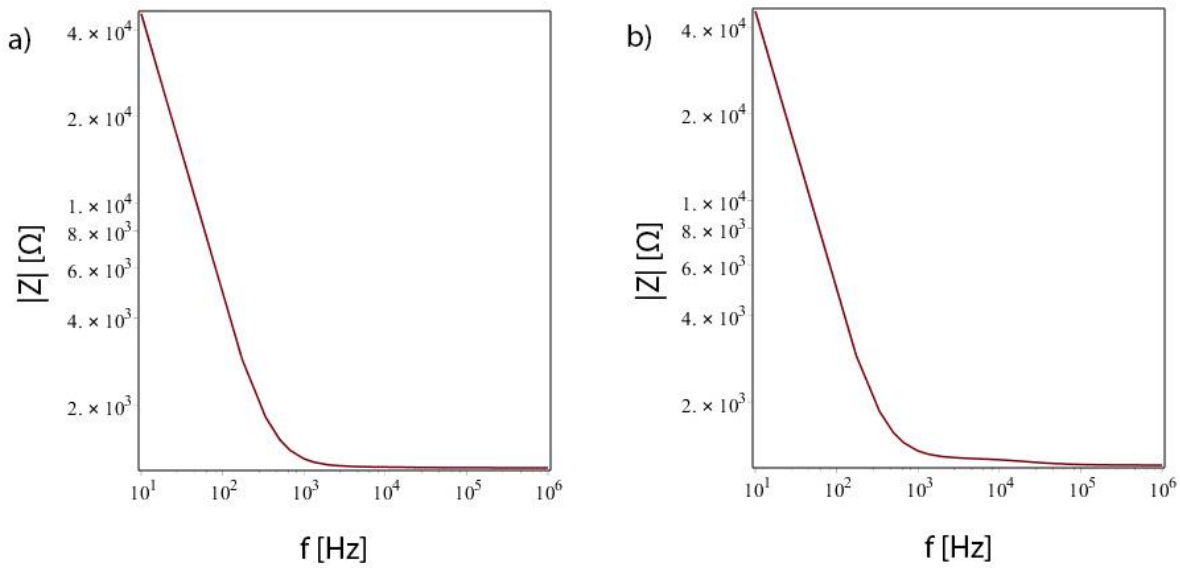

Figure 78 - Impedance plot of sensing system with ARPE-19 cells confluent on interdigitated electrodes in cell growth medium. a) original plot b) plot updated according to experimental values.

4.2.1.1.5 ITO Electrode Degradation

Degradation of the electrode or its coating may influence the measurements as well. Figure 61 displays the impedance measurements for the ITO electrode degradation test, where the culture sensing device had medium but no cells in the culture well, receiving the same medium changes as the cell-seeded devices. The measurements indicate that the electrodes may deteriorate over time, with an increase in $|\mathbf{Z}|$ of between 110 and 125 Ω for all frequencies over a 13-day timespan. Comparing with $|\mathbf{Z}|_{diff}$ of the ARPE-19 impedance plots, the medium alone seems to cause a higher impedance increase than the cell cultures. It may be that the cells shield the electrodes from degradation by contact with the medium, by reducing electrolyte mobility at the electrode surface. Follow-up measurements of the electrode degradation would be needed to ascertain whether the value above is accurate.

Crucially, the impedance increase in the degradation measurement run is almost uniform over the dispersion frequency range, which indicates that trends in $|\mathbf{Z}|_{diff}$ may be interpreted to arise from the ARPE-19 layer. The dispersion range indicates that this change stems from the cell layer itself, and not from some modification the cells might have done to the substrate; such a modification would not reflect cell membrane impedance dispersion.

4.2.1.1.6 Short Circuit and Air Measurements

Measurements of the wire contact area and of the electrodes with no electrolyte covering them were made to check whether the electrodes were isolated from each other. In the case of the 24 µm-digit (Figure 54) and 192 µm-digit electrodes, the wire contact area displayed almost frequency-independent resistance of approximately 48 Ω from 10 Hz to 1 MHz. Considering the rectangular shape of the measurement area, this is as expected.

The air impedance measurement, with values in the MΩ range at low frequencies, confirmed that the electrodes were sufficiently isolated from each other. Therefore, when measuring medium and cells that have considerably lower impedance than the air measurements, we can conclude that it is actually the medium and cells that are being measured, and not just the substrate.

4.2.1.2 Collagen-coated Electrodes

Electrode polarisation was apparent in the collagen-coated electrodes, with a high low-frequency impedance decreasing with increasing frequency (Figure 65).

The collagen-coated electrodes showed behaviour similar to the un-coated ones, with a similar dispersion in the ARPE-19 cells' 3 kHz – 300 kHz dispersion range (Figure 67). Cell attachment was similar to that of the un-coated electrodes as well (compare Figure 44 and Figure 63). The collagen coating seems to have caused a higher impedance from 1 kHz and towards higher frequencies, though the ARPE-19 dispersion is still discernible. The most notable effect of the collagen coating seems to have been a decrease in cell proliferation speed. This decrease in proliferation comes against expectations, as collagen is an established attachment-promotive coating. The poor proliferation may have been due to individual circumstances for this particular measuring device and need to be confirmed with follow-up studies.

4.2.1.3 TTIP/glycine-coated Electrodes

The TTIP/glycine-coated electrodes cause consistently higher $|\mathbf{Z}|$ values than the uncoated and collagen-coated electrodes (Figure 65). The phase angle in the early measurements is significantly higher than for un-coated and collagen-coated electrodes, but decreases over time to significantly lower values (Figure 68). Presumably, the substrate is in some way modified during the measurement run. It is difficult to ascertain a dispersion for the cells, as $|\mathbf{Z}|_{diff}$ for this coating was dominated by the change in impedance of the electrodes and/or coating while covered in cell culture medium (Figure 66). Since $|\mathbf{Z}|_{diff} > 1$ kΩ, and the dispersion spans 500 kΩ, the impedance increase is likely not caused by the ARPE-19 cell layer alone. It is possible that the surface triggered cell differentiation, but this is not discernible in microscope images, partly due to the decreased contrast of the ITO electrode microscopy. The dispersion range corresponds to a β-dispersion, indicating that it may be due to an increase of proteins in the system. Why the cells would do so would need investigation to ascertain.

An impedance measurement of the wire contact area of the electrodes showed a $|\mathbf{Z}|$ of 53.7 ± 0.8 Ω, frequency independent between 10 Hz and 1 MHz. The change in the coating's properties may be due to e.g. ion uptake in the coating, or dissolving, or a combination; though intuitively, if it was caused by dissolving only, the impedance should approach the impedance of the un-coated ITO electrodes.

Adjusting equation 9 for the increased resistance of the TTIP/glycine-coated electrodes results in an electrode resistance R_{el} of

$$R_{el} = R_c + R_d = 70\ \Omega + 140\ \Omega = 107.4\ \Omega + 214.8\ \Omega \approx 322.2\ \Omega$$

This increase in resistance is not large enough to account for the increase in impedance for the TTIP/glycine-coated sensing device.

4.2.1.4 $CaCO_3$-coated Electrodes

The $CaCO_3$-coated electrodes behaved differently than the other versions of the substrates. The measurements show no discernible influence from the ARPE-19 cells or from electrode polarisation (Figure 70). Rather, the impedance seems entirely resistive up to the 100 kHz-range, where the phase angle slowly decreases to -0.17 at 1 MHz, meaning it is still predominantly resistive. It should be safe to assume that the electrodes have been short-circuited by some modification during the ALD process. The term "short circuit" is used loosely here; the system |**Z**| for the $CaCO_3$-coated substrate is in all cases higher than 230 Ω.

The cause for this short circuiting was unclear. $CaCO_3$ is an insulator with an electronic band gap of 6.0 ± 0.35 eV [89] and a relative permittivity of 8.19 [90]. A $CaCO_3$ coating might change the electrode polarisation, but that does not explain the relatively low |**Z**| values when no medium was present in the culture well; this could be caused by diffusion of conductive material from the ITO electrodes either into or along the surface of the glass substrate, creating a conductive layer, albeit one with over 230 Ω resistance.

It also seemed that the overall |**Z**| was affected over time by the medium over the electrodes, as the measurement with no medium in the culture well is initially 236 ± 3 Ω in the frequency range 10 Hz – 1 MHz, compared to between 530 and 550 Ω for the electrodes covered with medium. This is counterintuitive, as the presence of an electrolyte should boost conductivity and not reduce it. It may be that the medium modifies the substrate. |**Z**| for the medium-covered electrodes in the same frequency range rises to 682 ± 11 Ω after 14 days, so the contact with the medium seems to increase |**Z**| over time. This indicates some modification of the substrate by the medium. At no point did the $CaCO_3$-coated electrodes show signs of electrode polarisation, so it is reasonable to assume that the film was not completely dissolved during the 6 days of the experiment.

The measurements show a *higher* impedance for the measurements of $CaCO_3$-coated ITO film, without electrodes, than for the electrode system with medium. An uneven distribution is not very likely, as the Si control slides that were used for measurements were placed in front of and behind the ITO electrode slides; a gradient in film thickness would be expected to show up as a significantly different film thicknesses for the two Si slides. They were measured by spectroscopic ellipsometry technique to 42.5 nm and 43.9 nm; not enough of a difference to warrant the observed difference in impedance. It is reasonable, then, to assume that the $CaCO_3$ film degrades over time both when exposed to medium and to air.

To investigate whether it was the nanofilm or the ALD process that caused this change in impedance, two follow-up experiments were performed. One was subjected ITO electrode slide to the same ALD program as the $CaCO_3$-covered one, but with the valves for the $Ca(thd)_2$ and CO_2 precursors closed. As an oversight, O_3 was still pulsed. The slide displayed conduction similar to that of the $CaCO_3$-covered one, with relatively low impedance when the circuit was open, frequency-independent $|\mathbf{Z}|$ in the measurement frequency range. This indicates, again, a short circuit.

The slide that received heat-treatment only did not share the short-circuit conductance profile, but had one rather similar to the un-coated electrodes. This indicates that he O_3 + heat exposure contributed significantly to the short circuiting. How an ALD deposition of O_3 would cause ITO electrodes to short circuit over a distance of 24 µm is unclear and would warrant further investigation.

During 10 days of submersion in cell culture medium, $|\mathbf{Z}|$ for the O_3-coated electrodes increases in the lower frequencies, indicating that electrode polarisation is then influencing the electrodes, probably because any conductive film has dissolved into the medium.

4.2.2 Substrate Biocompatibility

As mentioned in section 2.4, ITO has been demonstrated to promote cell attachment and growth. However, the attachment and proliferation rate of the custom-made ITO electrode culture devices were invariably inferior to commercially available culture vessels.

As can be seen in the phase-contrast microscope images of the cell cultures in sections 3.5.6, 3.5.8, and 3.5.9 (Figure 44, Figure 62, Figure 63, Figure 64, and Figure 69), cells eventually grew on all of the substrates, although not with the same speed and vigour as those seeded in commercially available cell culture flasks. While the culture flask cells were generally confluent after 3-5 days, the sensing devices only achieved up to 90 % confluence over a period of 6-14 days, depending on passage number and culture device.

Cell cultures on the “naked” ITO electrode substrates, i.e. the ones without any coating on top, reached 90 % confluence in 6 or 14 days in the case of the 24 µm-digit electrodes, and 6 days in the case of the 192 µm-digit ones. While the sample number is very small and conclusions are made with this taken into account, it is reasonable to assume that the width of the ITO electrode digits has little influence on cell attachment and proliferation. Again, follow-up experiments would need to be done to ascertain a correlation. The cell passage number, degree of cell differentiation, and circumstances during cell splitting likely has more influence. Trypsin, which is used to detach cells from their substrate, cleaves the attachment proteins of the cells so they are released from the substrate. The length of exposure to trypsin may influence their viability and therefore attachment ability. The passage used for the 24 µm-digit electrodes was not the same as the one used for the 192 µm-digit electrodes.

The same cell passage was used for the 192 µm-digit electrode measurements as the collagen- and $CaCO_3$-coated electrode measurements. Interestingly, collagen, a commonly employed substrate for promoting cell attachment, was the one least favoured as an attachment substrate by the ARPE-19 cells. Both $CaCO_3$ and 192 µm-digit electrodes achieved 90 % confluence after 6 days, at which point the collagen-covered substrate was only 50 % confluent; the collagen substrate only reached 90 % confluence after 14 days in culture. The parameters for the culture splitting, seeding, and measurements were similar for those three cultures. Again, due to the small sample size, this result can not be said to be conclusive; e.g. the collagen coating may have been deteriorated.

The ALD coatings of $CaCO_3$ and TTIP/glycine both permitted cell attachment and growth. Both promoted 90 % confluence within 6 days, which was considerably faster than the collagen coating, and at the same pace as the 192 µm-digit ITO electrodes. The TTIP/glycine device was seeded with cells from a different culture passage than those above, which may have influenced the properties of the cell culture, i.e. the cell proliferation may vary depending on exposure time to trypsin, number of cells pipetted out from the trypsinated culture, the age of the cells or their passing number.

4.2.3 Substrate Suitability for Optical Microscopy

One of the main goals of this thesis was to investigate a transparent material for electrode material. While the ITO electrodes are indeed transparent, the cells are significantly more difficult to see, as demonstrated in Figure 43. The microscope manufacturer Olympus informs that “Even with phase contrast objectives having correction collars that are designed for observation through thick glass or plastic, the image quality suffers when compared to cells imaged on thin (170 micrometer) cover glass plates” [91]. Using a thinner glass substrate would therefore probably improve image contrast significantly, but the reduced strength of the slides would need to be taken into account when evaluating wire/electrode interfaces.

The spring-loaded contacts used for this thesis would quite possibly break a glass slide of 170 µm thickness unless appropriate changes to the device design were made to counteract the contact springs. There were moments during assembly of the sensing device when pressure from the contact pressure was poorly counteracted by the rest of the construction, and while a 1 mm slide withstood the treatment, a 170 µm slide may not, and design changes would need to be done to mitigate it.

4.2.4 Suitability of the Sensing Device

One of the most important factors limiting or allowing cell growth seems to have been ventilation. Insufficient ventilation depletes the medium of CO_2, increasing the pH level as the CO_2 level drops. Too much ventilation allows the medium to evaporate. Therefore, finding a shape that allows just enough air circulation was vital. The cell culture well and lid eventually produced provided sufficient, but not too much, ventilation for the cells to survive

over time. There was still discernible evaporation, but with medium exchange every 3 days, humidity containment was adequate to keep sufficient medium in the culture wells. About 0.03 ml medium would evaporate over this timespan, corresponding to 30 % of the medium introduced to the well during a medium change.

Cell culture wells can be procured in various sizes and diameters. Initially, for this project, the dimensions of the culture wells were chosen to closely match those of the commercially available Corning Falcon 96 well cell culture plates, which have a well diameter of 6 mm and height of 10 mm. These wells were used as controls to test cell viability. When glass tubing was introduced as culture wells, tubes with 6.5 mm diameter were chosen to most closely match the Corning trays with the available resources. The height of the wells was kept at 10 mm.

The cultures were very sensitive to the shape of lid of the culture device. Several versions were tried, drawing inspiration from existing cell culture lids. Eventually, the lid that proved suitable had a 0.5 mm gap between the rim of the cell culture well and the ceiling of the lid, and a 0.5 mm difference between the outer diameter of the cell well and the inner diameter of the lid. The lid was made with a curtain around the rim, extending 6 mm down past the rim of the cell culture well, which limited evaporation and still allowed adequate circulation.

4.2.4.1 Component Materials

Initially, the wire mount and culture wells were machined from acrylic glass, but as requirements of the device shape became apparent, 3D-printed ABS plastic was used to facilitate more complex shapes. As 3D-printed material is porous, the wells required some form of lining, e.g. varnish or silicone. When it's desirable to limit the contact between the culture medium and any adhesive material, lining the culture wells with an adhesive or a varnish is a suboptimal. The lining material needs to release a minimal amount of chemicals, to not influence the cells' environment. In the successful sensing devices, glass tubing was used as culture well walls, limiting the contact between medium and adhesive to whatever adhesive is exposed at the bottom of the well after the well has been attached – with adhesive – to the ITO electrode/glass plate.

A glass well attached with aquarium silicone allowed cell attachment and growth, albeit at a slower rate than in the Corning culture wells.

In the device eventually used for the measurements, only the substrate with electrodes, the glass tube serving as culture well, and the aquarium silicone adhesive were in contact with the cell culture and medium. Rubber and other adhesives were toxic, while 3D printed plastic was impractical.

4.2.5 Cell layer properties derived from impedance values

For simplification of measurements, it may be desirable to limit measurements to one frequency. The characteristic frequency f_c is the apex of Im(**Z**) in the Nyquist plots, as shown

in Figure 57. It is often useful to measure changes in impedance at f_c, where the capacitance of the measured sample is greatest.

When the purpose is to measure degrees of proliferation accurately, having a range of f_c with variations depending on unknown conditions makes it non-trivial to make an assessment based on one frequency only, also because of changing ITO electrode electrical properties.

Evaluating the change in |**Z**| over the dispersion frequency range may be another simplified method of ascertaining level of confluence. However, As can be seen in Table 2, |**Z**| change alone can not be used to ascertain when the culture has reached confluence. However, when the culture has reached confluence, impedance data recorded during the cell proliferation may be used to analyse proliferation speed.

Differentiation may be easier to register. Some cell types show great increases in capacitance when they differentiate [20], and this may be exploited by measuring changes in capacitance to see when differentiation occurs.

4.3 RPE Culture

A comparison can be made between the ARPE-19 culture and the differentiated RPE culture reported by Onnela *et al*. [76]; the latter having a comparatively higher and more easily discernible impedance than the former at low frequencies, f < 1 kHz [76]. The measurements from the ITO sensing device at those frequencies were dominated by the electrode polarisation and varied to such a degree that discerning cell culture impedance in this frequency band would be difficult with the setup used in this thesis. Further experimentation with wires may allow less noise in the lower frequencies.

5 Conclusion

An impedance cell culture sensing device was constructed, which provided adequate growth conditions for ARPE-19 cells. The production of the device utilised laser scribing of a 350 nm ITO layer on a 1 mm soda lime glass slide to produce interdigitated electrodes, 3D printing ABS plastic to prototype and produce the wire mounts and device clamps, silicone adhesive available in aquarium shops, standard SiO_2 glass tubing, copper wires and spring-loaded gold contacts. The laser scribing and 3D printing processes were central and vital to the prototyping, as they are relatively fast and simple to execute; the laser ablation technique was also a premise of the thesis, as an alternative to more time-consuming microlithographic techniques that are often used in similar processes. With the available laser, scribing line width had a lower limit of 24 µm. For narrower electrode digit spacing, a laser with a more finely focused laser beam, or microlithography, would have to be used.

Experiments indicate that interdigitated ITO electrodes with no further coating may be used for impedance sensing of ARPE-19 cells, and that its sensitivity and consistency in the dispersion frequency range of the cells, 3 kHz to 400 kHz, is adequate to pick up the impedance profile of the cell layer. The variation in sensitivity for different digit widths and spacing of the electrodes was acceptably small in the range investigated, 24 µm and 192 µm, but narrower digits decrease current density, which is usually preferrable in order to disturb the cells minimally. The impedance values indicate that as the cells proliferate and the cell layer becomes more confluent, the impedance gradually changes, reflecting the changes in the cell layer.

The ITO electrodes and glass surface are conducive to cell attachment and proliferation, albeit less so than some commercially available cell culture vessels.

Measurements at frequencies below 1 kHz were dominated by electrode polarisation, and varied sufficiently within a frequency sweep as well as over time to render impedance measurements in this frequency range with this setup too inaccurate to discern cell culture impedance. This could preclude the technique from measuring differentiated RPE-cells, whose major dispersion lie in the 10 Hz – 1 kHZ range [76], unless modification is made to the measurement device to refine sensitivity and reduce noise in this frequency range. Shorter and better shielded wiring between the impedance analyser and the measurement device should ameliorate this to some extent.

The ITO electrodes were affected over time by the cell growth medium, their $|\mathbf{Z}|$ value rising throughout the measurement frequency range from 10 Hz to 1 MHz. Crucially, the $|\mathbf{Z}|$ increase in the ARPE-19 dispersion frequency range from 3 kHz to 400 kHz was constant over the range of frequencies. Impedance trends in the frequency range could reasonably be identified as being due to influence from the ARPE-19 cells, and not the impedance change in the ITO electrodes. It may be desirable to use a suitable coating to shield the ITO electrodes from the medium, and mitigate changes over time of the electrode properties.

Three types of coating were applied to the electrodes, to investigate biocompatibility and sensitivity:

- **Collagen** coating enabled similar cell proliferation and measurement capabilities as, but not obvious advantages over, the "naked" ITO electrodes.
- **TTIP/glycine** was not a successful candidate for electrode coating. Due to the lack of discernible cell layer dispersion, a TTIP/glycine coating of the kind tested in this thesis is not really suitable for impedance sensing of ARPE-19 cells.
- The **$CaCO_3$** ALD process effectively destroyed the electrodes in regards to their usefulness in measuring the cell culture. Results indicate that the O_3-pulsing during the ALD process contributes significantly to the destruction of the electrode system. As $CaCO_3$ is soluble in water and my dissolve during exposure to cell growth medium, the substrate coated with it may revert to a state similar to the un-coated slides over time as the $CaCO_3$ is dissolved. In experiments or production involving $CaCO_3$ as attachment-promoting substrate, an assessment should be made to evaluate whether it is practical to use the coating given the potentially limited lifespan of the film.

Though the different coatings deposited in this thesis were largely unsuccessful in improving the sensing devices, the functionality of collagen coating implies that a coating may be used without hindering impedance measurements.

The cell proliferation on the TTIP/glycine film shows that a hybrid organic/inorganic coating may at least have similar cell growth results as an uncoated slide. Measurement capabilities would have to be improved, but if one such film could be found, it could possibly be deposited by ALD technique, gaining the fine-tuned process control associated with the technique.

6 Onwards

The project has cast some light on the potential usefulness of ITO electrodes in impedance sensing, and also some associated problems. Both could be explored in follow-up research.

It might be useful to follow up this thesis by mapping how the changes in impedance reflect the changes in the cell layers. This can give a cell biology researcher valuable information about cell proliferation speed. The experiments would be relatively easy to set up, now that the sensing devices have been prototyped.

The cell layer sensing system can likely be improved in a number of ways. One obvious improvement would be the inclusion of better and shorter wires to reduce electric noise for the relatively low-voltage measurements performed in cell culture impedance sensing. Getting hold of a more biocompatible adhesive for the culture well might improve cell attachment and proliferation, though the exact reason for the reduced activity of the cells in the sensing devices compared to the Nunc^{TM} EasYFlasks is unclear, and may depend on several factors, including ventilation, adhesive, and substrate chemistry. A thinner glass slide would improve image contrast and ease of discerning the cells, but the sensing device would have to be modified to compensate for the reduced strength of the slide.

Though the ALD-coating attempted in this thesis failed in improving characteristics of the electrodes, efforts could be made to find other thin films that might both improve cell attachment and allow impedance sensing. Alternative ALD cycles for $CaCO_3$ deposition that don't include O_3 pulses could be researched, but since the film gradually dissolves, its practicality may be limited. Other ALD materials are probably more attractive. The fact that the ITO electrodes also degenerate under exposure to the cell growth medium indicates that a film deposited to make the ITO layer more resilient would be desirable. A hybrid film which enables impedance sensing could fulfil such a role. Alternatively, inorganic films could be investigated, e.g. if a monolayer of boron nitride, a polar film, could be deposited, it would be very interesting to investigate its performance.

Another extension of this thesis could be trials with different cell lines. For differentiated RPE cells, the sensing device would need to be improved to reduce noise. Any attachment-dependent culture might be tested, though, which includes bone, muscle, nerve and skin tissue, and is not limited to monolayer cultures. As skin tissue and bladder membranes have already been successfully grown and transplanted, a sensing device for proliferation monitoring may be desirable in production lines.

7 References

1. Kramer, B., *Electric Organ Discharge*, in *Encyclopedia of Neuroscience*, M.D.a.H. Binder, Nobutaka and Windhorst, Uwe, Editor. 2008, Springer: Berlin. p. 1050-1056.
2. Laboratory, S.P., *Lesser electric ray (Narcine bancroftii). Gulf of Mexico.*, Fish4345_-_Flickr_-_NOAA_Photo_Library.jpg, Editor. 2007: Wikepedia.
3. *Torpedo ray electric organs*, Torpedo_electric_organs.jpg, Editor.: https://en.wikipedia.org/wiki/Electric_ray#/media/File:Torpedo_electric_organs.jpg.
4. Grimnes, S. and O.G. Martinsen, *Bioimpedance and Bioelectricity Basics*. 2008.
5. Unknown, *Death of Georg W. Richmann*, Richmanns_Tod_1753.jpg, Editor., Wikimedia: https://commons.wikimedia.org/wiki/File:Richmanns_Tod_1753.jpg. p. Georg Wilhelm Richmann is killed, presumably by ball lightning.
6. Fricke, R., *The theory of electrolytic polarization.* Philosophical Magazine, 1932. **14**(90): p. 310-318.
7. Cole, K., *Electrical impedance of suspension of spheres.* The Journal of General Physiology, 1928. **12**(1): p. 8.
8. Cole, K., *ELECTRIC IMPEDANCE OF SUSPENSIONS OF ARBACIA EGGS. .* The Journal of General Physiology, 1928. **12**(1): p. 17.
9. Cole, K.S., *Electric phase angle of cell membranes.* Journal of General Physiology, 1932. **15**(6): p. 641-649.
10. Cole, K.S., *Permeability and impermeability of cell membranes for ions.* Cold Spring Harbor Symposia on Quantitative Biology, 1940. **8**: p. pp. 110-122.
11. Schwan, H.P., *Electrical properties of tissue and cell suspensions.* Advances in biological and medical physics, 1957. **5**: p. 147-209.
12. Giaever, I. and C.R. Keese, *MONITORING FIBROBLAST BEHAVIOR IN TISSUE-CULTURE WITH AN APPLIED ELECTRIC-FIELD.* Proceedings of the National Academy of Sciences of the United States of America-Biological Sciences, 1984. **81**(12): p. 3761-3764.
13. Giaever, I. and C.R. Keese, *MICROMOTION OF MAMMALIAN-CELLS MEASURED ELECTRICALLY.* Proceedings of the National Academy of Sciences of the United States of America, 1991. **88**(17): p. 7896-7900.
14. Scibase. *The Nevisense Product*. Available from: http://scibase.se/en/the-nevisense-product/.
15. Vogt, Y., *Svettemåler varsler farlig lavt blodsukker.* Apollon, 2011(3).
16. Rahman, A.R.A., J. Register, G. Vuppala, and S. Bhansali, *Cell culture monitoring by impedance mapping using a multielectrode scanning impedance spectroscopy system (CellMap).* Physiological Measurement, 2008. **29**(6): p. S227-S239.
17. Lucey, B.P., W.A. Nelson-Rees, and G.M. Hutchins, *Henrietta Lacks, HeLa Cells, and Cell Culture Contamination.* Archives of Pathology & Laboratory Medicine, 2009. **133**(9): p. 1463-1467.
18. Wang, M.H. and L.S. Jang, *A systematic investigation into the electrical properties of single HeLa cells via impedance measurements and COMSOL simulations.* Biosensors & Bioelectronics, 2009. **24**(9): p. 2830-2835.
19. Lee, R.M., H. Choi, J.S. Shin, K. Kim, and K.H. Yoo, *Distinguishing between apoptosis and necrosis using a capacitance sensor.* Biosensors & Bioelectronics, 2009. **24**(8): p. 2586-2591.
20. Wang, W., J. Yang, H. Liu, D. Lu, X.F. Chen, Z. Zenonos, L.S. Campos, R. Rad, G. Guo, S.J. Zhang, A. Bradley, and P.T. Liu, *Rapid and efficient reprogramming of somatic cells to induced pluripotent stem cells by retinoic acid receptor gamma and liver receptor homolog 1.* Proceedings of the National Academy of Sciences of the United States of America, 2011. **108**(45): p. 18283-18288.

21. Hildebrandt, C., H. Buth, S.B. Cho, Impidjati, and H. Thielecke, *Detection of the osteogenic differentiation of mesenchymal stem cells in 2D and 3D cultures by electrochemical impedance spectroscopy.* Journal of Biotechnology, 2010. **148**(1): p. 83-90.
22. Noll, T. and M. Biselli, *Dielectric spectroscopy in the cultivation of suspended and immobilized hybridoma cells.* Journal of Biotechnology, 1998. **63**(3): p. 187-198.
23. Ceriotti, L., J. Ponti, F. Broggi, A. Kob, S. Drechsler, E. Thedinga, P. Colpo, E. Sabbioni, R. Ehret, and F. Rossi, *Real-time assessment of cytotoxicity by impedance measurement on a 96-well plate.* Sensors and Actuators B-Chemical, 2007. **123**(2): p. 769-778.
24. Campbell, C.E., M.M. Laane, E. Haugarvoll, and I. Giaever, *Monitoring viral-induced cell death using electric cell-substrate impedance sensing.* Biosensors & Bioelectronics, 2007. **23**(4): p. 536-542.
25. Wang, R.H., Y. Wang, K. Lassiter, Y.B. Li, B. Hargis, S. Tung, L. Berghman, and W. Bottje, *Interdigitated array microelectrode based impedance immunosensor for detection of avian influenza virus H5N1.* Talanta, 2009. **79**(2): p. 159-164.
26. Wigley, C.B., *The cell culture laboratory*. Practical Approach Series; Basic cell culture, ed. J.M. Davis. 1994: Oxford University Press, Walton Street, Oxford OX2 6DP, England 200 Madison Avenue, New York, New York 10016, USA. 1-26.
27. Sutherland, F.W.H., T.E. Perry, Y. Yu, M.C. Sherwood, E. Rabkin, Y. Masuda, G.A. Garcia, D.L. McLellan, G.C. Engelmayr, M.S. Sacks, F.J. Schoen, and J.E. Mayer, *From stem cells to viable autologous semilunar heart valve.* Circulation, 2005. **111**(21): p. 2783-2791.
28. Tabakow, P., W. Jarmundowicz, B. Czapiga, W. Fortuna, R. Miedzybrodzki, M. Czyz, J. Huber, D. Szarek, S. Okurowski, P. Szewczyk, A. Gorski, and G. Raisman, *Transplantation of Autologous Olfactory Ensheathing Cells in Complete Human Spinal Cord Injury.* Cell Transplantation, 2013. **22**(9): p. 1591-1612.
29. Takahashi, K., K. Tanabe, M. Ohnuki, M. Narita, T. Ichisaka, K. Tomoda, and S. Yamanaka, *Induction of pluripotent stem cells from adult human fibroblasts by defined factors.* Cell, 2007. **131**(5): p. 861-872.
30. Institute, N., *The Nobel Prize in Physiology or Medicine 2012 - Press Release*. 2012, Nobel Media: Nobelprize.org.
31. Cyranoski, D. *Japanese woman is first recipient of next-generation stem cells*. 2014; Available from: http://www.nature.com/news/japanese-woman-is-first-recipient-of-next-generation-stem-cells-1.15915.
32. Doerner, S., *Dielektrische und akustische Spektroskopie als prozesstaugliche Analyseverfahren zur Charakterisierung fluid-disperser Systeme.* 2008, Faculty of Electrical Engineering and Information Technology. .
33. Justice, C., A. Brix, D. Freimark, M. Kraume, P. Pfromm, B. Eichenmueller, and P. Czermak, *Process control in cell culture technology using dielectric spectroscopy.* Biotechnology Advances, 2011. **29**(4): p. 391-401.
34. Ron, A., N. Fishelson, N. Croitoriu, D. Benayahu, and Y. Shacham-Diamand, *Theoretical examination of aggregation effect on the dielectric characteristics of spherical cellular suspension.* Biophysical Chemistry, 2009. **140**(1-3): p. 39-50.
35. Lackner, J.M. and W. Waldhauser, *Inorganic PVD and CVD Coatings in Medicine - A Review of Protein and Cell Adhesion on Coated Surfaces.* Journal of Adhesion Science and Technology, 2010. **24**(5): p. 925-961.
36. Gleixner, R. and P. Fromherz, *The extracellular electrical resistivity in cell adhesion.* Biophysical Journal, 2006. **90**(7): p. 2600-2611.
37. Brooker, R.J., *Biology*. 2011, New York: McGraw-Hill.
38. Selvakumaran, J., M.P. Hughes, J.L. Keddie, and D.J. Ewins, *Assessing biocompatibility of materials for implantable microelectrodes using cytotoxicity and protein adsorption studies*.

2nd Annual International Ieee-Embs Special Topic Conference on Microtechnologies in Medicine & Biology, Proceedings, ed. A. Dittmar and D. Beebe. 2002, New York: Ieee. 261-264.
39. *ABTECH Scientific, Inc.*; Available from: http://www.abtechsci.com/.
40. Matveeva, E., *Electrochemistry of the indium-tin oxide electrode in 1 M NaOH electrolyte.* Journal of the Electrochemical Society, 2005. **152**(9): p. H138-H145.
41. den Otter, M.W., *Approximate expressions for the capacitance and electrostatic potential of interdigitated electrodes.* Sensors and Actuators a-Physical, 2002. **96**(2-3): p. 140-144.
42. Mirtaheri, P., S. Grimnes, and O.G. Martinsen, *Electrode polarization impedance in weak NaCl aqueous solutions.* Ieee Transactions on Biomedical Engineering, 2005. **52**(12): p. 2093-2099.
43. Josefsberg, J.O. and B. Buckland, *Vaccine process technology.* Biotechnology and Bioengineering, 2012. **109**(6): p. 1443-1460.
44. Stacey, G., *CURRENT DEVELOPMENTS IN CELL CULTURE TECHNOLOGY*, in *New Technologies for Toxicity Testing*, M. Balls, R.D. Combes, and N. Bhogal, Editors. 2012, Springer-Verlag Berlin: Berlin. p. 1-13.
45. Paschos, N.K., W.E. Brown, R. Eswaramoorthy, J.C. Hu, and K.A. Athanasiou, *Advances in tissue engineering through stem cell-based co-culture.* Journal of Tissue Engineering and Regenerative Medicine, 2015. **9**(5): p. 488-503.
46. McAteer, J.A. and J. Davis, *Basic cell culture technique and the maintenance of cell lines*. Practical Approach Series; Basic cell culture, ed. J.M. Davis. 1994: Oxford University Press, Walton Street, Oxford OX2 6DP, England 200 Madison Avenue, New York, New York 10016, USA. 93-148.
47. Roberts, P.L., *Sterilization*. Practical Approach Series; Basic cell culture, ed. J.M. Davis. 1994: Oxford University Press, Walton Street, Oxford OX2 6DP, England 200 Madison Avenue, New York, New York 10016, USA. 27-55.
48. Zernike, F., *Phase contrast, a new method for the microscopic observation of transparent objects.* Physica, 1942. **9**(7): p. 686-698.
49. Zernike, F., *Phase contrast, a new method for the microscopic observation of transparent objects Part II.* Physica, 1942. **9**: p. 974-986.
50. Prize, N. *The Nobel Prize in Physics 1953*. Available from: http://www.nobelprize.org/nobel_prizes/physics/laureates/1953/.
51. Egeberg, *Working principle of phase contrast microscopy.*, Working_principle_of_phase_contrast_microscopy.gif, Editor. 2012, Wikimedia Commons: https://commons.wikimedia.org/wiki/File:Working_principle_of_phase_contrast_microscopy.gif.
52. Wegener, J., C.R. Keese, and I. Giaever, *Electric cell-substrate impedance sensing (ECIS) as a noninvasive means to monitor the kinetics of cell spreading to artificial surfaces.* Experimental Cell Research, 2000. **259**(1): p. 158-166.
53. Strauss, O., *The role of retinal pigment epithelium in visual functions.* Ophthalmologe, 2009. **106**(4): p. 299-304.
54. Unknown, *Retinal pigment epithelium*. Oxford Journals, http://hmg.oxfordjournals.org/content/19/21/4229/F1.expansion.html.
55. Carter, H.V., *Anatomy of the Retina*, Gray881.png, Editor. 1858, Lee and Febiger: Anatomy of the Human Body. p. Cross-section drawing of retina.
56. Dunn, K.C., A.E. AotakiKeen, F.R. Putkey, and L.M. Hjelmeland, *ARPE-19, a human retinal pigment epithelial cell line with differentiated properties.* Experimental Eye Research, 1996. **62**(2): p. 155-169.

57. Burridge, K., K. Fath, T. Kelly, G. Nuckolls, and C. Turner, *FOCAL ADHESIONS - TRANSMEMBRANE JUNCTIONS BETWEEN THE EXTRACELLULAR-MATRIX AND THE CYTOSKELETON.* Annual Review of Cell Biology, 1988. **4**: p. 487-525.
58. Ward, M.D. and D.A. Hammer, *Morphology of cell-substratum adhesion. Influence of receptor heterogeneity and nonspecific forces.* Cell biophysics, 1992. **20**(2-3): p. 177-222.
59. Jungbauer, S., R. Kemkemer, H. Gruler, D. Kaufmann, and J.P. Spatz, *Cell shape normalization, dendrite orientation, and melanin production of normal and genetically altered (haploinsufficient NF1)-melanocytes by microstructured substrate interactions.* Chemphyschem, 2004. **5**(1): p. 85-92.
60. Uttayarat, P., G.K. Toworfe, F. Dietrich, P.I. Lelkes, and R.J. Composto, *Topographic guidance of endothelial cells on silicone surfaces with micro- to nanogrooves: Orientation of actin filaments and focal adhesions.* Journal of Biomedical Materials Research Part A, 2005. **75A**(3): p. 668-680.
61. Oakley, C. and D.M. Brunette, *THE SEQUENCE OF ALIGNMENT OF MICROTUBULES, FOCAL CONTACTS AND ACTIN-FILAMENTS IN FIBROBLASTS SPREADING ON SMOOTH AND GROOVED TITANIUM SUBSTRATA.* Journal of Cell Science, 1993. **106**: p. 343-354.
62. Chen, C.S., M. Mrksich, S. Huang, G.M. Whitesides, and D.E. Ingber, *Geometric control of cell life and death.* Science, 1997. **276**(5317): p. 1425-1428.
63. Curtis, A.S.G. and C.D. Wilkinson, *Reactions of cells to topography.* Journal of Biomaterials Science-Polymer Edition, 1998. **9**(12): p. 1313-1329.
64. Cartwright, T. and G.P. Shah, *Culture media*. Practical Approach Series; Basic cell culture, ed. J.M. Davis. 1994: Oxford University Press, Walton Street, Oxford OX2 6DP, England 200 Madison Avenue, New York, New York 10016, USA. 57-91.
65. Fedoroff, S. and A. Richardson, *Protocols for Neural Cell Culture*. 2008: Humana Press.
66. Westas, E., L.M. Svanborg, P. Wallin, B. Bauer, M.B. Ericson, A. Wennerberg, K. Mustafa, and M. Andersson, *Using QCM-D to study the adhesion of human gingival fibroblasts on implant surfaces.* Journal of Biomedical Materials Research Part A, 2015. **103**(10): p. 3139-3147.
67. Lv, C., X.J. Wang, A. Govindasamy, H. Tsuboi, M. Koyama, M. Kubo, H. Ookawa, and A. Miyamoto, *Tight-binding quantum chemical calculations of electronic structures of indium tin oxide.* Japanese Journal of Applied Physics Part 1-Regular Papers Brief Communications & Review Papers, 2005. **44**(4B): p. 2806-2809.
68. Tak, Y.H., K.B. Kim, H.G. Park, K.H. Lee, and J.L. Lee, *Criteria for ITO (indium-tin-oxide) thin film as the bottom electrode of an organic light emitting diode (vol 411, pg 12, 2002).* Thin Solid Films, 2009. **517**(15): p. 4490-4490.
69. Hong, C.H., J.H. Shin, B.K. Ju, K.H. Kim, N.M. Park, B.S. Kim, and W.S. Cheong, *Index-Matched Indium Tin Oxide Electrodes for Capacitive Touch Screen Panel Applications.* Journal of Nanoscience and Nanotechnology, 2013. **13**(11): p. 7756-7759.
70. Zhang, L., Y.J. Zhou, L. Guo, W.W. Zhao, A. Barnes, H.T. Zhang, C. Eaton, Y.X. Zheng, M. Brahlek, H.F. Haneef, N.J. Podraza, M.H.W. Chan, V. Gopalan, K.M. Rabe, and R. Engel-Herbert, *Correlated metals as transparent conductors.* Nature Materials, 2016. **15**(2): p. 204-+.
71. Lu, J.L., J.W. Elam, and P.C. Stair, *Atomic layer deposition-Sequential self-limiting surface reactions for advanced catalyst "bottom-up" synthesis.* Surface Science Reports, 2016. **71**(2): p. 410-472.
72. Nilsen, O., K.B. Klepper, H.O. Nielsen, and H. Fjellvag, *Deposition of Organic- Inorganic Hybrid Materials by Atomic Layer Deposition*, in *Atomic Layer Deposition Applications 4*, A. Londergan, et al., Editors. 2008, Electrochemical Society Inc: Pennington. p. 3-14.
73. Klepper, K.B., O. Nilsen, and H. Fjellvag, *Growth of thin films of Co3O4 by atomic layer deposition.* Thin Solid Films, 2007. **515**(20-21): p. 7772-7781.

74. Lodewijks, K. *Spectroscopic Ellipsometry*. Available from: http://www.kristoflodewijks.be/?page_id=262.
75. Love, C.J., *Separation of even and odd terms*. 2016: http://www.mapleprimes.com/questions/211460-Series-Of-Bessel-Functions#comment227147. p. Forum discussion.
76. Onnela, N., V. Savolainen, K. Juuti-Uusitalo, H. Vaajasaari, H. Skottman, and J. Hyttinen, *Electric impedance of human embryonic stem cell-derived retinal pigment epithelium.* Medical & Biological Engineering & Computing, 2012. **50**(2): p. 107-116.
77. Toimela, T., H. Maenpaa, M. Mannerstrom, and H. Tahti, *Development of an in vitro blood-brain barrier model-cytotoxicity of mercury and aluminum.* Toxicology and Applied Pharmacology, 2004. **195**(1): p. 73-82.
78. Nevala, H., T. Ylikomi, and H. Tahti, *Evaluation of the selected barrier properties of retinal pigment epithelial cell line ARPE-19 for an in-vitro blood-brain barrier model.* Human & Experimental Toxicology, 2008. **27**(10): p. 741-749.
79. Mannermaa, E., M. Reinisalo, V.P. Ranta, K.S. Vellonen, H. Kokki, A. Saarikko, K. Kaarniranta, and A. Urtti, *Filter-cultured ARPE-19 cells as outer blood-retinal barrier model.* European Journal of Pharmaceutical Sciences, 2010. **40**(4): p. 289-296.
80. Wegener, J., M. Sieber, and H.J. Galla, *Impedance analysis of epithelial and endothelial cell monolayers cultured on gold surfaces.* Journal of Biochemical and Biophysical Methods, 1996. **32**(3): p. 151-170.
81. Vos, M., G.G. Marmitt, Y. Finkelstein, and R. Moreh, *Determining the band gap and mean kinetic energy of atoms from reflection electron energy loss spectra.* Journal of Chemical Physics, 2015. **143**(10): p. 11.
82. Lebron, I., D.A. Robinson, S. Goldberg, and S.M. Lesch, *The dielectric permittivity of calcite and arid zone soils with carbonate minerals.* Soil Science Society of America Journal, 2004. **68**(5): p. 1549-1559.
83. Bansal, N.P. and R.H. Doremus, *Chapter 14 - Dielectric Properties*, in *Handbook of Glass Properties*. 1986, Academic Press: San Diego. p. 450-499.
84. Bagnaninchi, P.O., M. Dikeakos, T. Veres, and M. Tabrizian, *Complex permittivity measurement as a new noninvasive tool for monitoring In vitro tissue engineering and cell signature through the detection of cell proliferation, differentiation, and pretissue formation.* Ieee Transactions on Nanobioscience, 2004. **3**(4): p. 243-250.
85. supplies, S. *Indium-Tin-Oxide (ITO) Coated Slides & Coverslips*. Indium-Tin-Oxide (ITO) Coated Slides & Coverslips]. Available from: http://www.2spi.com/category/ito-coated-substrates/light-microscopy/.
86. Raciukaitis, G., M. Brikas, M. Gedvilas, and T. Rakickas, *Patterning of indium-tin oxide on glass with picosecond lasers.* Applied Surface Science, 2007. **253**(15): p. 6570-6574.
87. Kvalvik, J.N., *Bioactive surfaces by atomic layer deposition*, in *Department of Physics*. 2015, University of Oslo: https://www.duo.uio.no/bitstream/handle/10852/47763/Masteroppgave_Julie_Nitsche_Kvalvik_final.pdf. p. 118.
88. Tolba, E., W.E.G. Muller, B.M.A. El-Hady, M. Neufurth, F. Wurm, S.F. Wang, H.C. Schroder, and X.H. Wang, *High biocompatibility and improved osteogenic potential of amorphous calcium carbonate/vaterite.* Journal of Materials Chemistry B, 2016. **4**(3): p. 376-386.
89. Medeiros, S.K., E.L. Albuquerque, F.F. Maia, E.W.S. Caetano, and V.N. Freire, *Electronic and optical properties of CaCO3 calcite, and excitons in Si@ CaCO3 and CaCO3@ SiO2 core-shell quantum dots.* Journal of Physics D-Applied Physics, 2007. **40**(18): p. 5747-5752.

90. Roberts, S., *DIELECTRIC CONSTANTS AND POLARIZABILITIES OF IONS IN SIMPLE CRYSTALS AND BARIUM TITANATE.* Physical Review, 1949. **76**(8): p. 1215-1220.
91. Douglas B. Murphy, K.R.S., Michael W. Davidson. *Comparison of Phase Contrast and DIC Microscopy*. 2012; Available from: http://www.olympusmicro.com/primer/techniques/dic/dicphasecomparison.html.
92. Hamilton, *Hamilton Company conductance probes*. Hamilton Company, http://www.hamiltoncompany.com/products/process-analytics/sensors/conductivity.
93. Novocontrol, *Novotech interdigitated electrode 150 um.*
94. Ibidi. *ECIS system*. Available from: http://ibidi.com/xtproducts/en/Instruments-Accessories/ECIS-Electric-Cell-Substrate-Impedance-Sensing.
95. Ibidi, *ECIS electrodes*.
96. Malleo, D., J.T. Nevill, L.P. Lee, and H. Morgan, *Continuous differential impedance spectroscopy of single cells.* Microfluidics and Nanofluidics, 2010. **9**(2-3): p. 191-198.

Appendices

Appendix A - Design Iterations

The designs and prototypes of the device went through several iterations to accommodate the necessary changes for the device to function adequately (Figure 79 and Figure 80).

Creating and maintaining the cells' necessary environment for proliferation and survival was an ongoing process, and evolved during the project. The cells died repeatedly in the devices until a working prototype was achieved.

Rapid evaporation was a problem in the early runs. When investigated, the water pan in the bottom of the incubator proved to be empty; when this was filled, evaporation was less of a problem, but still a present one. The cell well lid shape and material was adjusted several times to limit evaporation, allow sufficient ventilation for O_2 and CO_2 exchange, and biocompatibility. Lids were made from acrylic, 3D-printed ABS plastic with and without epoxy or silicone lining, and eventually, glass tubing.

Version 1 (Figure 79 a and c) of the device featured 4 pairs of electrodes, a machined acrylic wire mount which was glued in place with epoxy or construction adhesive, and a machined acrylic lid. It was discarded due to evaporation of the medium.

Version 2 (Figure 79 b and d) had 3D-printed ABS plastic parts. The glass plate and wire mount were made wider to facilitate application of the epoxy glued to fix them together, as well as a lid with a "curtain" to improve ventilation. It was discarded due to glue toxicity.

Version 3 (Figure 79 c and f) had a glass culture well cut from a tube of SiO_2 glass, separated from the wire mount to reduce the pressure on the glass plate, and to minimise contact between the cell culture medium and adhesive or plastic. It was discarded due to being difficult to assemble and handle without damaging the components, as parts were positioned close together and the wire mount was not fixed to the substrate. Its lid was 3D-printed in ABS plastic and lined with silicone.

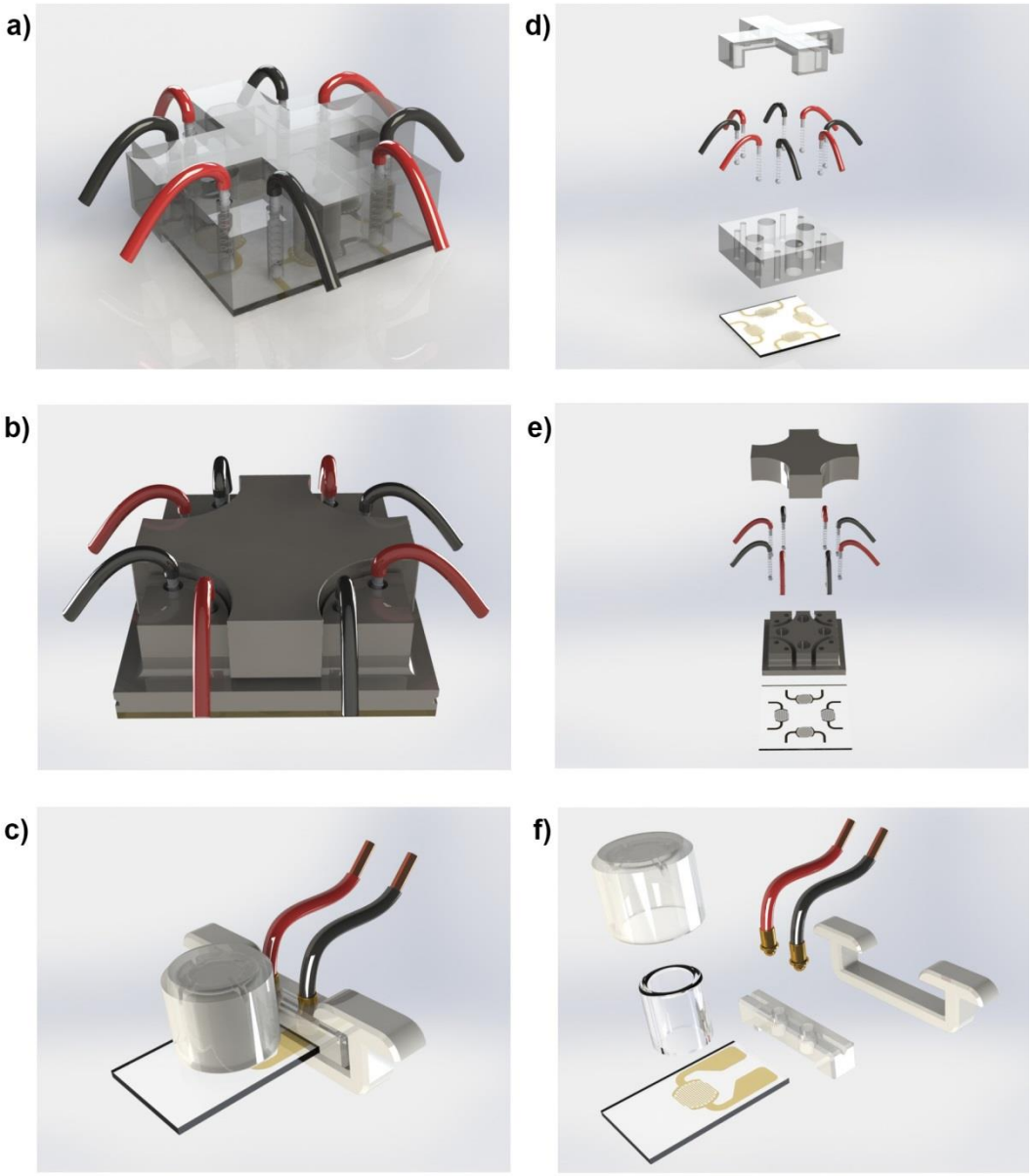

Figure 79 - Design iterations of the sensing device. a): Version 1: 4 electrode pairs in with wires in plexiglass mount glued to substrate. b): Version 2: 4 electrode pairs with wires in ABS mount glued to substrate. c): Version 3: 1 electrode pair, glass tube culture well fixed with silicone, cell well separated from wire mount, ABS well lid. d), e) and f): exploded view of a), b) and c).

Version 4 (Figure 80 a and d) avoided the use of adhesive by ensuring pressure on the glass cell culture well and sealing the interface between the well and the substrate with a rubber o-ring. It was focused on ease of assembly, where it succeeded. It failed due to toxicity of the rubber o-ring.

Version 5 (Figure 80 b and e) was successful. It was easy to assemble and significantly sturdy to survive handling and experiments. It featured a glass lid to eliminate the need for silicone lining. It enabled cell attachment and proliferation, and impedance measurements of the culture. It was used for the majority of the experiments described in section 3.3.

Version 6 (Figure 80 c and f) was created to enable measurement on slides that were cut for device version 2. Glass wells were fixed by silicone. It was also successful in enabling cell attachment and growth, and measurements. It was used only for one TTIP/glycine slide.

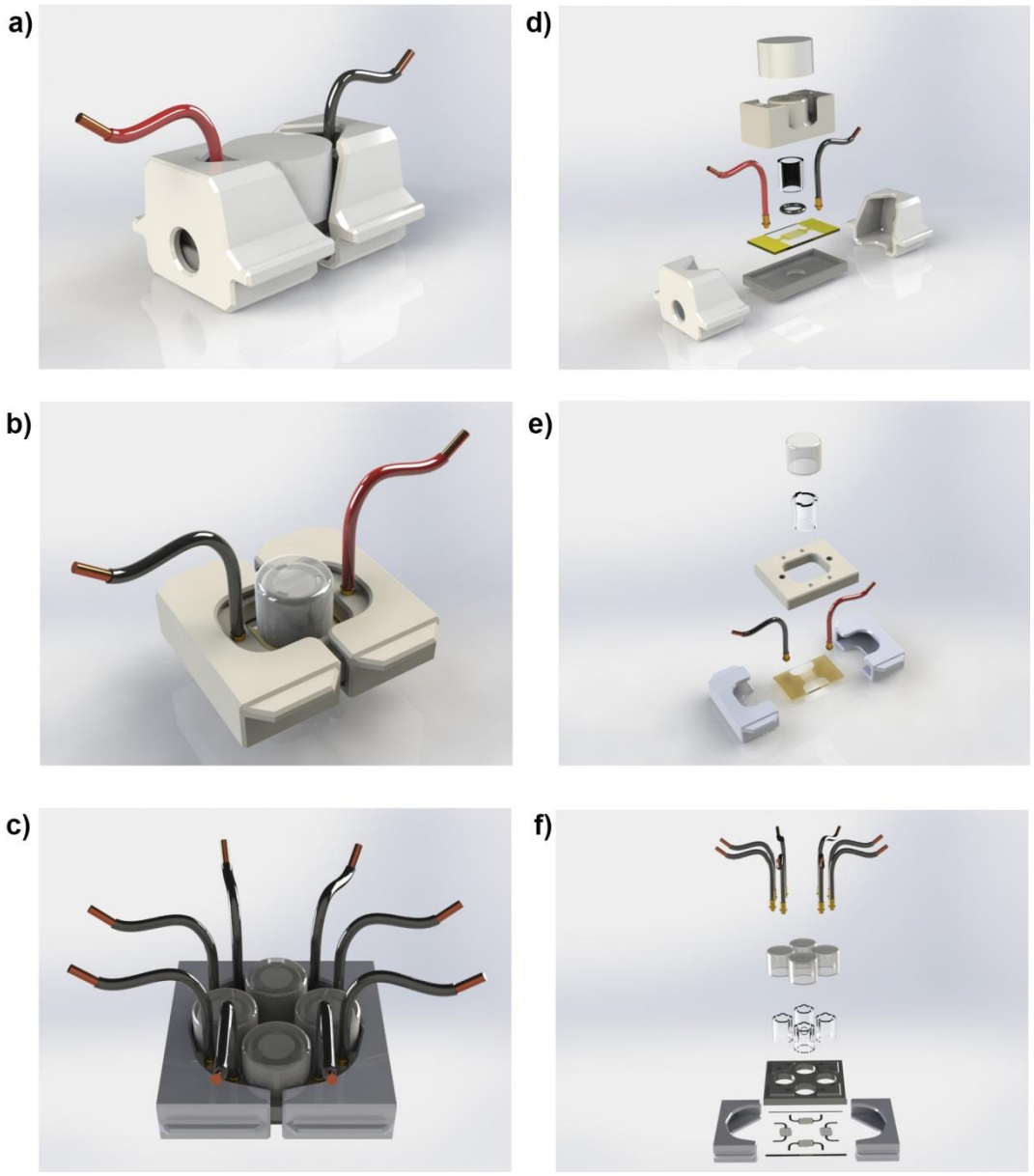

Figure 80 - Design iterations of the sensing device. In all 3 versions, wires are held in place by an ABS plastic mount fixed mechanically. a): 1 electrode pair with cell well and wire mount separated, culture well fixed to substrate with silicone. b): 1 electrode pair with mount fixed by clips, the culture well held in place mechanically with rubber o-ring to waterproof the bottom of the well and a "bed" to prevent breakage from pressure from the culture well. c): 4 electrode pairs with cell wells and wire mount separated. Culture wells fixed with aquarium silicone. d), e) and f): exploded views.

Appendix B - Electrics and Dielectrics

Admittance is the inverse of impedance, and is denominated by **Y**, so **Y** = 1/**Z**. It is measured in the SI unit siemens (S). In complex terms,

$$\mathbf{Y} = G + jB \quad [\mathrm{S}] \tag{21}$$

where *G* is conductance, *j* is the imaginary unit, and *B* is susceptance. Complex admittance is useful when considering a conductive material with capacitive properties. When measuring circuits with resistors and capacitors in parallel, it is simpler to evaluate them in terms of admittance than impedance. In a non-inductive circuit, $B = \omega C$, where ω is the angular frequency of the current, and *C* is capacitance.

In a circuit with admittances $\mathbf{Y}_1$, $\mathbf{Y}_2$, $\mathbf{Y}_3$, … in *series*, the expression for total admittance $\mathbf{Y}_\mathrm{S}$ is determined by the relation

$$\frac{1}{\mathbf{Y}_\mathrm{S}} = \frac{1}{\mathbf{Y}_1} + \frac{1}{\mathbf{Y}_2} + \frac{1}{\mathbf{Y}_3} + \cdots \tag{22}$$

which in a circuit with a resistor *R* and capacitor *C* in *series* yields the relation

$$\mathbf{Y}_\mathrm{S} = \frac{R + \frac{j}{\omega C}}{R^2 + \frac{1}{\omega^2 C^2}} \quad [\mathrm{S}] \tag{23}$$

where *j* is the imaginary unit and ω is the angular frequency of the current.

For a circuit with admittances $\mathbf{Y}_1$, $\mathbf{Y}_2$, $\mathbf{Y}_3$, … in *parallel*, the total admittance $\mathbf{Y}_\mathrm{P}$ is

$$\mathbf{Y}_\mathrm{P} = \mathbf{Y}_1 + \mathbf{Y}_2 + \mathbf{Y}_3 + \cdots \quad [\mathrm{S}] \tag{24}$$

which in a circuit with a resistor *R* and capacitor *C* in *parallel* yields the relation

$$\mathbf{Y}_\mathrm{P} = \frac{1}{R} + j\omega C \quad [\mathrm{S}] \tag{25}$$

where *j* is the imaginary unit and ω is the angular frequency of the current.

Capacitance is the ability to store electric charge; it is the denoted by *C* and measured in the SI derived unit farad (F). For a parallel-plate capacitor, the capacitance $C = Q / V$, where *Q* and –*Q* are the charges on the two capacitor plates, and *V* is the voltage between them. In the same capacitor, the capacitance can be expressed in terms of the permittivity of the material between the plates:

$$C = \varepsilon \frac{A}{d} \quad [\mathrm{F}] \tag{26}$$

where ε is the permittivity of the material between the plates, A is the area of the plates and d is the distance between the plates.

Conductance, usually expressed by G and measured in the SI unit siemens (S), is the inverse of resistance: $Y = 1 / R = I / V$, and 1 S = 1 / 1 Ω = 1 A / 1 V, and is a value for how easily current passes through a material.

Current density, measured in A/m^2 and usually denoted by **J**, is a vector with a magnitude equal to the current per cross-sectional area. It can be expressed by the equation

$$I = \int \mathbf{J}\, d\mathbf{A} \quad [\mathrm{A}] \tag{27}$$

where I denotes current [A], **J** denotes current density [A/m^2] and **A** denotes area [m^2]. Current density can also be expressed in terms of conductivity **σ** and electric field **E**:

$$\mathbf{J} = \boldsymbol{\sigma}\mathbf{E} \quad [\mathrm{A/m^2}] \tag{28}$$

In an electrolytic conductor, the current density is given by:

$$\mathbf{J} = (nze\mathbf{v})_+ + (nze\mathbf{v})_- \quad [\mathrm{A/m^2}] \tag{29}$$

where n denotes charge carrier density, z denotes electric charge per carrier, e is the elementary electric charge, **v** is the charge velocity, and the + and – subscripts denote cations and anions, respectively [4].

High current density can be very damaging to tissue. It's often said that it's not high voltage that are dangerous, it's high current; this is, however, also dependent on current density. A low current may still be dangerous if the current density is high enough, and a higher current may be tolerable if the current density is low, i.e. the current is spread out wide and thin enough.

Electric current, measured in the SI unit ampere (A) and usually denoted in equations by the symbol I, is a measure of flowing electric charge. Electric charge is a fundamental property of subatomic particles (some particles have 0 charge), and is measured in the SI-derived units coulomb (C) or elementary charge (e) and usually denoted by the symbol Q or q; 1 C corresponds to approximately 1.602×10^{19} e. An electron has a charge of –e, while a proton has a charge of +e. 1 ampere equals 1 coulomb of charge flowing across a surface in one second, 1 A = 1 C/s, or, in the standard equation symbolism, $I = Q / t$, where t is the usual

symbol for time, when the charge flow is steady. More generally, current can be expressed as the rate of charge flow across a given surface,

$$I = \frac{dQ}{dt} \quad [\mathrm{A}] \tag{30}$$

where *I* denotes current, *Q* denotes charge [C], and *t* denotes time [s].Current as a concept is divided into DC, where the direction of the charge flow is constant, and AC, where the charge flow oscillates.[8] Bioimpedance measurements usually utilises weak currents, in the µA or low mA range, and frequencies in the kHz-MHz range.

Electric potential energy, or just *electric potential*, measured in the SI unit volt (V), is a measure of the electric potential energy a charge would have at a given point in space. It defined as the work that would be performed by an electric field in moving a unit positive electrical charge from that point to infinity. Voltage is the difference in electric potential energy between two points, and is denoted by V or U in equations. 1 volt is equal to 1 joule (J) of energy per coulomb. For AC, used in mains supplies around the world[9], the voltage (and current) follows a sine wave, and the voltage declared is actually the root mean square (rms) of the peak voltage. Bioimpedance measurements usually utilise AC with voltage in the lower mV range.

Impedance is the complex representation of electrical resistance in a medium. It is denominated by **Z** and is measured in the SI unit ohm (Ω). In complex terms,

$$\mathbf{Z} = \mathbf{R} + \mathbf{jX} \quad [\Omega] \tag{31}$$

where R is resistance, X is reactance and j is the imaginary unit, $\sqrt{1}$. In an ideal capacitor with no resistance and no loss, $R = 0$ and $X = 1 / \omega C$, where ω is the angular frequency of the current and C is the capacitance of the capacitor. *j* is used as the symbol for the imaginary unit to avoid confusion with the symbol for electric current, I or i.

When measuring circuits with resistors and capacitors in series, it is simpler to evaluate them in terms of impedance than admittance. According to Kirchoff's circuit laws, and similar to resistance, the total impedance $\mathbf{Z}_S$ of a circuit with impedances $\mathbf{Z}_1$, $\mathbf{Z}_2$, $\mathbf{Z}_3$, … in *series* increases with the number of impedance elements,

$$\mathbf{Z}_S = \mathbf{Z}_1 + \mathbf{Z}_2 + \mathbf{Z}_3 + \cdots \quad [\Omega] \tag{32}$$

[8] The frequency of the Norwegian residential mains supply, which carries AC, is currently 50 Hz, with small variations.

[9] In Norway, the voltage of the mains supply is 230V; the peak voltage is 230V · √2= 325V.

which in a circuit with a resistor *R* and a capacitor *C* in *series* yields the relation

$$\mathbf{Z}_{\mathrm{S}} = R + \frac{1}{j\omega C} \quad [\Omega] \tag{33}$$

where *j* is the imaginary unit and ω is the angular frequency of the current.

In a circuit with impedances $\mathbf{Z}_1$, $\mathbf{Z}_2$, $\mathbf{Z}_3$, … in *parallel*, the total impedance $\mathbf{Z}_{\mathrm{P}}$ is determined by the relation

$$\frac{1}{\mathbf{Z}_{\mathrm{S}}} = \frac{1}{\mathbf{Z}_1} + \frac{1}{\mathbf{Z}_2} + \frac{1}{\mathbf{Z}_3} + \cdots \tag{34}$$

which in a circuit with a resistor *R* and a capacitor *C* in *parallel* yields the relation

$$\mathbf{Z}_{\mathrm{P}} = \frac{R(1 - j\omega CR)}{1 + \omega^2 C^2 R^2} \quad [\Omega] \tag{35}$$

where *j* is the imaginary unit and ω is the angular frequency of the current.

Permittivity, ε, is a measure of how a material is affected by and how it affects an electric field, and is related to and caused by polarisation in the material. Relative permittivity[10] ε_r is the ratio of a material's permittivity to the permittivity of vacuum, ε_0, so that $\varepsilon = \varepsilon_r\ \varepsilon_0$.

Permittivity is dependent on the current frequency, and when AC is passed through a medium, its phase may be changed. Therefore it is useful to treat permittivity as a complex value when AC is involved. The expression then becomes

$$\boldsymbol{\varepsilon} \equiv \varepsilon' - j\varepsilon'' \equiv (\varepsilon_{\mathrm{r}}' - j\varepsilon_{\mathrm{r}}'')\varepsilon_0 \qquad [\mathrm{F/m}] \tag{36}$$

where $\boldsymbol{\varepsilon}$ is the complex permittivity, ε' is the real part of the permittivity, ε'' is the imaginary part of the permittivity, and *j* is the imaginary unit, used instead of the usual *i* to avoid confusion with *I* or *i* as the usual symbols for current. For materials with only electronic charge carriers, permittivity usually varies insignificantly in DC and in AC with frequencies up to 10^{15} Hz. Materials with larger charge carriers like ions and polar molecules will experience variations in permittivity at lower frequencies (see section on "Dispersions").

[10] Relative permittivity is also called "dielectric constant". This term is deprecated in contexts of physics, but still in use in contexts of chemistry.

Reactance can be seen as a circuit element's resistance to a *change* of current in the circuit, either by inductive reactance or capacitive reactance. It can also be interpreted as the degree to which an element stores and releases energy with each oscillation of an AC circuit. Reactance is only observed for changing current, which usually means AC. It is denominated by *X* and measured in the SI unit ohm [Ω]. Inductive reactance is proportional to the current frequency and the element's inductance, while capacitive reactance is inversely proportional to the current frequency and the element's capacitance. In cell culture impedance sensing (and bioimpedance in general), inductive reactance can largely be ignored, as its contributions are usually negligible, while capacitive reactance is one of the main properties measured and interpreted.

Capacitive reactance can be described as the capacitive element's resistance to the electric field created by charges accumulated at the capacitor's plates. The resistance is due to the polarisable elements in the dielectric between the capacitive plates realigning due to the magnetic field, generating an electric field of their own, which opposes the capacitor plates' electric field. This opposition rises as the electric field over the dielectric rises. When the frequency increases, the build-up of charge on the capacitor plates will be smaller, resulting in a weaker electric field, again resulting in a weaker opposing electric field in the dielectric.

Capacitive reactance is expressed as

$$X_C = -\frac{1}{\omega C} = -\frac{1}{2\pi f C} \quad [\Omega] \tag{37}$$

where ω is the angular frequency of the current, C is capacitance, and f is the current frequency. Since capacitance is proportional to permittivity, i.e. $C \propto \varepsilon$, it follows that capacitive reactance is inversely proportional to ε, i.e. $X_C \propto \varepsilon$.

Inductive reactance is expressed by

$$X_L = \omega L = 2\pi f L \quad [\Omega] \tag{38}$$

where ω is the angular frequency of the current, L is inductance, and f is the current frequency.

Resistance is a measure of a medium's resistance to electric current, is measured in the SI unit ohm (Ω), and usually represented in equations by an *R*. The resistance of a medium is proportional to the voltage required to pass a specific current; $R = V / I$, and in unit terms this relationship can be expressed as 1 Ω = 1 V / 1 A.

Susceptance (not to be confused with susceptibility γ) can be seen as a circuit element's "willingness" to allow a change in current. It is denoted by *B* (not to be confused with

magnetic flux density, also represented by *B*) and measured in siemens [S]. Similar to reactance, susceptance can be divided into inductive susceptance and capacitive susceptance.

Capacitive susceptance is expressed as

$$B_C = \omega C = 2\pi f C \quad [\mathrm{S}] \tag{39}$$

where ω is the angular frequency of the current, C is capacitance, and f is the current frequency.

Inductive susceptance is expressed by

$$B_L = \frac{1}{\omega L} = \frac{1}{2\pi f L} \quad [\mathrm{S}] \tag{40}$$

where ω is the angular frequency of the current, L is inductance, and f is the current frequency.

Appendix C - Bessel Functions

Bessel functions are the solutions $y(x)$ of the differential equation

$$x^2\frac{d^2y}{dx^2} + x\frac{dy}{dx} + (x^2 - \alpha^2)y = 0 \tag{41}$$

where α is a complex number, and the order of the Bessel function. This is a second-order differential equation and consequently has two linearly independent solutions. Bessel functions of the first kind are denoted J_α, while those of the second kind are denoted Y_α.

J_α can be defined as

$$J_\alpha = \sum_{m=0}^{\infty} \frac{(-1)^m}{m!\,\Gamma(m+\alpha+1)}\left(\frac{x}{2}\right)^{2m+\alpha} \tag{42}$$

where $\Gamma(z)$ is the gamma function:

$$\Gamma(t) = (n-1)! \tag{43}$$

A plot of the zeroth order Bessel function of the first kind is shown in Figure 81.

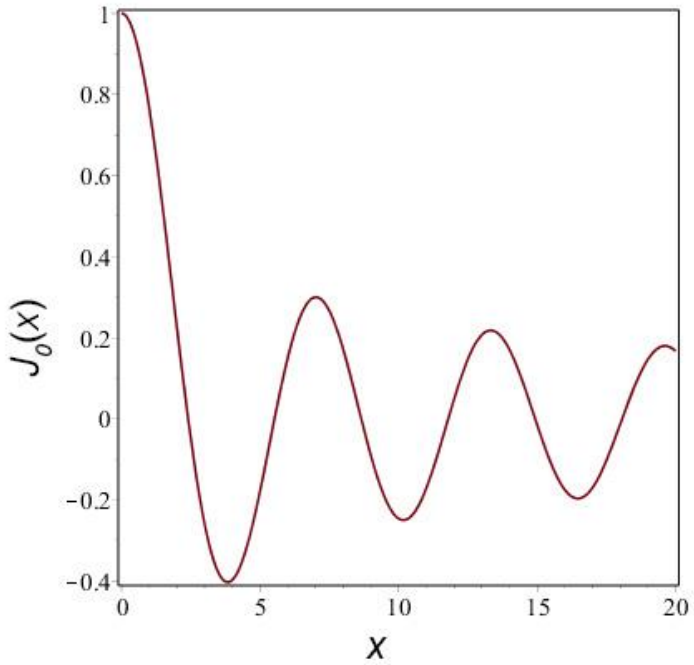

Figure 81 - Zeroth order Bessel function of the first kind.

Appendix D – Equipment Used in This Thesis

The following equipment was used in this thesis:

Name	Manufacturer	Equipment type
DraftSight 2015	Dassault Systémes	Drafting software
Dulbecco's modified Eagle's medium with Ham's F-12 nutrient mixture	Dulbecco	Cell culture medium
Dulbecco's phosphate-buffered saline	Dulbecco	Cell culture buffer
F - 120 Sat reactor	ASM Microchemistry	ALD reactor
Fetal bovine serum	Gibco	Cell culture serum
Inkscape	Inkscape Project	Vector graphics software
ITO Coated Glass Plate	SPI Supplies	300 mm x 300 mm x 1 mm thick glass coated with 350 nm ITO by sputtering
Kojair KR-105	Kojair	Class II microbilogical safety cabinet
Maple	Maplesoft	Computer algebra system
Diaphot ELWD 0.3	Nikon	Phase contrast microscope
No More Nails	Pattex	Construction adhesive
Nunc^{TM} filter cap EasYFlasks	Thermo Scientific	Cell culture flasks, 25 cm^2 and 75 cm^2
Origin 2016	OriginLab Corporation	Graphing & analysis software
P/S Solution	ScienCell	Antibiotic
Parasilico	DL Chemicals	Aquarium silicone
Power Epoxy Universal	Loctite	Two-component adhesive
PowerLine E Laser Cutter	ROFIN	Laser cutter
Rotofix 32	Hettich Lab Technology	Centrifuge
Sciospec ISX-3v2	Sciospec	Single channel impedance analyser
Series II Water Jacketed CO_2 Incubator	ThermoForma	Incubator
Silikon	Casco	Filler silicone
Solidworks 2013	Dassault Systémes	CAD software
Trypsin-EDTA (1X)	Gibco	Trypsin
Ultimaker 2+	Ultimaker	3D printer
Universal Adhesive	JBL Haru	Aquarium adhesive

Appendix E - Vitality of ARPE-19 Cells

The ARPE-19 cell culture was subjected to a toxicity test described in section 3.4.5., where 6 25 cm^2 EasyFlask cell culture bottles had been prepared in advance with smears of different adhesives on the cell culture substrate inside the bottle. Big (~3 cm^2) and small (~0.5 cm^2) smears of epoxy (Figure 82), construction adhesive and silicone were deposited, 1 smear in each, on the cell culture substrates of the bottles, and left to dry, before the culture was split at 1:2 density and seeded in the bottles. Cells grew and proliferated well in both bottles containing an epoxy smear. In the bottles with small smears of construction adhesive and silicone the cells also proliferated. In the bottle with a large smear of construction adhesive, the cells died out after a week. In the bottle with a large smear of silicone, the cells died out after 2 weeks.

After an initial run of 1 week of normal medium changes every 3 days, the cells in the toxicity test bottles were left to their own devices for a prolonged time. The survivability of some of the cultures was remarkable. In all the bottles with small smears of different adhesives, and in the bottle with a big smear of epoxy, the cells were alive and confluent 19 days after the last medium change. The cells were, in this last medium change, given 8 ml of medium per 25 cm^2 bottle, just above the upper limit of the recommended amount of 0.2-0.3 ml/cm^2, which for a 25 cm^2 bottle resolves to 7.5 ml.

A similar experiment was performed in a 25 cm^2 bottle, and the ARPE-19 culture in this bottle was also alive after 1.5 months without medium change.

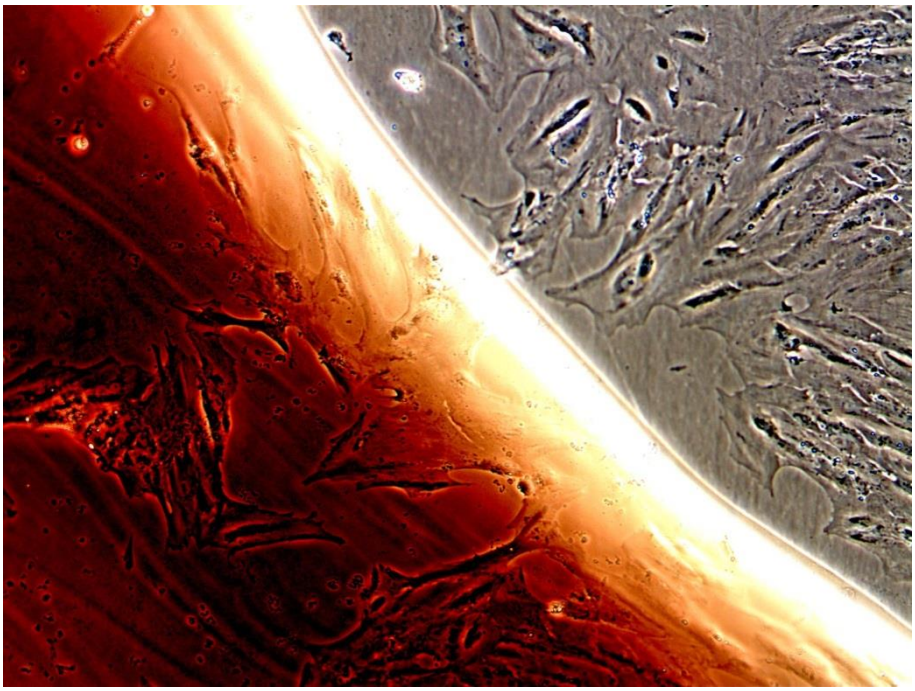

Figure 82 - ARPE-19 cells growing near and on a smear of epoxy. The red colour of the epoxy has been absorbed from the cell culture medium.

Appendix F - Impedance Sensing Equipment

F.1 - Commercial Equipment

A signal generator and analyser is necessary, and often combined in a separate unit, which can be coupled with a computer to record data. The sensors vary according to manufacturer and intended use: Probes used in liquids and suspensions, plate capacitors to measure films and bulk properties, and substrate electrodes to measure surface properties, films or attached cell cultures.

Solartron produces some of the most commonly used impedance analysers, including the '1260A Impedance/Gain-phase analyser' and '1294 Impedance Interface'.

Sciospec also produces impedance analysers, some of them portable, like the Sciospec single channel impedance analyzer ISX-3v2, which was used in this thesis.

Probes produced by the manufacturers **Aber Instruments** and **Hamilton Company** are made for suspension measurements and include a probe with a ring electrode (Figure 83) measuring a choice of frequencies, used to insert into the suspension, and which is registered by a regular PC running appropriate, proprietary software. Disposable probes are available to streamline the monitoring process and reduce the need for on-site cleaning and sterilisation [92].

Novocontrol produces interdigitated electrodes with a 150 µm (Figure 84) or 75 µm wide digits. The electrode digits have a height of 35 µm, which means that the electrode pattern would probably be a significant influence on cell attachment and proliferation, should the electrodes be used in a cell culture with attached cells. Their website and newsletter "Dielectrics Newsletter" indicate they would be suitable for measuring liquids and materials where sensitivity in the bulk of the materials is not necessary [93].

Figure 83 - Hamilton suspension probes. From [92].

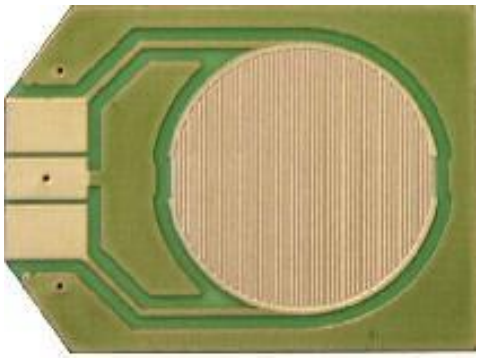

Figure 84 - Novocontrol interdigitated electrodes, 150 µm wide digits.From [93].

Ibidi systems produce their ECIS (Electrical Cell Impedance Sensing) equipment (Figure 85) for substrate impedance sensing, similar to the Novocontrol setup, and with different electrode designs (Figure 86). Their interdigitated electrodes are made from gold, and measure down to 0.1 mm digit thickness, with 0.545 mm between digits. The patterns are

produced by depositing a polymer film on top of a gold electrode, and then etching away the pattern for the electrode. The electrode is then recessed from the substrate. The thickness of the polymer on top of the electrode is 1-5 µm.

The ECIS system was developed by Ivar Giaever and Jens Feder, and was the first commercially produced system of cell culture impedance sensing [94].

Figure 85 - The Ibidi ECIS system. Cell growth array with electrodes in the background (not to scale). From [94].

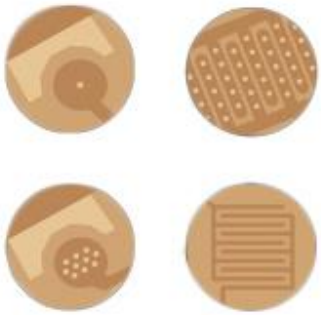

Figure 86 - Different types of Ibidi ECIS electrodes. The brightest areas are areas where the polymer film has been etched off, and the gold electrode is exposed. In the bottom right electrode, no film has been deposited on the electrode, and the dark lines are the exposed gold electrodes. Based on [95]

Abtech produces cell culture impedance sensing equipment with interdigitated electrodes with digit width measuring down to 2 µm, and they offer electrodes made from gold, ITO (Figure 87), and platinum (Figure 88) [39].

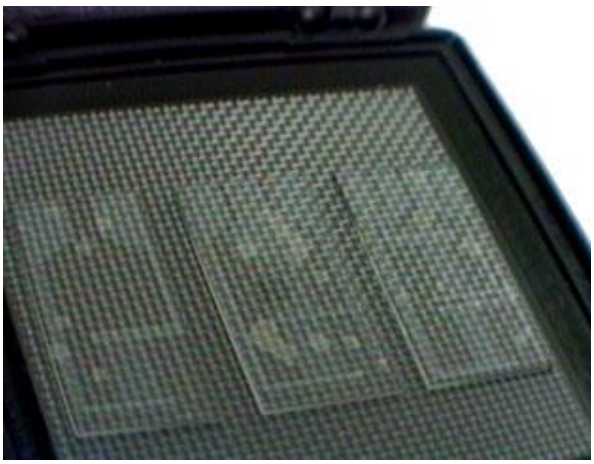

Figure 87 Abtech interdigitated ITO electrodes. From [39].

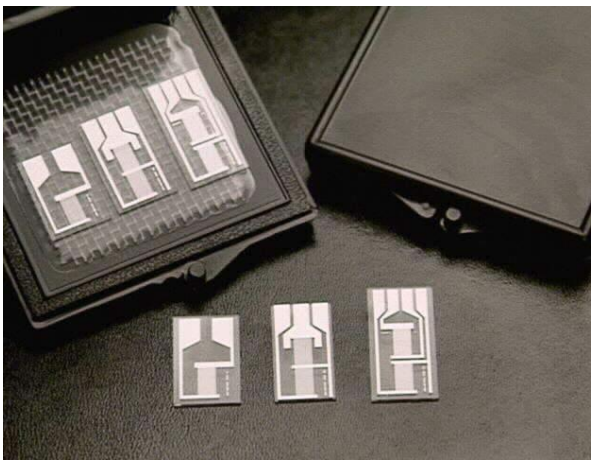

Figure 88 - Abtech interdigitated platinum electrodes. From [39].

F.2 - Experimental Equipment

Custom-made equipment for specific research is offered by several manufacturers, e.g. Ibidi. Researchers themselves have produced different setups, according to the needs of the experiments. Microchannel devices of different designs were produced by Lee *et al.* (Figure

89) [19] and by Malleo *et al.* (Figure 90) [96] to measure single cells, and a multiple electrode device was constructed by Rahman *et al*. to measure cell proliferation (Figure 91) [16].

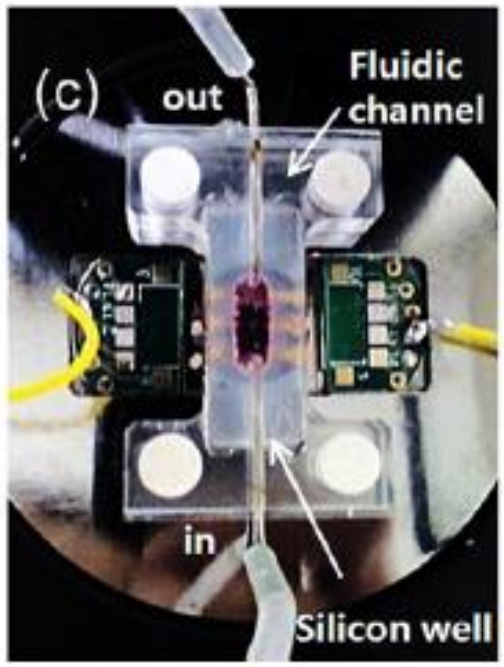

Figure 89 - Microchannel impedance sensing device by Lee *et al.* From [19]

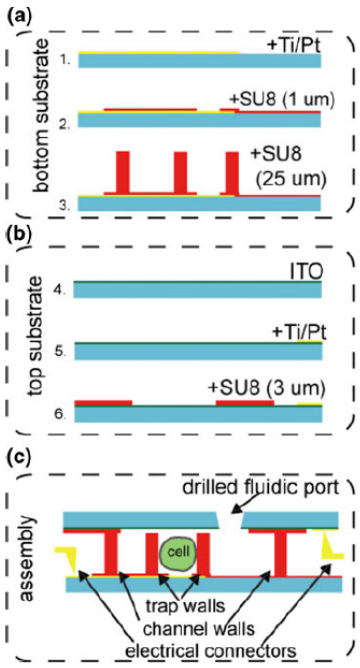

Figure 90 - Microchannel device by Malleo *et al.* ; scetch of manufacturing process. a) bottom substrate with walls b) top substrate with contacts c) assembly of top and bottom substrates. From [96].

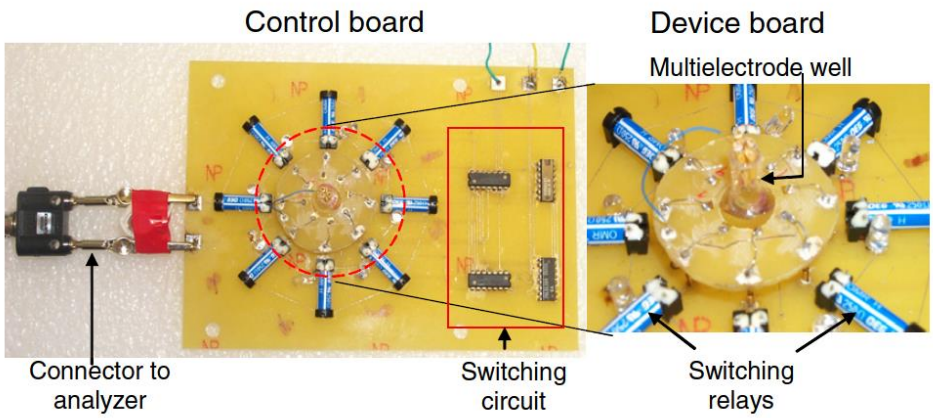

Figure 91 - Multielectrode impedance sensing setup by Rahman *et al*. From [16].

Appendix G - Calculations

Capacitance of interdigitated electrodes (3.2.1):

$$C \approx pq\frac{4}{\pi a}\varepsilon\sum_{n=1}^{\infty}\frac{1}{2n-1}J_0^2\left(\frac{(2n-1)\pi s}{2a}\right)$$

$$= 0.006\text{ m}\cdot 0.006\text{ m}\cdot\frac{4}{\pi\cdot(0.000024\text{ m}+0.000024\text{ m})}\cdot 70.8\text{ nF/m}$$

$$\cdot\sum_{n=1}^{\infty}\frac{1}{2n-1}\cdot J_0^2\cdot\left(\frac{(2n-1)\cdot\pi\cdot 0.000024\,m}{2\cdot(0.000024\,m+0.000024\,m)}\right)=0.531\text{ nF}$$

Resistance of interdigitated ITO electrodes (3.2.1.1):

$$R_{el}=R_c+R_d=\ 2\cdot n_{sc}\cdot 35\ \Omega+\frac{1}{\left(n_f\cdot\frac{1}{35\ \Omega\cdot n_{sf}}\right)}=n_{sc}\cdot 70\ \Omega+\frac{1}{\left(\frac{w_{tot}}{w_f}\cdot\frac{1}{35\ \Omega\cdot\frac{l_f}{4\cdot w_f}}\right)}$$

$$=n_{sc}\cdot 70\ \Omega+\frac{4\cdot 35\ \Omega\cdot l_f}{w_{tot}}$$

Horizontal resistance of ECM layer (3.2.1.2):

$$R_{\text{hor}}=\rho\cdot\frac{l}{A}=\frac{l}{\sigma\cdot p_{\text{tot}}\cdot h}=\frac{2.4\cdot 10^{-5}\text{m}}{1\frac{\text{S}}{\text{m}}\cdot 0.38\text{ m}\cdot 1.0\cdot 10^{-7}\text{m}}\approx 630\ \Omega$$

Vertical resistance of ECM layer (3.2.1.2):

$$R_{\text{ver}}=\rho\cdot\frac{l}{A}=\frac{l}{\sigma\cdot A}=\frac{1.0\cdot 10^{-7}\text{m}}{1\frac{\text{S}}{\text{m}}\cdot 1.8\cdot 10^{-5}\text{m}^2}=5.5\text{ m}\Omega$$

Resistance of medium (3.2.1.4):

$$R_{\text{m}}=\rho\cdot l/A\approx(1\ \Omega\cdot\text{m}\cdot 2.4\cdot 10^{-5}\text{ m})/(0.383\text{ m}\cdot 2.4\cdot 10^{-5}\text{m})=2.6\ \Omega$$

Total impedance of equivalent circuit (3.2.1.6):

$$\mathbf{Z}_{\text{tot}}=\mathbf{Z}_{\text{el}}+\frac{1}{\frac{1}{\mathbf{Z}_{\text{c}}}+\frac{1}{\mathbf{Z}_{\text{ECM}}}}=\frac{1}{\frac{1}{R_{\text{el}}}+j\omega C_{\text{el}}}+\frac{\mathbf{Z}_{\text{c}}\mathbf{Z}_{\text{ECM}}}{\mathbf{Z}_{\text{c}}+\mathbf{Z}_{\text{ECM}}}=\frac{R_{\text{el}}}{1+R_{\text{el}}j\omega C_{\text{el}}}+\frac{\mathbf{Z}_{\text{c}}R_{\text{ECM}}}{\mathbf{Z}_{\text{c}}+R_{\text{ECM}}}$$

Laser output (Section 3.4.1.1):

$P = I^2R$ where P = 16 W and I = 32 A. Then

$$R\ =\frac{P}{I^2}\ =\frac{16\text{ W}}{(32\text{ A})^2}=0.015625\ \Omega$$

and for a current of 16 A, the expected power output would be:

$$P = I^2R = (16\ \text{A})^2 \cdot 0.015625\ \Omega = 4\ \text{W}$$

$W = P \cdot t = 4\ \text{W} \cdot 1 \cdot 10^{-6}\ \text{s} = 4 \cdot 10^{-6}\ \text{J}$

Scribing area for a 24 µm diameter laser beam (Section 3.4.1.1):

$A = \pi r^2 = \pi \cdot (12 \cdot 10^{-4}\ \text{cm})^2 = 4.52 \cdot 10^{-6}\ \text{cm}^2$

Laser pulse fluence (Section 3.4.1.1):

Fluence $H_e = W / A = 4 \cdot 10^{-6}\ \text{J} / 4.52 \cdot 10^{-6}\ \text{cm}^2 = 0.88\ \text{J/cm}^2$